THESIS

STATISTICAL PROPERTIES OF CLIPPED SPECKLE PATTERN AND ITS APPLICATIONS TO OPTICAL CORRELATOR

Akifumi OGIWARA

Graduate School of Electronic Science and Technology

Shizuoka University

February 1992

To my parents,

Who were much less surprised than I was when it turned out that their little boy was writing this thesis.

CONTENTS

ABSTRACT

The present thesis is concerned with a fast and precise correlation measurement using binarized speckle signals. In this paper, the statistical properties of clipped speckle signals are investigated and the implementation of an optical nonlinear correlator is presented based on them.

The accuracy of the peak detection in speckle correlation technique is studied by using a computer simulation. The computer simulation for various optical systems shows that the clipping technique has the advantage of the accurate peak detection of the speckle cross-correlation function.

The differences of the accuracy of the peak detections among logical AND, logical NOR, logical XOR, and clipped intensities of 1 and -1 for the clipped correlation are studied theoretically and experimentally. The obtained results show that the accuracy of the peak detections varies depending on the intensity threshold level and the employed logical operations. However, it is proved that the logical XOR and (1,-1) operations are equivalent to each other.

To calculate the correlation function of a two-dimensional speckle intensity, the method of the optical parallel processing is employed. For this purpose, the intensity and phase modulation characteristics of a liquid crystal television (LCTV) as a spatial light modulator are investigated. The effects of the binarization for the speckle signals on the diffraction efficiency are also discussed theoretically and experimentally. Based on the results, the optical correlators for speckle interferometry are proposed by using LCTVs and nonlinear Optic RAM detectors.

Chapter 1. PREFACE

Since the advent of laser, the speckle phenomena have attracted strong attention of many investigators and have been studied by them. As a result, a wide variety of applications using speckle patterns have been found up to now. In those applications of laser speckle patterns, the intensity correlation technique is often used to determine the transient or the dynamic characteristics of a light scattering object. However, it takes a long time to process the signal in a normal correlator because the signal must be digitized through an A/D converter which has several gray scales and the digitized signal must be processed by using full-bit registers and multiplexers. Although the fast Fourier transform (FFT) method is often used to reduce the processing time, it is not enough to realize the " real-time correlator "

Recently it has been recognized that the clipped correlation technique is a useful method for the speckle measurements. The clipping correlation technique is very useful, because the electronics required to process the signal are so reduced that the correlation function can be calculated quickly: N bit-shift register can be reduced to 1-bit on-off register; multiplexers can be replaced by simple logical gates (AND, XOR, and so on). The idea of the clipping correlation and its applications have been presented by several investigators.[1-9] The main purpose of this thesis is how to implement a fast and precise measurement using binarized speckle signals. For this purpose, statistical properties of clipped speckle signals are investigated and a system implementation for an optical correlator is presented.

Chapter 2 discusses a brief summary of the fundamental properties and basic formulations of doubly clipped signal of speckle intensity.

Chapter 3 discusses the accuracy of the peak detection of the speckle correlation function. The dependence of the intensity clipping threshold on the accuracy of the peak detection is very important in the practical use of the clipping correlation technique. However, it is difficult to perform the explicit analysis on the problem. Therefore, the accuracy of the peak detection in speckle correlation technique is studied by using a computer simulation. The shape of the clipped correlation function sharpens compared with the nonclipped one. It is expected that the peak position of the clipped cross-correlation function can be determined more accurately than that of the nonclipped one. The computer simulation for certain optical systems

shows that the clipping technique has the advantage of the accurate peak detection in the speckle cross-correlation function.

In chapter 4, several methods of the logical operations for the intensity clipping are studied to evaluate the accuracy of the peak detection of the clipped correlation function. The theoretical background of the clipped correlation function by using several logical operations is discussed. The differences of the accuracy among logical AND, logical NOR, logical XOR, and clipped intensities of 1 and -1 are studied theoretically and experimentally. The obtained results show that the accuracy of the peak detections varies depending on the intensity threshold level and the employed logical operation. However, it is proved that the logical XOR and (1,-1) operations are equivalent to each other.

In chapter 3 and 4, the analyses have been devoted to one-dimensional 1-bit digital clipping correlation for speckle intensity. However, for the case such as the vector velocity and displacement measurements, we have to treat a two-dimensional speckle intensity pattern. The direct application of the one-dimensional clipping technique to this problem seems to be almost impossible because of the complicated hardware design and the cost for the realization. Thus, a new concept is required to settle the problem. The most useful candidate is the optical parallel processing for the two-dimensional signal. The matched filtering introduced by Vander Lugt is one of the early and famous techniques in optical information processing.[10] Goodman also proposed an alternative approach to it.[11] Although the techniques were very useful ones to implement an optical parallel processing, they were inefficient for a real-time purpose because photographic films were used in those technique.

To settle the problem, spatial light modulators (SLMs) instead of the films have been developed.[12,13] Because of interesting features of the device such as incoherent-to-coherent image conversion, spatial information storage, and light amplification, a lot of studies using those devices have been done by many researchers. Horner has studied the theoretical background for the use of SLMs in optical pattern recognition.[14-20] Javidi has analyzed the optical correlation and deconvolution problems based on the operation of SLMs.[21-35] The applications of SLMs for information processing have been experimentally conducted by Yu, et.al.[36,37] In spite of those studies, the

SLMs have not been still widely used because of their costs and problems such as sensitivity for light and low spatial resolution.

On the other hand, a liquid crystal television (LCTV) has been recently used as a spatial light modulator in the field of optical information processing because of the low cost of the device and the ease of the commercial availability.[38-46] In chapter 5, the intensity and phase modulation characteristics of LCTV as a SLM are investigated. The effects of the binarization for the speckle signals on the diffraction efficiency are also discussed theoretically and experimentally. Based on the results, the system considerations for the optical correlator to process the two-dimensional speckle intensity pattern are given.

In chapter 6, the optical correlators for speckle interferometry are proposed by using LCTV and nonlinear Optic RAM detector. To demonstrate the usefulness of the system, the vector velocity measurement of a light scattering object is presented.

Chapter 2. FUNDAMENTALS OF SPECKLE CLIPPING CORRELATION

To overcome the practical difficulties of a fast real-time digital correlator, the procedure of clipping or one-bit quantization of a signal is frequently used. The digital correlator usually consists of an N-bit shift register (N is the number of digitized bits of a signal) and multiplexers. Therefore, the speed of the calculation is limited by the bits of the signal and the operation speed of the multiplexers. But, for the clipping correlation, the N-bit shift register can be reduced to 1-bit on-off register, and the multiplexers can be replaced by simple logical gates (AND, XOR, and so on). As a result, high-speed correlation is achieved. It is very important to investigate the fundamental properties of clipped speckle patterns for the actual applications.

This chapter is devoted to a brief summary of the basis of doubly clipped speckle intensity. We assume that the speckle amplitude under consideration obeys a zero mean complex Gaussian random process. The clipped signal of the speckle intensity I' has only two levels:

$$I' = \begin{cases} 1 & I \geq b\langle I\rangle, \\ 0 & I < b\langle I\rangle, \end{cases} \tag{2-1}$$

where $b\langle I\rangle$ is the clipping threshold. The doubly clipped correlation function of two intensities I'_1 and I'_2 is defined by

$$\langle I'_1 I'_2\rangle = \int_0^\infty \int_0^\infty I_1 I_2 \, P(I_1, I_2)\, dI_1 dI_2$$

$$= \int_{b_1\langle I_1\rangle}^\infty \int_{b_2\langle I_2\rangle}^\infty P(I_1, I_2)\, dI_1 dI_2 \,. \tag{2-2}$$

$P(I_1,I_2)$ is the joint probability density function of the speckle intensities I_1 and I_2, and is given by the following modified Bessel function $I_0(x)$ [47]

$$P(I_1,I_2) = \frac{1}{<I_1><I_2>(1-\mu^2)} \exp\left(- \frac{I_1/<I_1> + I_2/<I_2>}{1-\mu^2} \right) I_0\left(\frac{2\mu}{1-\mu^2} \sqrt{\frac{I_1 I_2}{<I_1><I_2>}} \right),$$

(2-3)

where μ is the nonclipped correlation factor which is defined by using the complex speckle amplitudes A_1 and A_2 as follows:

$$\mu = \frac{|<A_1 A_2^*>|}{\sqrt{<|A_1|^2><|A_2|^2>}} .$$

(2-4)

For a nonclipped signal of speckle intensity, the correlation function has a well-known simple form and is given by

$$<I_1 I_2>_{nonclip} = <I_1><I_2> (1 + \mu^2) .$$

(2-5)

On the other hand, substituting Eq.(2-3) into Eq.(2-2), the clipped correlation function is expanded by an infinite series of the nonclipped correlation factor μ [1,4]

$$r(\mu) = <I'_1 I'_2> = \sum_{n=0}^{\infty} a_n \mu^{2n},$$

(2-6)

where the coefficient a_n in the expansion is related to the clipping thresholds and given by

$$a_n = \exp(- b_1 - b_2) L_n^{-1} (b_1) L_n^{-1} (b_2) .$$

(2-7)

$L_n(x)$ is a Laguerre polynomials and is defined by

$$L_n^{(\alpha)}(x) = \frac{1}{n!} e^x x^{-\alpha} \frac{d^n}{dx^n}\left(e^{-x} x^{n+\alpha}\right)$$

$$= \sum_{m=0}^{n} \binom{n+\alpha}{n-m} \frac{1}{m!} (-x)^m . \qquad (2\text{-}8)$$

Fig.2-1 shows the plots of the clipped correlation as a function of the correlation factor for various values of the clipping thresholds. From this figure, we can find that the coefficient of the clipped correlation function varies abruptly near the correlation factor μ=1 while it varies slowly for small values of μ. Using this figure, the nonclipped correlation function can be restored from the clipped one.

Figs.2-2 (a) and (b) show examples of nonclipped and clipped intensities of a time varying speckle. Figs.2-3 (a) and (b) show the corresponding correlation functions. As is expected from the theoretical calculation in Fig. 2-1, the width of the clipped correlation function in Fig.2-3 (b) is narrower than that of the nonclipped one in Fig.2-3 (a), in particular around the peak position.

Next, we consider the two limiting cases. When the correlation factor μ goes to zero (i.e., no correlation), it is easily shown that

$$\langle I'_1 I'_2 \rangle_{\mu=0} = \langle I'_1 \rangle \langle I'_2 \rangle = \exp(-b_1 - b_2) . \qquad (2\text{-}9)$$

On the other hand, when the correlation factor is equal to unity, the clipped correlation becomes

$$\langle I'_1 I'_2 \rangle_{\mu=1} = \begin{cases} \exp(-b_1) & b_1 \geq b_2 \\ \exp(-b_2) & b_1 < b_2 \end{cases} . \qquad (2\text{-}10)$$

Most of concern is when the intensities to be correlated obey the same statistics and the clipping levels of the two intensities also have the same

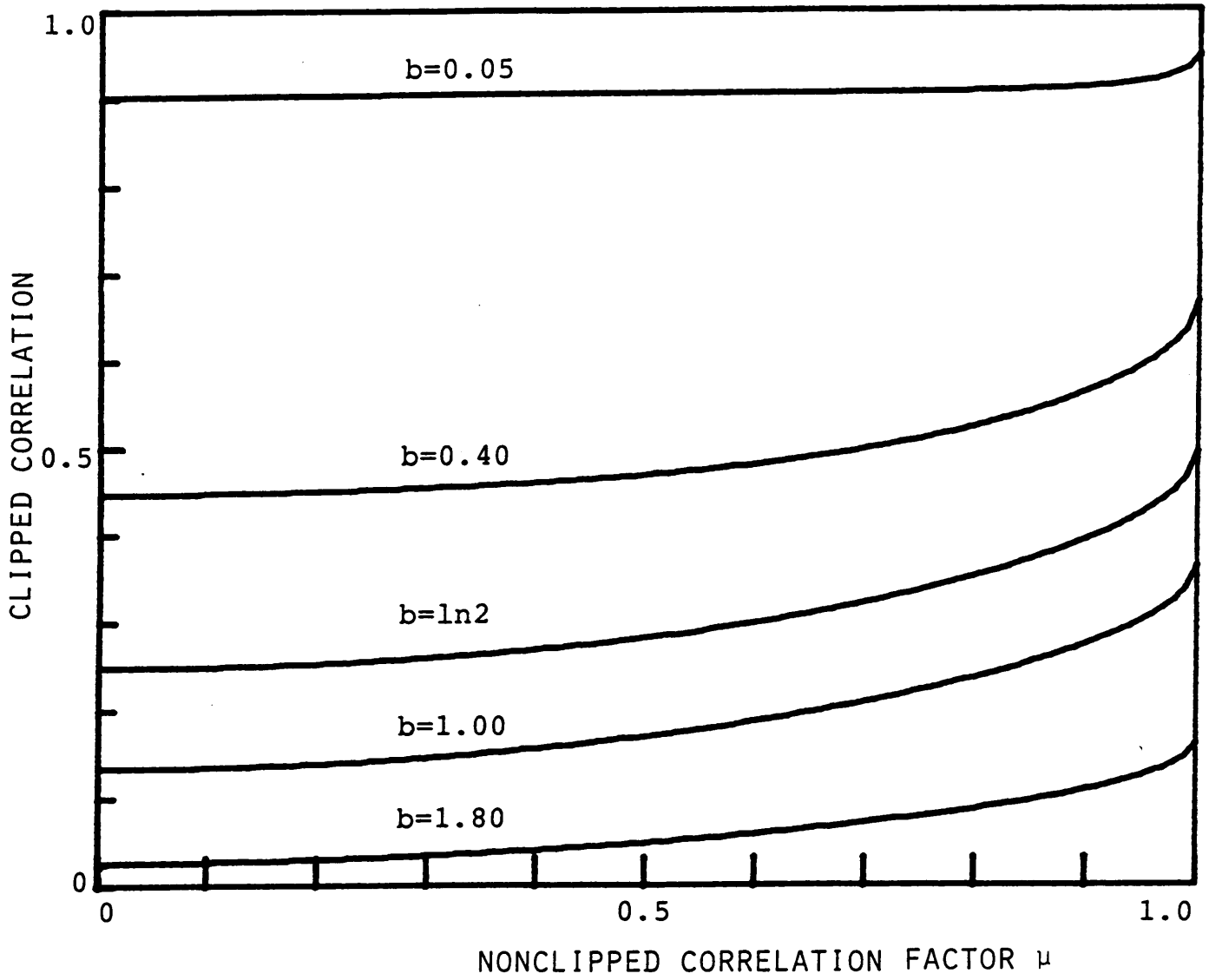

Fig.2-1 Plot of clipped correlation as a function of correlation factor for various values of the clipping threshold.

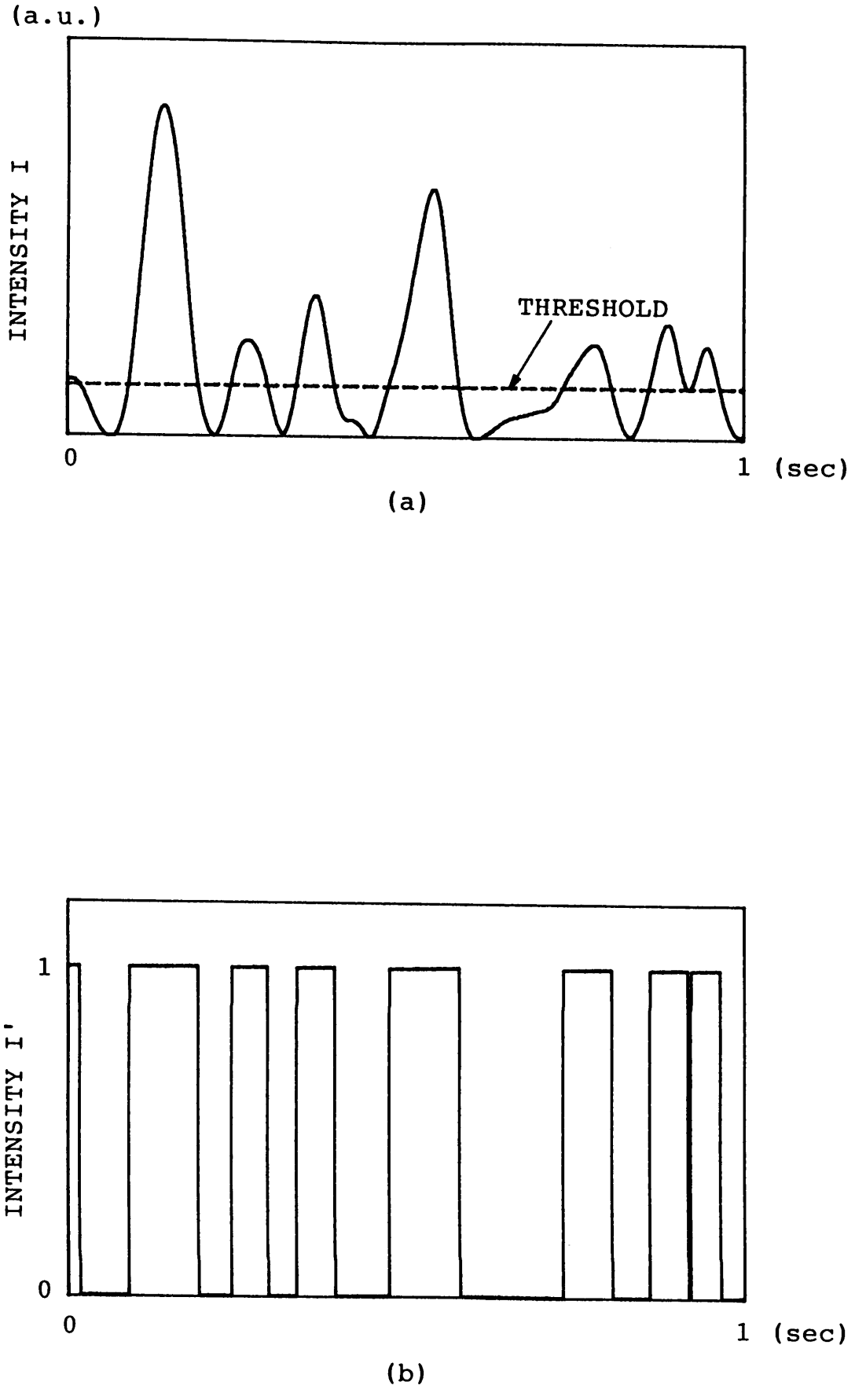

Fig.2-2 Example of nonclipped (a) and clipped (b) intensities.

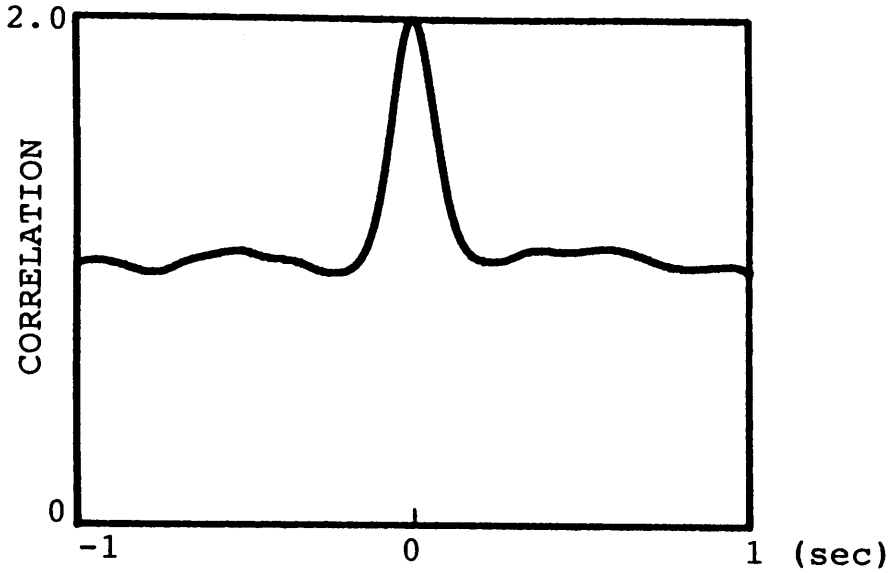

(a)

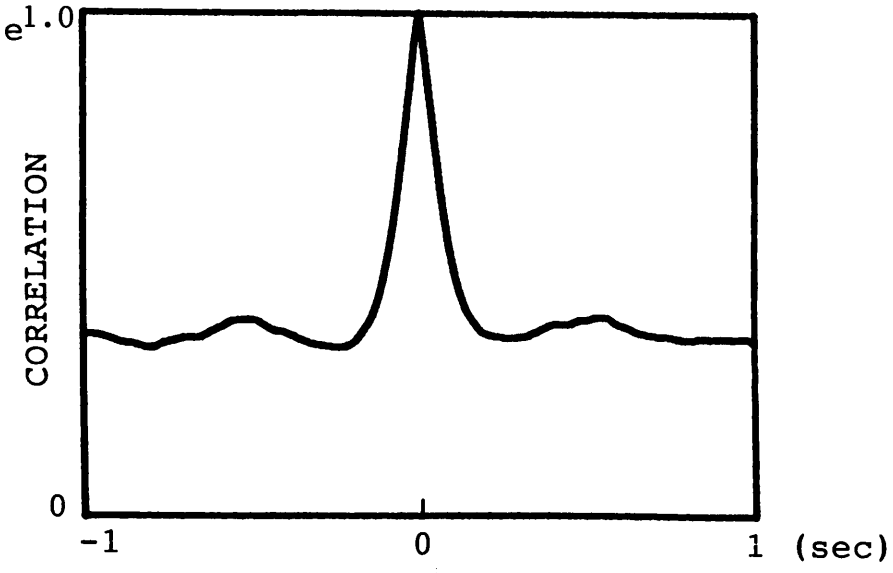

(b)

Fig.2-3 Correlation functions corresponding to those of Fig.2-2.

value. For this particular case, putting $\langle I_1\rangle=\langle I_2\rangle=\langle I\rangle$ and $b_1=b_2=b$, the dynamic range of the clipped correlation function becomes

$$D = \langle I'_1 I'_2\rangle_{\mu=1} - \langle I'_1 I'_2\rangle_{\mu=0}$$

$$= e^{-b}(1 - e^{-b}) \ . \qquad (2\text{-}11)$$

By differentiating D with a clipping threshold b, we can find that the maximum dynamic range of the correlation function occurs at the clipping threshold level of b=ln2.[4] At this threshold level, in the actual clipped speckle intensity signal having a finite data length (see Fig. 2-2 (b)), the number of the data points above the threshold is the same as that below the threshold:

$$\langle I'\rangle = \exp(-\ln 2) = \frac{1}{2} \ . \qquad (2\text{-}12)$$

In the following chapters, some statistical aspects of speckle clipping and their applications will be given based on the statistical properties of the doubly clipped signal of speckle intensity discussed here.

Chapter 3. ACCURACY OF PEAK DETECTION IN SPECKLE CLIPPING CORRELATION

3-1. Introduction

In many applications of laser speckle patterns, the intensity correlation technique is used to determine the transient or dynamic characteristics of a laser light scattering object. The intensity clipping technique is often used to measure the correlation of speckle pattern, because it takes a long time to process the signal in a normal digital correlator. The idea and importance of the clipped correlation function to the speckle measurements have been discussed in the several papers.[1-9] The method of the signal clipping is advantageous in speckle measurements because the electronics required to process the correlation are so reduced that the correlation function can be calculated quickly.

One of the problems of intensity clipped correlation is how we can derive the nonclipped correlation factor from the clipped correlation. Pedersen[1] and Marron and Morris[4] have derived the analytical form of the doubly clipped correlation function of a speckle intensity. We have also investigated the width of a clipped correlation function and compared the theory with the experiment.[8,48] Another important aspect of the technique in the clipped correlation is how to accurately find the peak position of the cross-correlation function. The peak position of the cross-correlation function of a speckle pattern is directly related to the physical quantities of a light scattering object, such as displacement or velocity. A usual speckle correlation function has a bell shaped function which is dependent on the transfer function of an actual optical system. On the other hand, the clipped correlation has an acute function compared with the nonclipped one. Therefore, we can expect more accurate detection of the peak position of a clipped correlation function than that of a nonclipped one.

In this chapter, we discuss the accuracy of the peak detection of clipped and nonclipped correlation functions of speckle patterns.[49] The shape of the clipped correlation function also depends on the threshold of the clipping level as has been discussed in chapter 2. The accuracy of the peak detection is also affected by additive noises involved in the optical system and the electronic circuit used in the signal processing. The computer simulation is employed to find the accuracy of the peak detection of the cross-correlation

function of speckle patterns. Two translation states of speckles, i.e., pure and modified speckle translations have been adopted to compare the SNRs in the cross-correlation functions between them. In the pure translation state, the speckle transverses across the observation plane unchanging its fine structure. But, if the speckle translates across the observation plane losing its identity, i.e., the modified translation state, the peak height of the cross-correlation along the speckle motion is always less than unity. Therefore, it is expected that the SNR in the modified translation state is less than that of the pure translation. A random phase screen is assumed for the light scattering object and the speckle patterns having pure and modified translation states are simulated. The obtained results show the practical advantage of the peak detection of the clipped correlation function, especially in the pure translation state.

3-2 Clipped Correlation Function of Speckle Intensity

As is shown in chapter 2, the doubly clipped correlation function of the speckle intensities having the same statistics is given by

$$r(\mu) = \langle I'_1 I'_2 \rangle = \sum_{n=0}^{\infty} \mu^{2n} \exp(-2b) \{ L_n^{-1}(b) \}^2 \ . \tag{3-1}$$

Fig.3-1 shows the plot of the clipped correlation function having different clipping thresholds against the correlation factor μ^2 of the nonclipped intensity. To see the effect of the clipping threshold on the width of the clipped correlation function, we used the normalized function of the correlation

$$R(\mu) = \frac{r(\mu) - r(0)}{r(1) - r(0)} \ . \tag{3-2}$$

As is seen from this figure, the width of the clipped correlation function is narrower than the nonclipped one. This property establishes that the correlation of the clipped signal will yield a more accurate detection of the peak position than that of the nonclipped one. It is emphasized that the

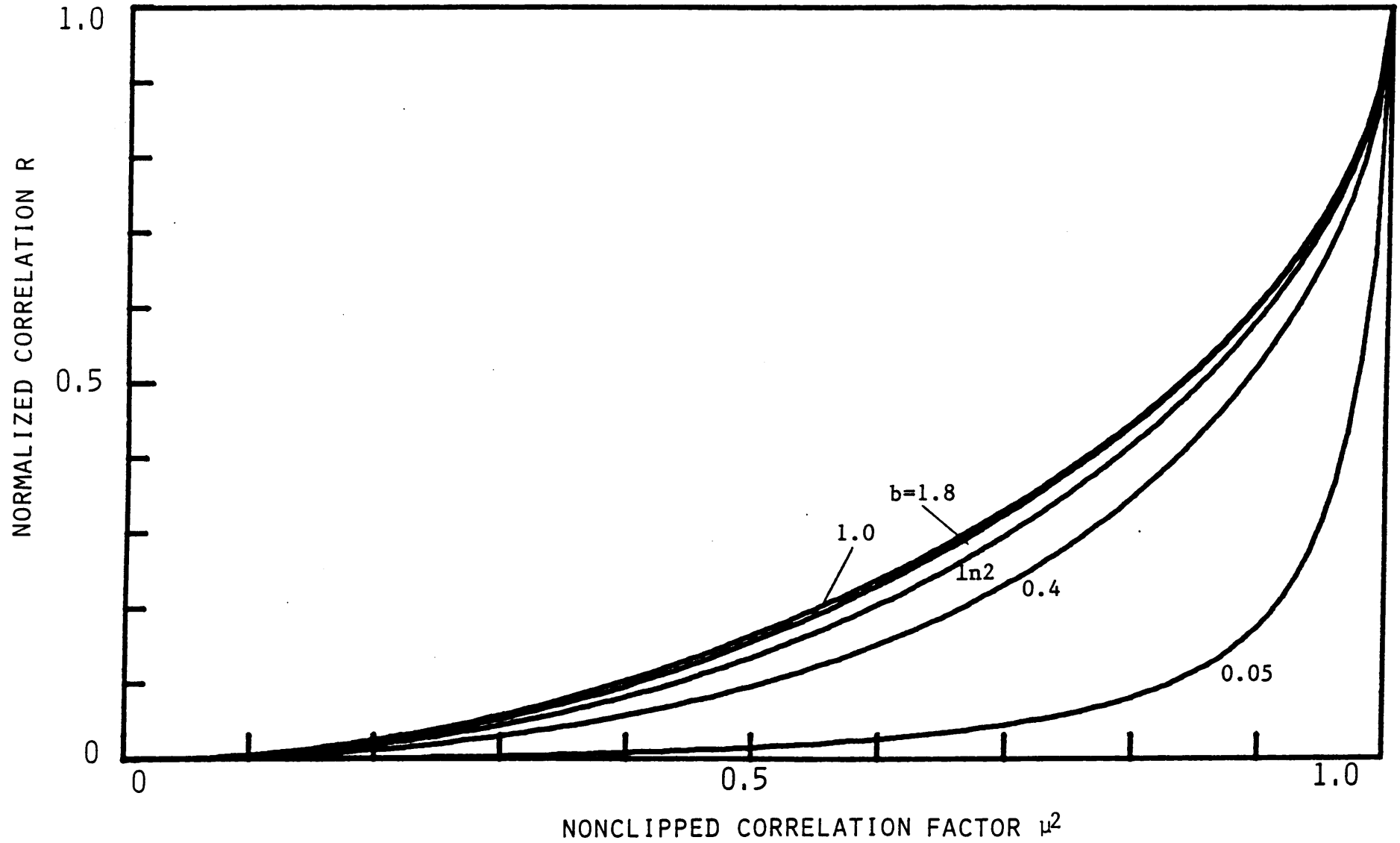

Fig.3-1 Normalized correlation coefficient R for various values of the clipping threshold versus the nonclipping correlation factor μ.

clipping technique is especially suited for the speckle applications based on the cross-correlation method since the cross-correlation measurement requires a good accuracy of peak detection of the function. However, it has been pointed out in chapter 2 that the dynamic range of the clipped correlation function takes its maximum when the threshold is b=ln2. The dynamic range decreases rapidly as the clipping threshold increases or decreases from the value. Therefore, we must take care of a noise effect, i.e., a SNR of the signal, together with a clipping threshold when we consider the accuracy of the peak detection of the cross-correlation function.

Figs.3-2(a) and (b) show examples of the cross-correlation functions of the nonclipped and clipped speckle patterns in a two lens imaging system. Theoretical background of the calculation of the cross-correlation function is discussed in the following section. The speckle translates across the image plane without changing its micro structure in this case. It is noted from this figure that the correlation function of the clipped speckle pattern is narrower than that of nonclipped one.

Figs.3-3(a) and (b) also show examples of the cross-correlation functions in a single lens imaging system. In this optical system, a speckle translates across the observation plane as changing its fine structure and, as a result, the correlation peak decreases as the correlation offset increases. The peak value of the clipped correlation function decreases more rapidly than that of the nonclipped one and the width of the function becomes broad. Therefore, the accuracy of the detection of the peak position is predicted to be worse in this optical system.

3-3. Simulation of Speckle Correlation

The computer simulation is made up with three processes. First, a random phase of a light scattering object is simulated. Then, a pair of speckle patterns for a certain optical system is generated. Finally, the clipped and nonclipped cross-correlation functions are calculated. The simulation is conducted with a NEWS (SONY 32-bit engineering work station) computer.

A. Random Phase Object

We assume that laser speckle patterns to be correlated are produced by a phase object

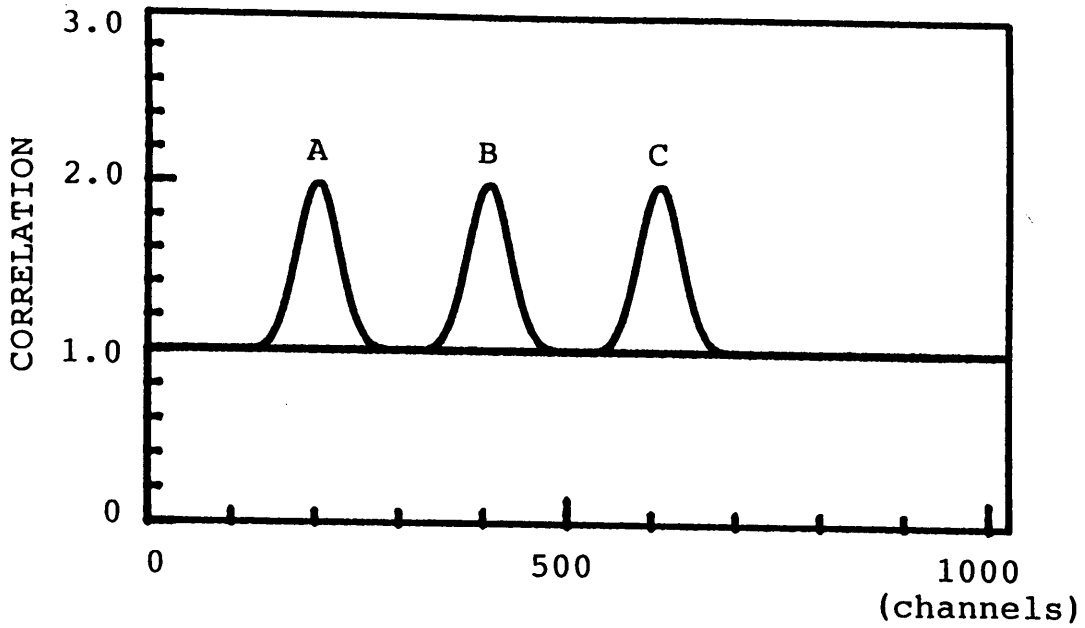

(a)

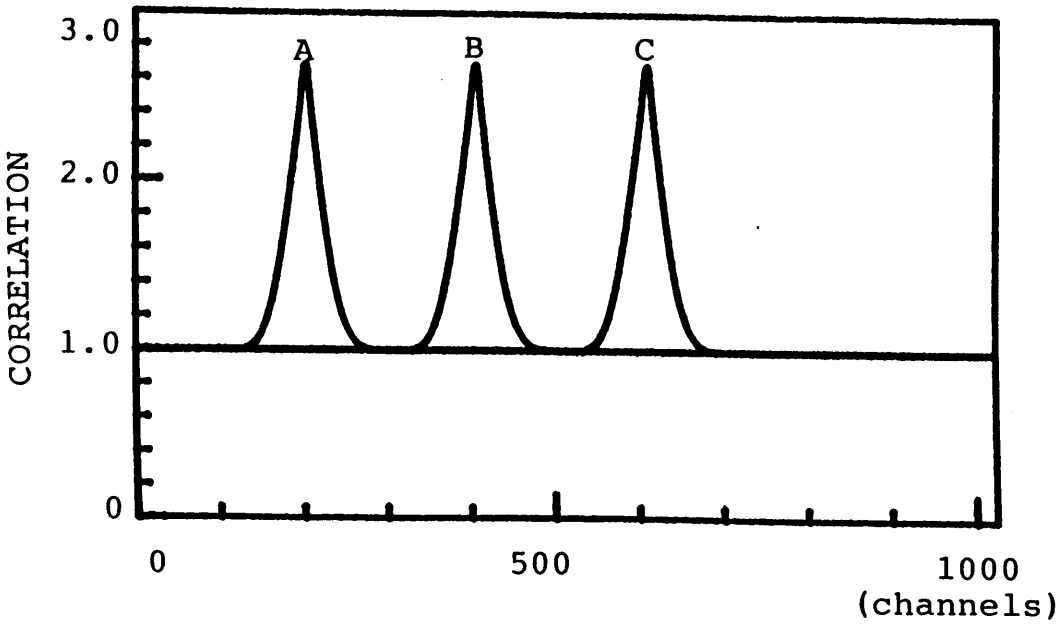

(b)

Fig.3-2 Example of nonclipped and clipped cross-correlation functions theoretically calculated for the pure translation of speckle: (a) nonclipped cross-correlation and (b) clipped cross-correlation. The offsets of the correlations are 200, 400, and 600 channels from A to C, respectively.

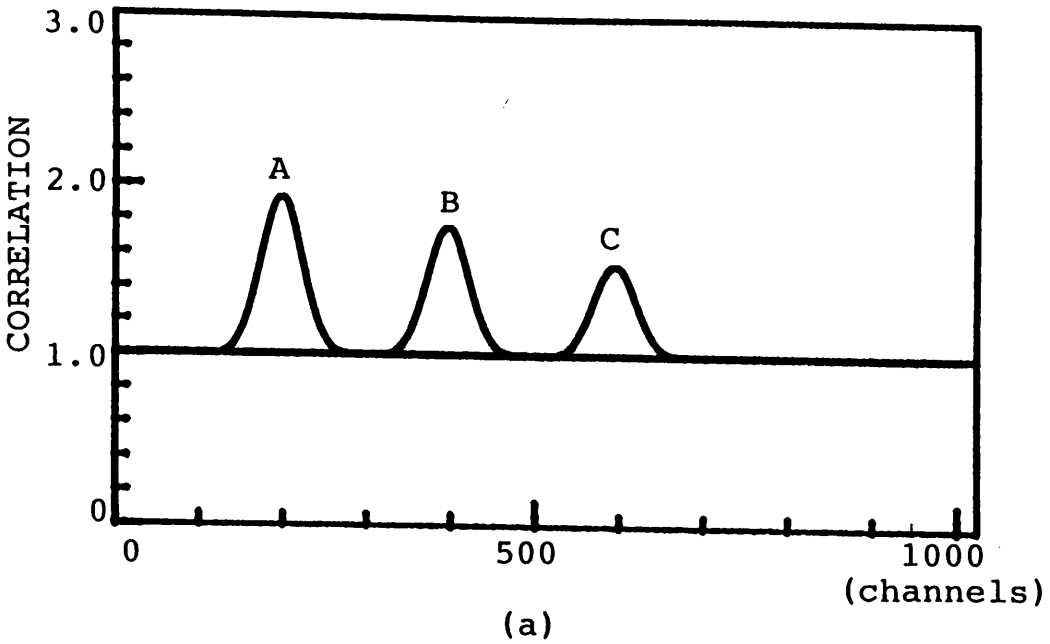

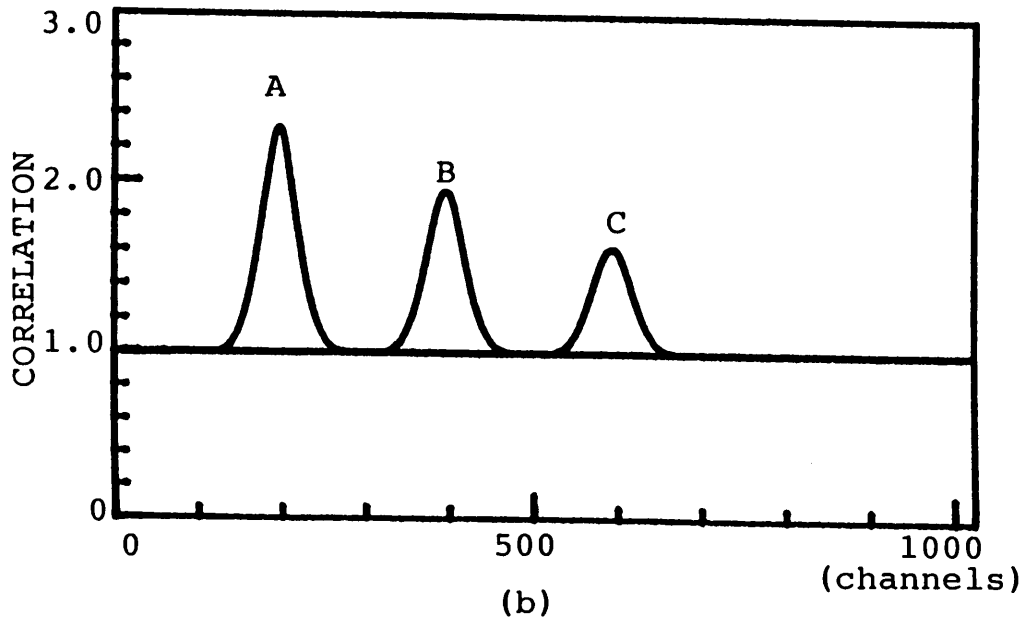

Fig.3-3 Example of nonclipped and clipped cross-correlation functions theoretically calculated for the modified translation of speckle: (a) nonclipped cross-correlation and (b) clipped cross-correlation. The offsets are the same values as those in Fig.3-2.

$$u_O(\mathbf{x},t) = \exp\{i\phi(\mathbf{x},t)\} \ , \qquad (3\text{-}3)$$

where $\mathbf{x}$ is the vector coordinate on the object plane and ϕ is the random phase produced by the scattering from the object at time t. By using the computer, the generation of a random phase object which consists of 8192 sampling points is made in almost the same manner as in Ref.50. The Gaussian statistics is assumed for both the probability density function and correlation function of the random phase. To generate many speckle patterns, this process is repeated.

B. Two Lens imaging System

Our primary concern is to find the peak position of clipped and nonclipped cross-correlation functions of speckle patterns. Therefore, we need a speckle pattern which translates across the observation plane. Then the imaging speckle patterns are investigated. First, we studied a speckle pattern in a two lens imaging system. The speckle pattern appeared at the image plane of the two lens imaging system and translated across the observation plane without changing its fine structures. Therefore, theoretically, the peak value of the nonclipped cross-correlation function is always equal to unity under the plane wave illumination to the object.

Using a Gaussian soft aperture approximation[51] in the two lens imaging system, the transfer function of the imaging system is expressed by

$$K(\mathbf{X},\mathbf{x}) = \int_{-\infty}^{\infty} \exp\left(-\frac{|\mathbf{r}|^2}{q^2} \right) \exp\{ -i\frac{k}{f}(\mathbf{x}-\mathbf{X})\mathbf{r} \}\, d^2\mathbf{r} \ , \qquad (3\text{-}4)$$

where k is a wave number of an illuminating light to the phase object, q is the radius of the aperture function at the back focal plane of the first lens (i.e., the Fourier plane of the object), f is the focal length of the lens, and $\mathbf{r}$ and $\mathbf{X}$ are the vector coordinate at the Fourier and image planes, respectively. Then, the complex amplitude of a speckle pattern at the imaging plane is given by

$$u(\mathbf{X},t) = \int_{-\infty}^{\infty} u_0(\mathbf{x},t)\, K(\mathbf{X},\mathbf{x})\, d^2x \ , \tag{3-5}$$

In the following simulation, the plane wave illumination of a laser light to the object is assumed.

To compare the simulation with the theoretical calculation, we refer to the theoretical results derived in Ref.51. The cross-correlation function in the two lens imaging system is calculated as follows:

$$\mu^2 = \exp\left\{ -\frac{1}{(l_0/v)^2} (\tau - \tau_d)^2 \right\} \ , \tag{3-6}$$

where $\tau=t_1-t_2$ is the variable of the time correlation, τ_d is the time delay of the correlation given by l/v ($l=x_1-x_2$ being the distance of the two detectors in the observation plane), and l_0 is the spatial size of the speckle pattern and is given by

$$l_0 = \frac{2f}{kq} \ . \tag{3-7}$$

From the calculated 8192 points of the phase ϕ, a speckle amplitude with 2048 sample points having a certain arbitrary offset is simulated by using Eq.(3-5). The complex amplitude is calculated numerically by the computer and the intensity distribution is obtained by the square modulus of the complex amplitude.

C. Single Lens Imaging System

The speckle pattern produced at the image plane of a single lens imaging system is simulated also by using a Gaussian soft aperture approximation having an aperture radius q. We use the following optical transfer function:

$$K(\mathbf{X},\mathbf{x}) = \exp\left\{ \frac{ik}{2}\left(\frac{|\mathbf{X}|^2}{p_2} + \frac{|\mathbf{x}|^2}{p_1}\right) \right\}$$

$$\times \int_{-\infty}^{\infty} \exp\left(-\frac{|\mathbf{r}|^2}{q^2}\right) \exp\left\{ -ik\left(\frac{\mathbf{x}}{p_1} - \frac{\mathbf{X}}{p_2}\right) \mathbf{r} \right\} d^2\mathbf{r} \ , \tag{3-8}$$

where p_1 and p_2 are the distances from the object to the lens and from the lens to the image plane, respectively. The cross-correlation function in the single lens imaging system is calculated theoretically as follows:[51]

$$\mu^2 = \exp\left\{ -\frac{1}{(l_o/v)^2} (\tau - \tau'_d)^2 \right\} \exp\left\{ -\left(\frac{p_1}{p_2}\right)^2 \left(\frac{l^2}{l'^2_o + q^2}\right) \right\} \ , \tag{3-9}$$

where τ'_d is also the time delay of the correlation and again l'_o is the spatial size of the speckle in the imaging system and is given by

$$l'_o = \frac{2p_1}{kq} \ . \tag{3-10}$$

Calculating the speckle amplitude by substituting Eq.(3-8) into Eq.(3-5), the speckle intensity variation is also simulated for the single lens imaging system. The speckle pattern in a single lens imaging system always translates across the image plane with deforming its fine structure. Therefore, the peak value of the normalized cross-correlation is always less than unity.

D. Cross-Correlation Using Simulated Speckle Patterns

Fig.3-4 shows a set of the simulated speckle patterns for a two lens imaging system. The phase used to calculate the intensity in Fig.3-4(b) is shifted by a certain offset from that in Fig.3-4(a). Using these simulated speckle patterns, both the clipped and nonclipped cross-correlation functions are calculated by the computer. The generation of 500 pairs of speckle patterns having a certain offset is repeated. Then the clipped and nonclipped cross-correlation functions are calculated. Finally, the fluctuations of the position of the correlation peak are estimated.

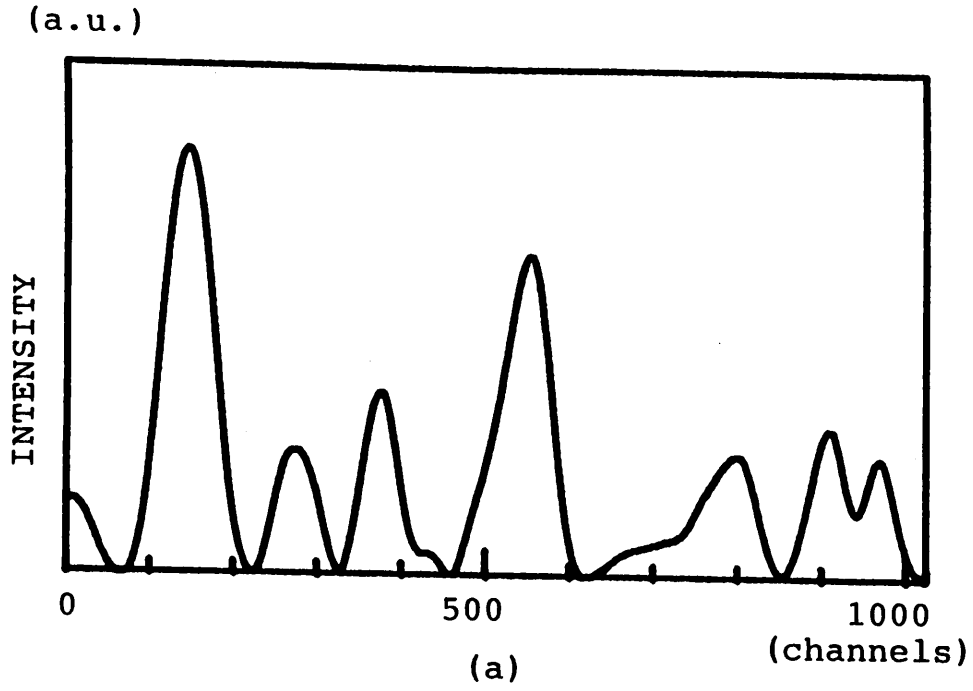

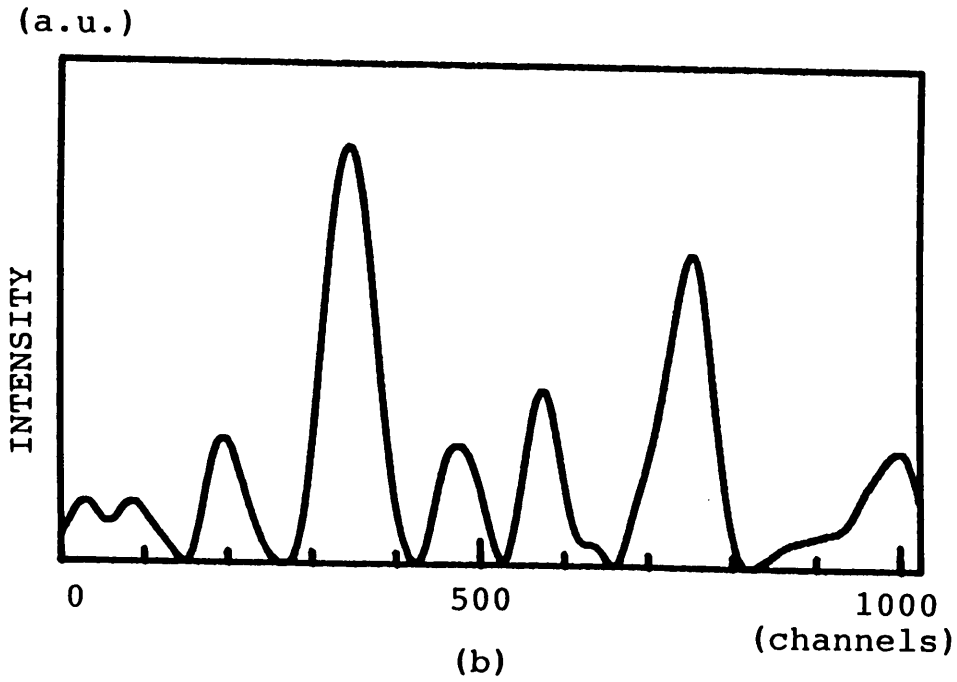

Fig.3-4 Example of the simulations of the pure translation state of speckle patterns produced by the two lens imaging system. The correlation offset is 200 channels.

3-4. Results and Discussions

A. Two Lens Imaging System

The clipped and nonclipped cross-correlation functions are calculated from the simulated speckle patterns (see Fig.3-4). The averaged nonclipped and clipped correlation functions in the two lens imaging system are shown in Fig.3-5. In Fig.3-5(b), the clipping threshold is chosen to be a mean intensity of the speckle intensity variations. The correlation length and time delay of these correlation functions can be compared with the theoretical calculation in Fig.3-2. The offsets of the correlation functions are 200, 400, and 600 channels from A to C in the figure.

Fig.3-6 shows the distribution of the fluctuations of the peak position for the nonclipped cross-correlation functions. In this figure, the vertical axis is the total number of speckle pattern to be correlated. The peak fluctuation increases as the correlation offset increases. On the other hand, Fig.3-7 shows that for the clipped cross-correlation functions, the peak fluctuation increases with the increase of the correlation offset, though the rms fluctuation is smaller than that of nonclipped one which is shown in Fig.3-6. Furthermore, this trend becomes clear for the case of the large correlation offset. In this simulation, the standard deviation of the distribution of the peak fluctuation for the clipped cross-correlation having the offset of 600 channels is 2.37 channels, whereas the corresponding standard deviation for the nonclipped cross-correlation is 7.26 channels. The peak fluctuation becomes smaller to the extent of about one third of that of the nonclipped case. It is said that the clipping technique has the advantage of the peak detection of the cross-correlation function and is suitable for accurate measurements of an object velocity or displacement based on the speckle cross-correlation method.

In practical measurements, the noises encountered in the optical system and the electronic circuits usually affect the SNR of the peak detection.[52] We also studied the noise effects on the accuracy of the peak detection. Fig.3-8 shows an example of speckle signal added with a white noise. The SNR defined by $\langle I \rangle / \sigma_S$ (σ_S is the standard deviation of the noise amplitude) is chosen to be 20 in this figure. The fluctuation of the peak detection is calculated for the noise speckle signal. Fig.3-9 shows the distributions of peak detection of the nonclipped and clipped cross-correlation functions having the noise in speckle signals. The offset of the correlation is chosen to

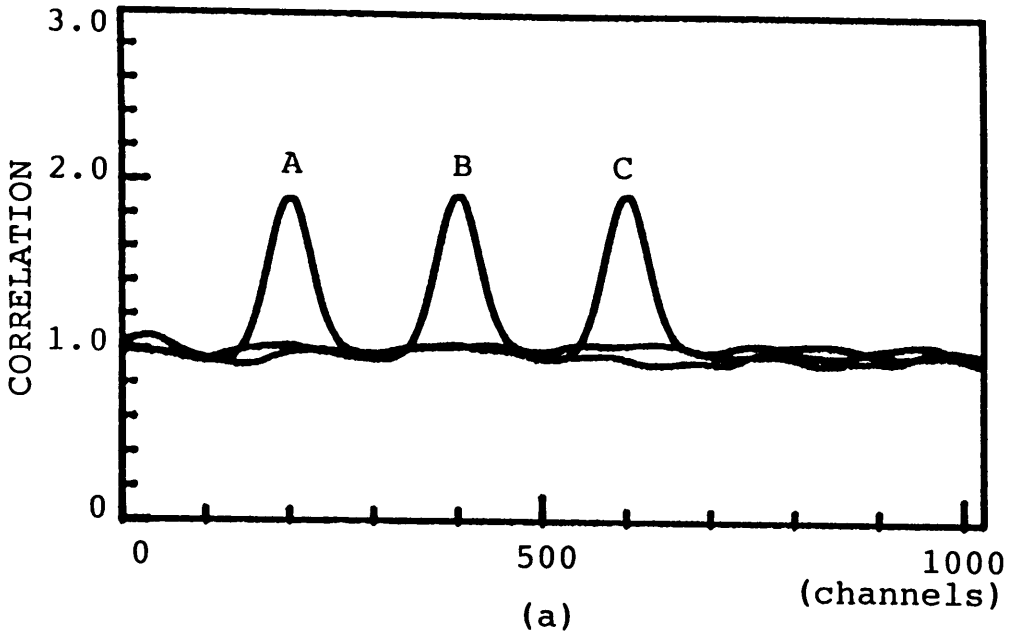

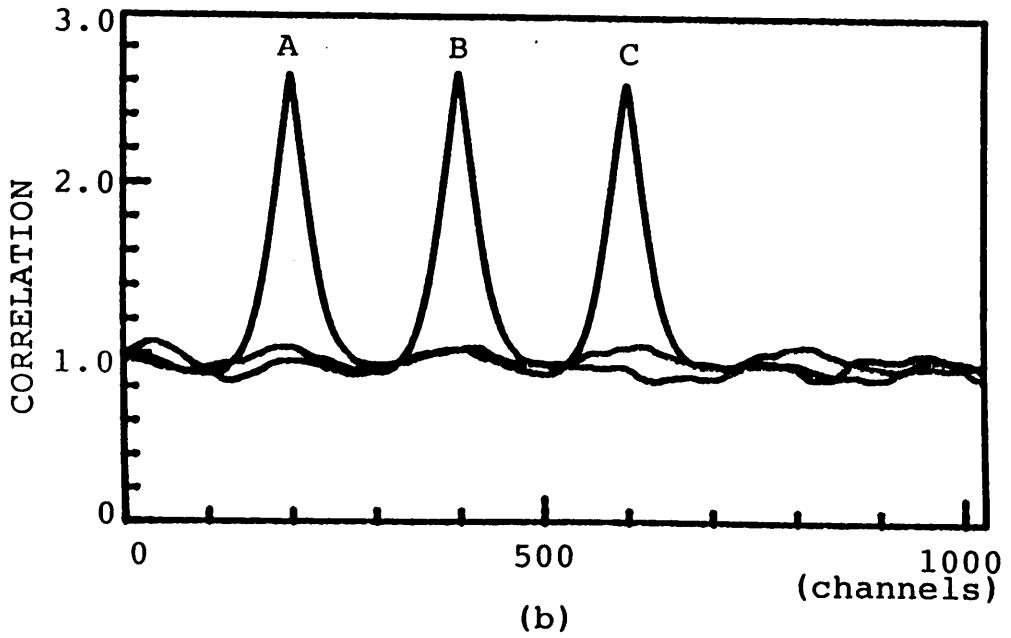

Fig.3-5 Simulated cross-correlation functions in the two lens imaging system: (a) nonclipped cross-correlation and (b) clipped cross-correlation. The offsets are the same values as those in Fig.3-2.

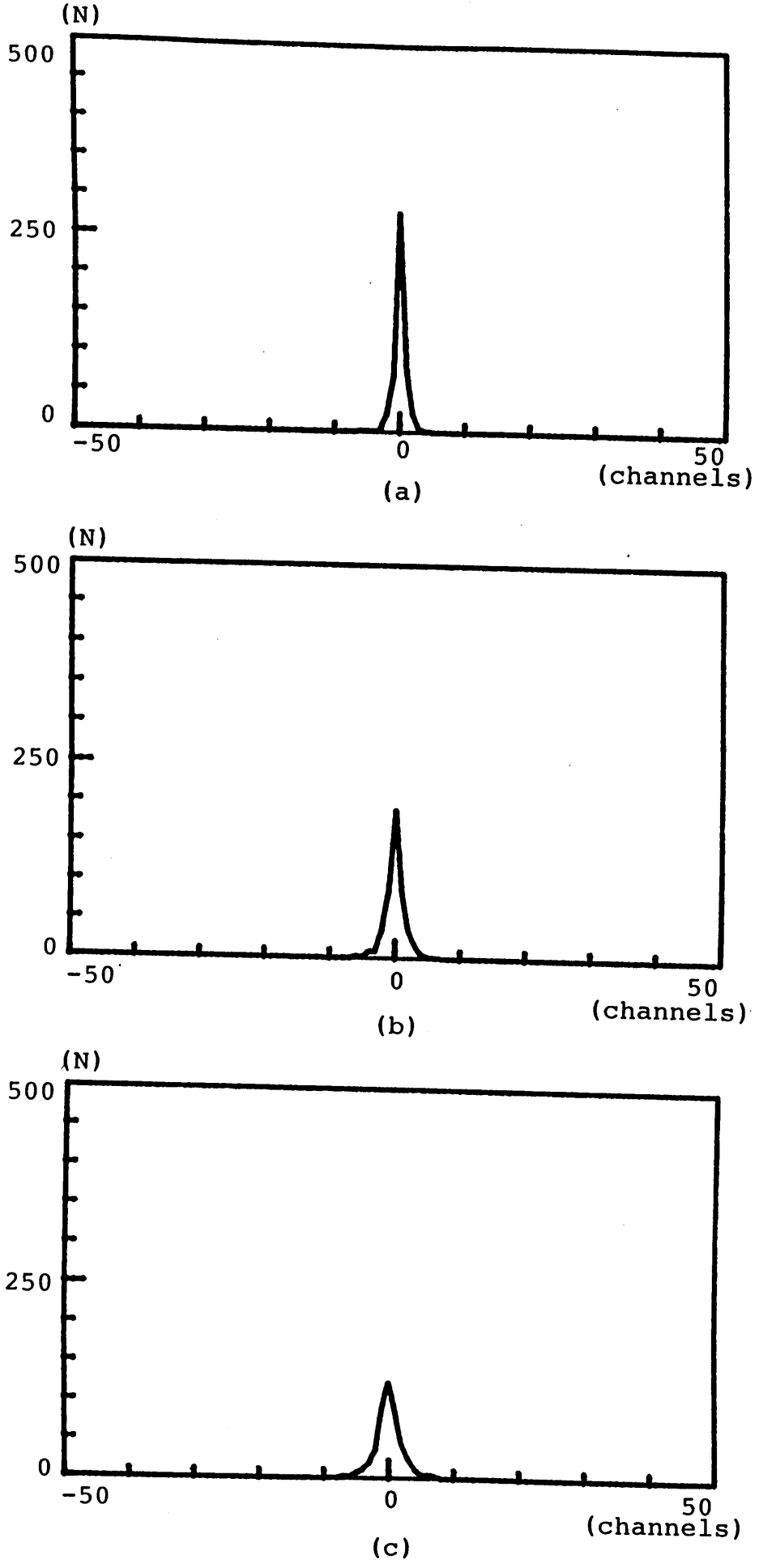

Fig.3-6 Peak fluctuation of nonclipped cross-correlation function in the two lens imaging system. The offsets of the correlation are 200, 400, and 600 channels, from (a) to (c).

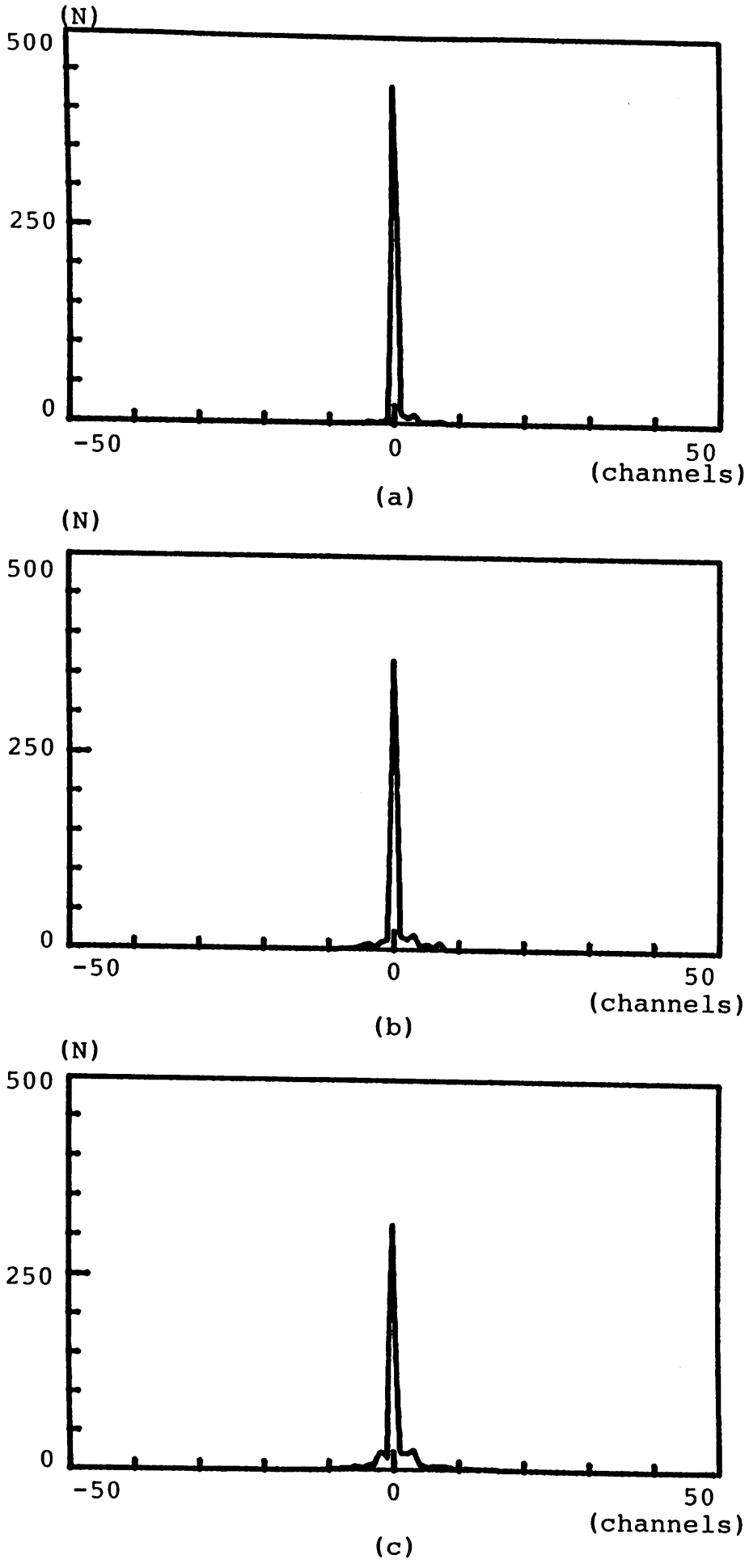

Fig.3-7 Peak fluctuations of clipped cross-correlation function corresponding to Fig.3-6.

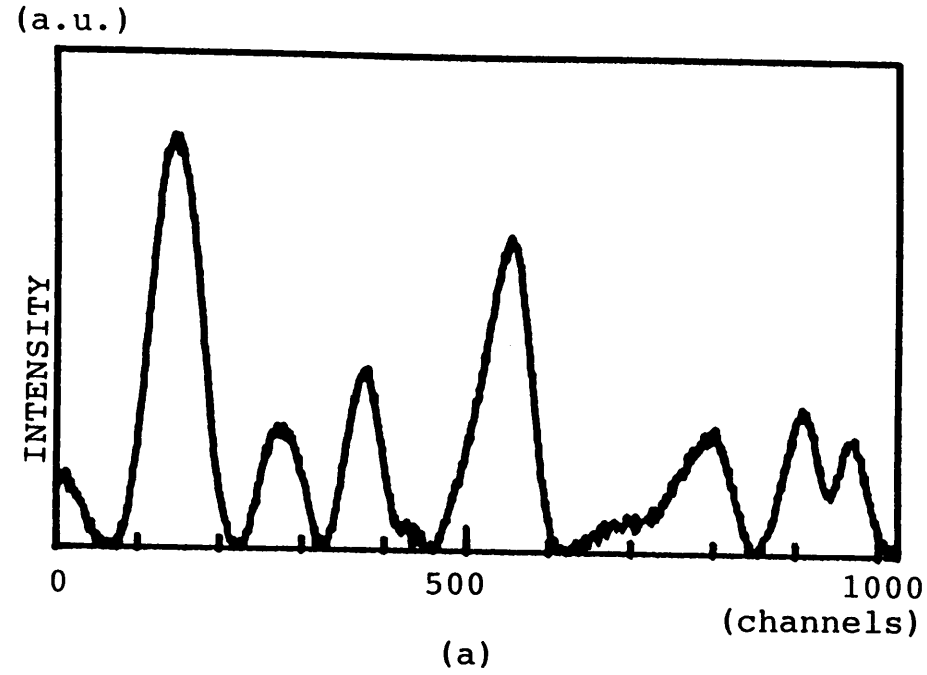

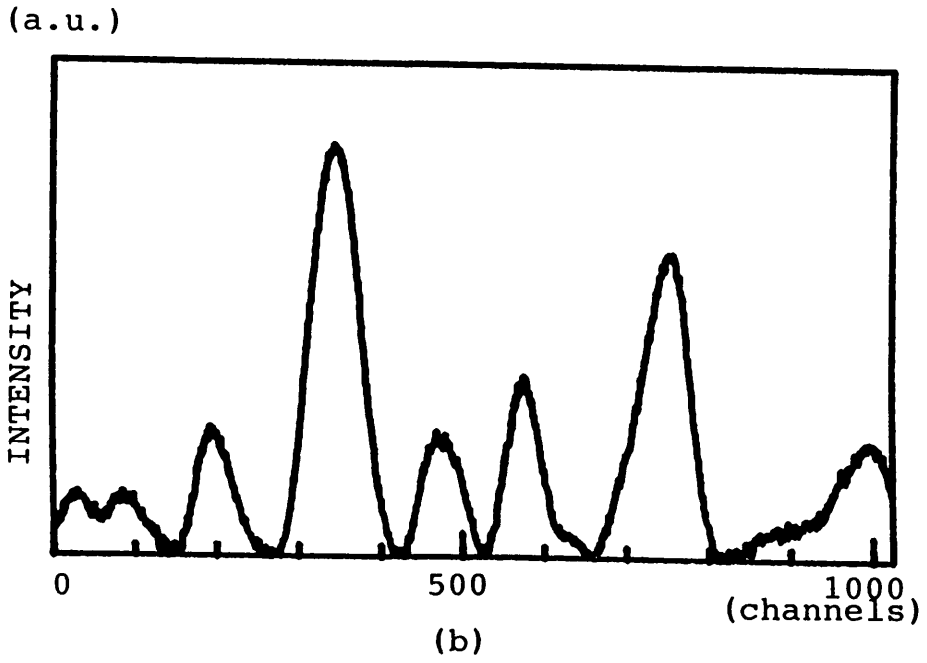

Fig.3-8 Speckle patterns added with a white noise.

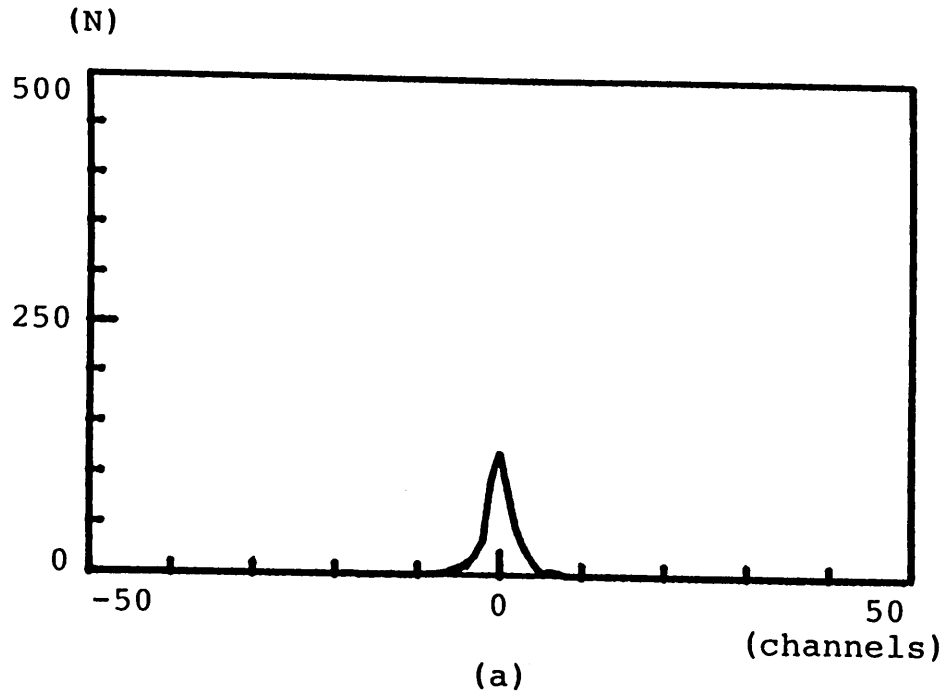

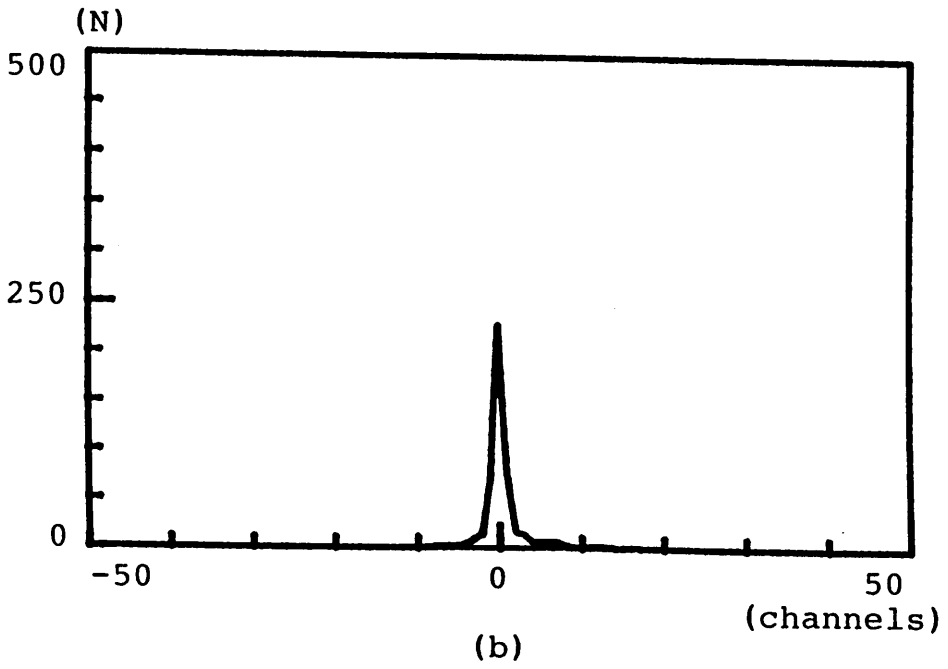

Fig.3-9 Peak fluctuations of the speckle patterns with a white noise: (a) nonclipped case and (b) clipped case.

be 600 channels in this figure. A comparison of this figure with Figs.3-6(c) and 3-7(c) shows that the noise has little effect on the accuracy of the peak detection for the nonclipping case but the accuracy of the peak detection becomes worse for the clipped case. However, for a low noise level, the peak detection of the correlation function of the clipped signal is still better than that of nonclipping one. It can be said that the clipping technique is suited for the accurate measurement of the correlation function of a speckle signal.

B. Single Lens Imaging System

Fig.3-10 shows examples of simulated speckle patterns in the single lens imaging system. Because of the quadratic term of the phase in the single lens optical transfer function described in Eq.(3-8), the modified translation of speckle signals can be observed as is seen in this figure. The correlation offset is 200 channels in this figure. The averaged cross-correlation functions of nonclipped and clipped signals are shown in Fig.3-11. The clipping threshold is also equal to the mean intensity and the correlation offsets are 200, 400, and 600 channels from A to C.

The distribution of the peak positions for the nonclipped speckle correlation function is shown in Fig.3-12, while Fig.3-13 shows the distribution of the peak position for clipped speckle correlation functions. The fluctuations of the peak positions both for the nonclipped and clipped correlation functions increase and the accuracy of the peak detection becomes worse as the correlation offset increases. However, the clipping technique is still effective for estimating the peak position for the correlation having a small offset. In the state of the modified translation, the peak height of the correlation function is always less than that of the pure translation state. As is seen from Fig.3-1 which shows the plots of the factor of a clipped correlation versus that of nonclipped one, we can find that the factor of the clipped correlation function varies abruptly near the correlation factor $\mu=1$ while it varies slowly for small values of μ. For this case, the clipped correlation function in the state of a modified translation does not have a sharp peak compared with that of the pure translation. In the modified translation state, the clipping technique may not be suited for a measurement of the correlation peak when signal to be correlated has a large offset.

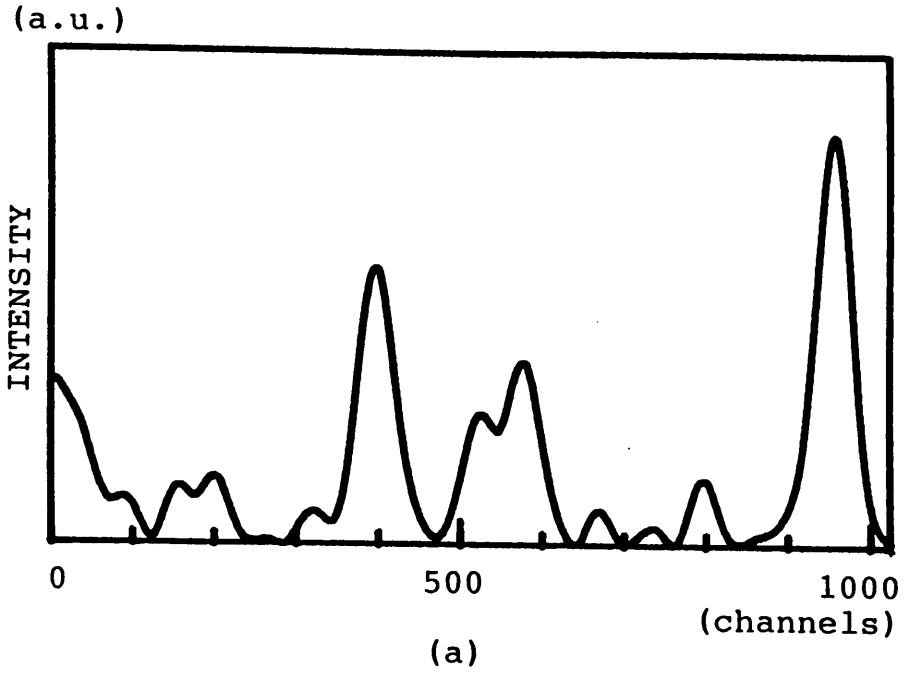

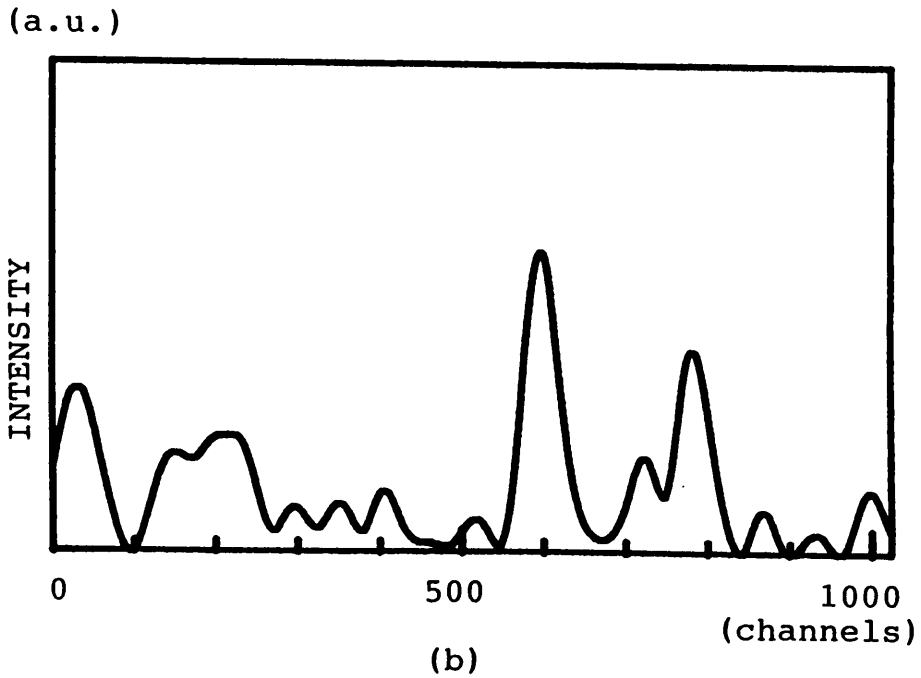

Fig.3-10 Example of the simulation of modified translation state of speckle patterns in the single lens imaging system. The correlation offset is 200 channels.

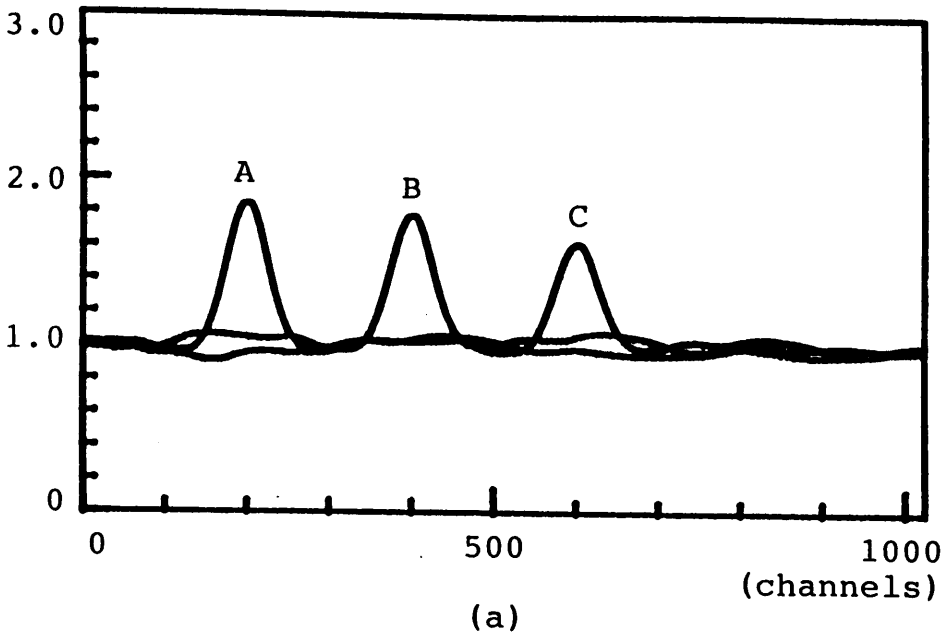

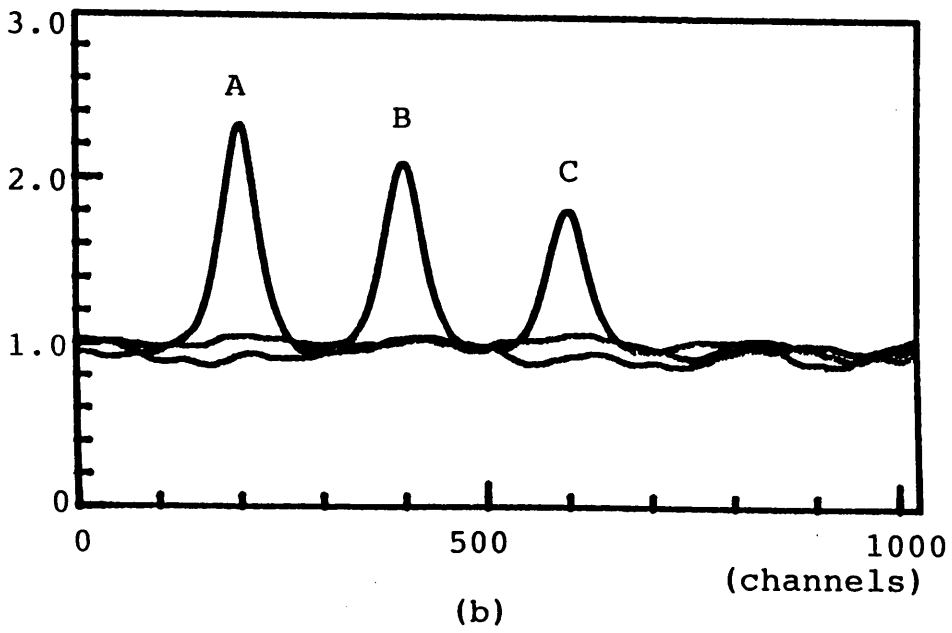

Fig.3-11 Simulated cross-correlation function in the single lens imaging system: (a) nonclipped correlation and (b) clipped correlation. The correlation offsets are the same values as those in Fig.3-2.

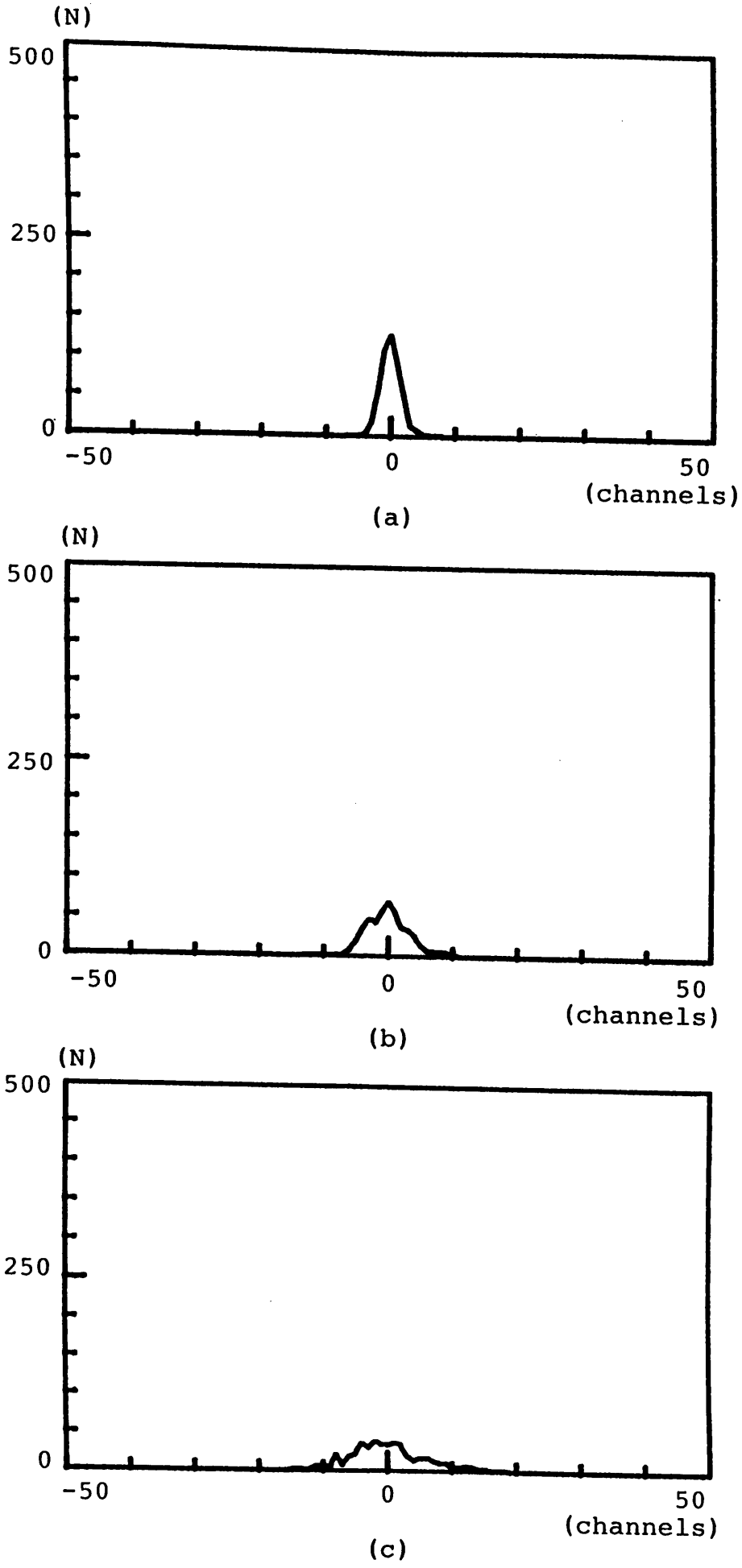

Fig.3-12 Peak fluctuations of nonclipped cross-correlation function in the single lens imaging system. The correlation offsets are 200, 400, and 600 channels from (a) to (c), respectively.

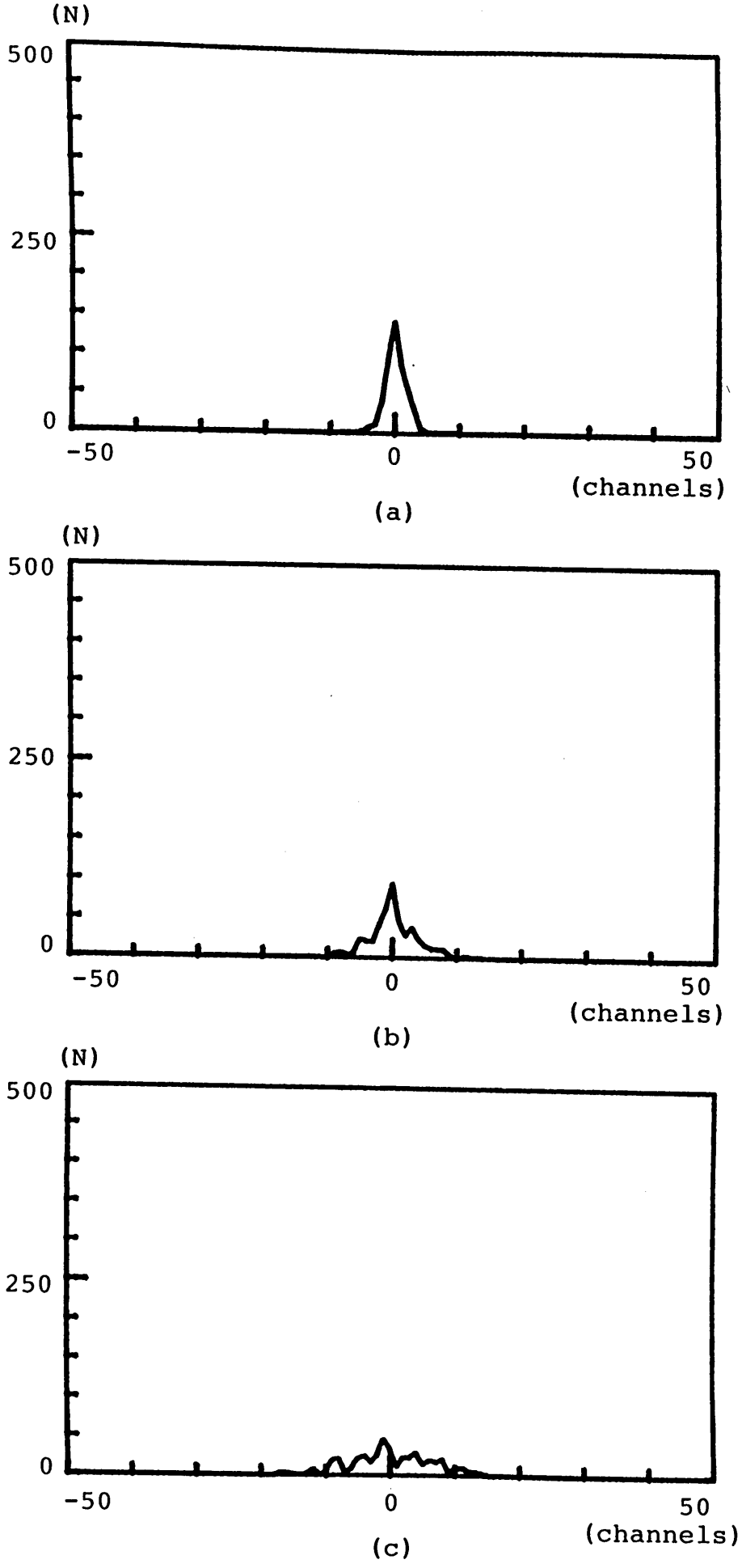

Fig.3-13 Peak fluctuations of clipped cross-correlation function corresponding to Fig.3-12.

Chapter 4. VARIOUS LOGICAL OPERATIONS IN SPECKLE CLIPPING CORRELATION

4-1. Introduction

The high speed calculation of the correlation function is realized by the intensity clipping technique because of the simplicity of the technique and the reduction of the processing electronics. The accuracy of the peak detection for the clipped and nonclipped correlation function was investigated by a computer simulation in chapter 3. Another problem is the dependence of the accuracy on a logical operation in the calculation of a clipped correlation function.

There are several definitions for the clipped signals of speckle intensity. One of them is the usual method of the signal clipping, i.e., a 1-bit digitization of the intensity. In this digitization, the clipped intensity is set to be unity for the intensity above or equal to a certain threshold, while zero for the intensity below it. Another possible definition of the digitization is that the clipped signals have two values 1 and -1 corresponding to intensities above and below the threshold, respectively. Using these definitions, the correlation function is calculated based on several logical operations as shown in Fig.4-1. Churnside has suggested that the (1,-1) method can extract more information from the clipped signal than other cases.[3] However, Marron and Morris have pointed out that these definitions are equivalent.[6]

In this chapter, we examine the accuracy of the peak detection of the cross-correlation function for several methods of the clipped signals of speckle intensity.[53] The theoretical background of the correlation function calculated by the logical operations of the clipped intensity is discussed. We also present experiments performed by using a special interface board of a microcomputer, which is developed for acquiring speckle signals with high speed. Using this system, the accuracy of the peak detections for the four methods of logical operations, i.e., logical AND, logical NOR, logical XOR, and clipped intensities of 1 and -1, is discussed. The obtained results show that the logical XOR and (1,-1) operations are equivalent. It is also known that the accuracy of the peak detections for the logical operations depends on the clipping thresholds.

AND		
1	1	1
1	0	0
0	1	0
0	0	0

NOR		
1	1	0
1	0	0
0	1	0
0	0	1

XOR		
1	1	0
1	0	1
0	1	1
0	0	0

(1,-1)		
1	1	1
1	-1	-1
-1	1	-1
-1	-1	1

Fig.4-1 Possible logical operations for clipped speckle signal.

4-2. Logical operation of Clipped Signal

In this section, we discuss the correlation functions for several logical operations of clipped speckle intensity signals. As is discussed in chapter 2, the most simple definitions of clipped speckle intensity is

$$I' = \begin{cases} 1 & I \geq b\langle I\rangle \\ 0 & I < b\langle I\rangle \end{cases} . \tag{4-1}$$

For the logical AND operation of the clipped intensity, the correlation function is written by

$$R_{AND} = \int_{b\langle I\rangle}^{\infty} \int_{b\langle I\rangle}^{\infty} P(I_1,I_2)\ dI_1 dI_2 , \tag{4-2}$$

where $P(I_1,I_2)$ is the joint probability density function defined by Eq.(2-3). Eq.(4-2) can be also expanded by an infinite series of the correlation factor μ:

$$R_{AND} = \sum_{n=0}^{\infty} \mu^{2n} \exp(-2b) \{ L_n^1(b) \}^2 . \tag{4-3}$$

The nonclipped correlation factor can be regained from the relation of the clipped correlation factor in Eq.(4-3).

Here, we consider the dynamic range of the correlation function which is defined by the difference between the correlation peak and uncorrelated values of the function. It is discussed in chapter 2 that the maximum dynamic range for the correlation function given by Eq.(4-3) is

$$R_{AND}(\mu=1) - R_{AND}(\mu=0) = \frac{1}{4} . \tag{4-4}$$

Eq.(4-4) shows that the dynamic range of clipped correlation function falls one quarter of that of nonclipped one as is also pointed out in the case for integrated speckle intensity.9

Next, we treat the logical XOR operation (or equivalently the logical EX-NOR operation) of the clipped signals in which the product of the clipped intensities has the value of unity when one of the speckle intensity is above threshold and the other is below it or vice versa. Then the clipped correlation function for the logical XOR operation is defined by

$$R_{XOR} = \int_{b<I>}^{\infty} \int_{0}^{b<I>} P(I_1,I_2)\, dI_1 dI_2 + \int_{0}^{b<I>} \int_{b<I>}^{\infty} P(I_1,I_2)\, dI_1 dI_2 \ . \tag{4-5}$$

Substituting the joint probability density function in Eq.(2-3) into Eq.(4-5), one can obtain4

$$R_{XOR} = -\,2R_{AND} + 2\exp(-b) \ , \tag{4-6}$$

where R_{AND} is the clipped correlation function defined in Eq.(4-3). We can also calculate the maximum dynamic range of the correlation function for the logical XOR operation in the same manner as that of the logical AND operation,

$$R_{XOR}(\mu=1) - R_{XOR}(\mu=0) = -\frac{1}{2} \ . \tag{4-7}$$

The minus sign in Eq.(4-7) means that the minimum value of the function which is appeared in the lower side of the uncorrelated value corresponds to the peak of the usual correlation function. In the case of the logical XOR operation, the value of the dynamic range of the correlation function becomes twice that for the logical AND operation.

Another possible definition of the clipped signal for calculating the correlation function is given by

$$I' = \begin{cases} 1 & I \geq b\langle I\rangle \\ -1 & I < b\langle I\rangle \end{cases} . \qquad (4\text{-}8)$$

The correlation function of this clipped signal is calculated by the joint probability density function in Eq.(2-3) as

$$R(1,-1) = \int_0^{b\langle I\rangle}\int_0^{b\langle I\rangle} P(I_1,I_2)\,dI_1dI_2 + \int_{b\langle I\rangle}^{\infty}\int_{b\langle I\rangle}^{\infty} P(I_1,I_2)\,dI_1dI_2$$
$$- \int_{b\langle I\rangle}^{\infty}\int_0^{b\langle I\rangle} P(I_1,I_2)\,dI_1dI_2 - \int_0^{b\langle I\rangle}\int_{b\langle I\rangle}^{\infty} P(I_1,I_2)\,dI_1dI_2$$

$$= 4R_{AND} - 4\exp(-b) + 1 . \qquad (4\text{-}9)$$

The maximum dynamic range of the correlation function of Eq.(4-9) is also calculated for the clipping threshold of b=ln2 as

$$R(1,-1)\,(\mu=1) - R(1,-1)\,(\mu=0) = 1 . \qquad (4\text{-}10)$$

The maximum dynamic range of the clipped correlation function for (1,-1) logic is the same as that of the nonclipped one. It seems that the dynamic range in Eq.(4-10) has twice the value of that for the logical XOR operation (four times the value compared with that of the logical AND operation) and that the perfect information of the nonclipped correlation function can be recovered for the (1,-1) logic in concerning with the dynamic range. However, the clipped signals have only two values, i.e., the values above and below threshold, so that the maximum information for the clipped case is reduced to one half of that of nonclipped one. As a matter of fact in the derivation of Eq.(4-10) or Eq.(4-9), the same information is counted twice. This is readily explained as follows. Since $P(I_1,I_2)$ is a probability density function, the following relation is always satisfied for any value of the probability density function:

$$\int_0^{b<I>}\int_0^{b<I>} P(I_1,I_2)\,dI_1dI_2 + \int_{b<I>}^{\infty}\int_{b<I>}^{\infty} P(I_1,I_2)\,dI_1dI_2$$

$$= 1 - \int_{b<I>}^{\infty}\int_0^{b<I>} P(I_1,I_2)\,dI_1dI_2 - \int_0^{b<I>}\int_{b<I>}^{\infty} P(I_1,I_2)\,dI_1dI_2 \ . \qquad (4\text{-}11)$$

Substituting Eq.(4-11) into Eq.(4-9), Eq.(4-9) reduces to Eq.(4-5) except for a factor of two. This factor is only originated from the mathematical process, so that the information contained in Eq.(4-9) is the same as that in Eq.(4-5). The evidence of this fact is demonstrated as the experimental result in the following section. However, Eq.(4-5) and Eq.(4-9) should be distinguished from Eq.(4-2) because these equations evaluate both of the information of the clipped signals above and below threshold while Eq.(4-2) only contains the information of the intensity above threshold. In the next section, we conduct the experiments to compare the accuracy of the correlation function based on clipping methods of these different logical operations.

4-3. Experiments and Discussions

Fig.4-2 shows the experimental setup for clipped correlation function of four different logical operations, AND, NOR, XOR, and (1,-1). The object of a rotating ground glass plate of #400 is illuminated by a plane wave of a 30 mW He-Ne laser. The object is imaged by two lenses together with a pinhole located at the back focal length of the first lens. The focal lengths of two lenses are 100 and 400 mm, respectively. The radius of the pinhole is 1.0 mm. One-dimensional Plasma-Coupled Device (PCD) array detector which contains 1024 elements with 25μm spacing is placed in the observation plane. The detected intensity signal is stored in a microcomputer through an interface board developed for the fast data acquisition. Using this system, a total of 1000 samples of the speckle pair having a certain time offset is acquired. Throughout the following experiment, the time offsets of the cross-correlation are chosen to be 410, 820, and 1430 ms. From the obtained data, the speckle intensity signals are binarized at a certain threshold level

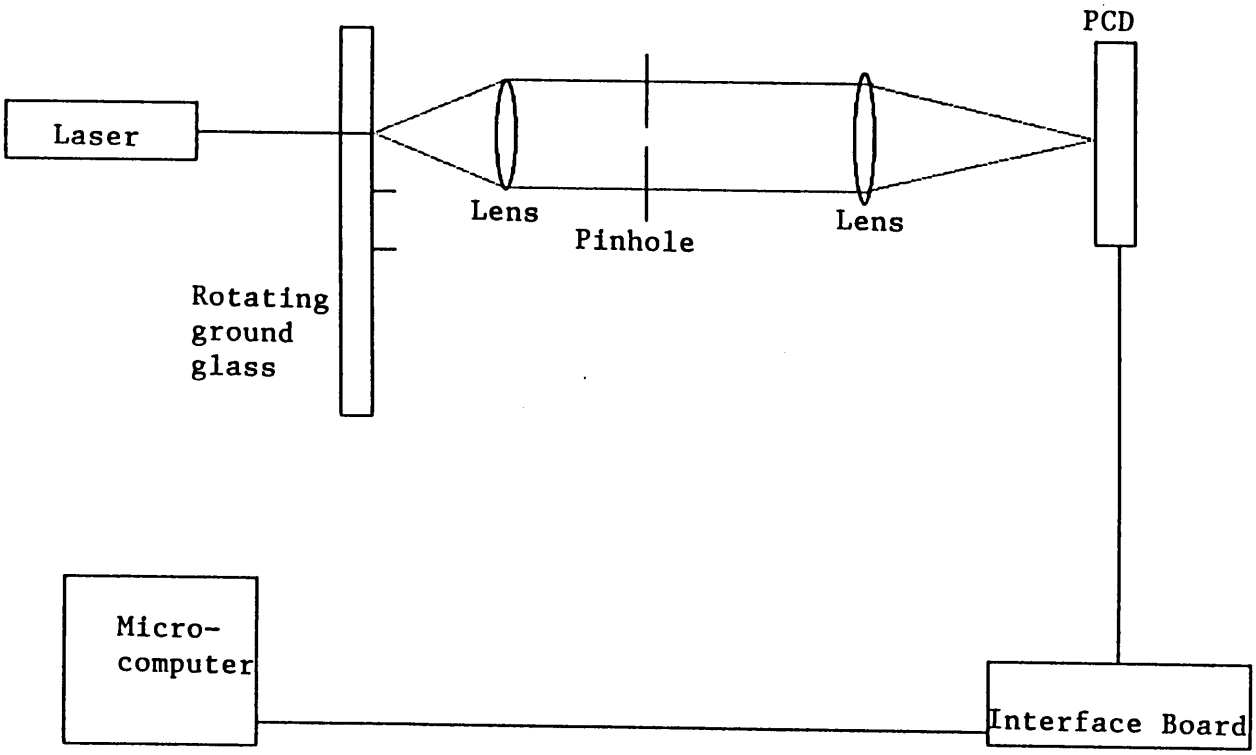

Fig.4-2 Schematic illustration of the experimental setup.

and the clipped cross-correlation functions having 512 points data length are calculated by the software on the computer. Thus, the distribution of the peak positions of the correlation functions is obtained from the calculated cross-correlation functions for each logical operation. By evaluating these peak distributions, we compare the accuracy of the peak detection among the different logical operations.

Fig.4-3(a) shows the cross-correlation functions of logical AND operation having three time offsets. Fig.4-3(b) is the cross-correlation function for the complementary clipping which corresponds to the logical NOR operation of the clipped signals. Figs.4-3(c) and (d) show the cross-correlation functions of logical XOR and (1,-1) operations for three time offsets, respectively. In Fig.4-3, a threshold level is chosen as the averaged intensity of the speckle signals and the correlation functions are normalized by the value of 512. From these figures, (1,-1) operation method seems to be the best concerning the dynamic range of the correlation function. However, as it is already discussed in section 4-2, the information involved in Fig.4-3(c) is the same as that in Fig.4-3(d).

Fig.4-4 shows the distributions of the peak positions obtained from the clipped cross-correlation functions such as shown in Fig.4-3. The time offset is chosen to be 1430 ms and the clipping threshold level is 2.0 <I>. As is seen in this figure, the distributions of XOR and (1,-1) are the same, whereas they are different from those of the other logical operations, although the same nonclipped speckle intensity signals are used in the calculations.

To see the effects of the logical operations and the clipping threshold level on the peak detection, the relation between the standard deviation of peak distributions and the clipping threshold of speckle intensity is shown in Fig.4-5. Figs.4-5(a), (b), and (c) correspond to the time offsets of 410, 820, and 1430 ms, respectively. As is already discussed, XOR and (1,-1) logical operations are equivalent and the obtained deviations entirely coincide with each other. This result represents that the clipped correlation function calculated by the (1,-1) logic does by no means have more information than that of the logical XOR operation. Except for the equivalence of the logical XOR and (1,-1) operations, the accuracy of the peak detections varies depending on the threshold level and the method of the logical operation. The good accuracy of the peak detections is obtained for each logical operation at the clipping threshold around the average intensity level. We

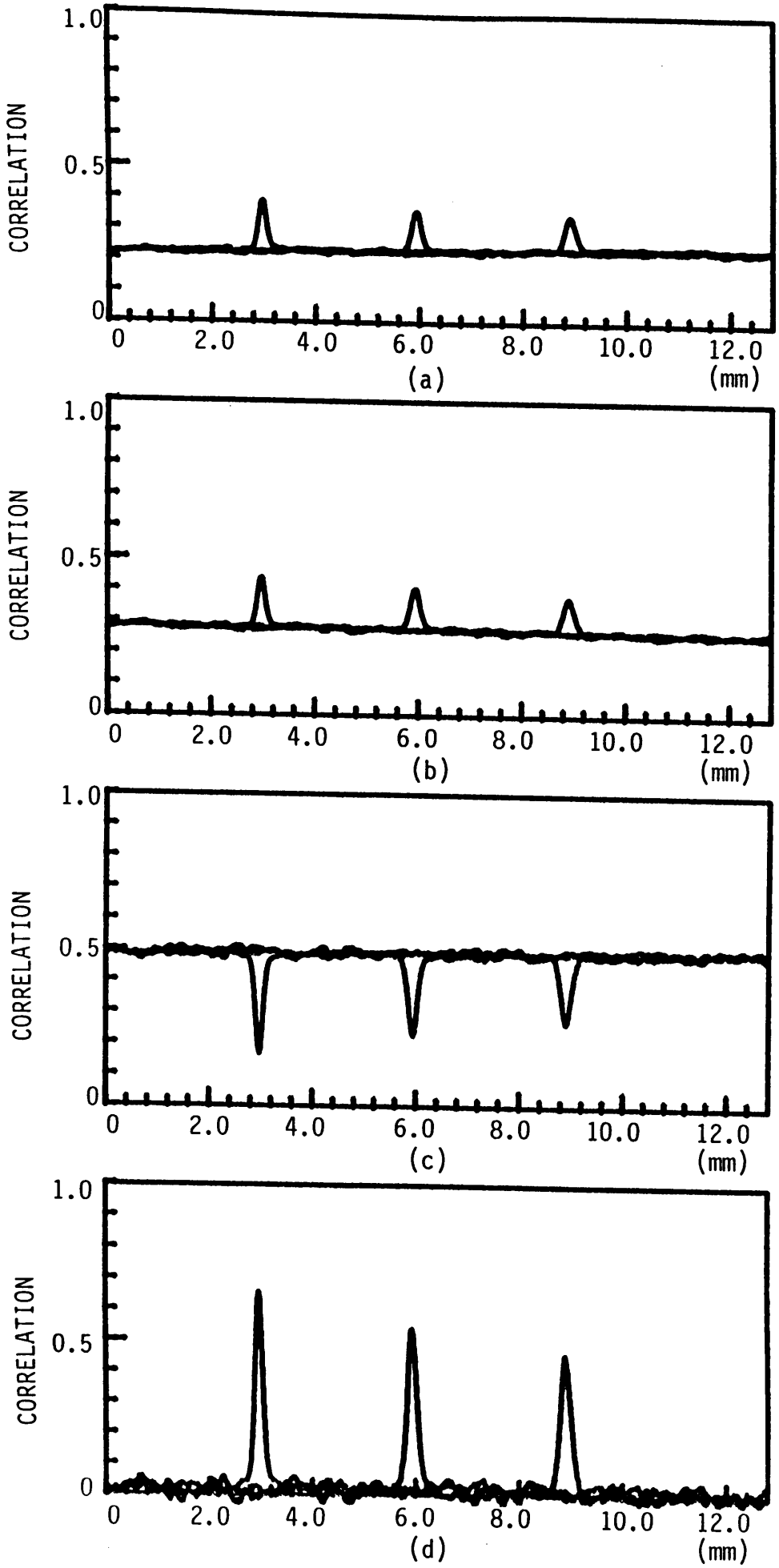

Fig.4-3 Examples of clipped cross-correlation functions: (a) logical AND, (b) complementary clipping (i.e., logical NOR), (c) logical XOR, and (d) (1,-1) logic.

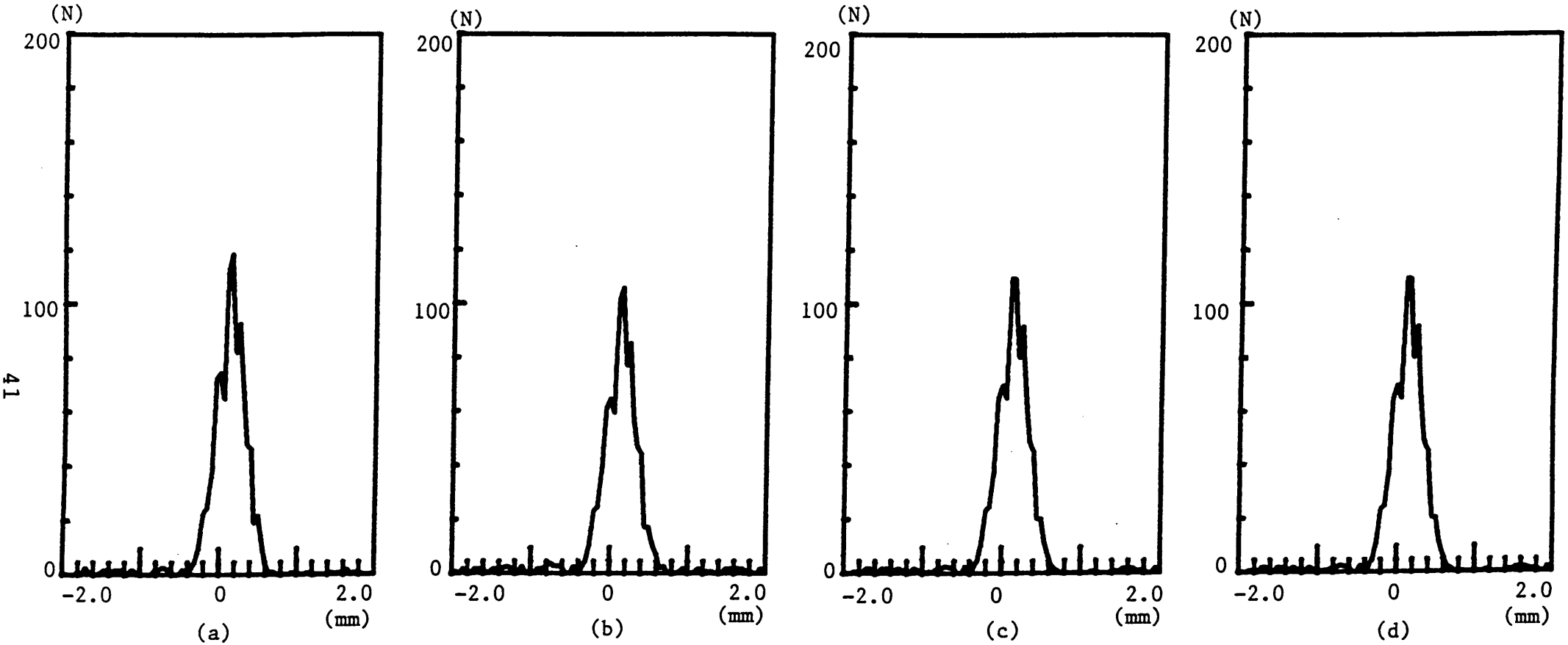

Fig.4-4 Distributions of the correlation peak positions: (a) logical AND, (b) logical NOR, (c) logical XOR, and (d) (1,-1) logic.

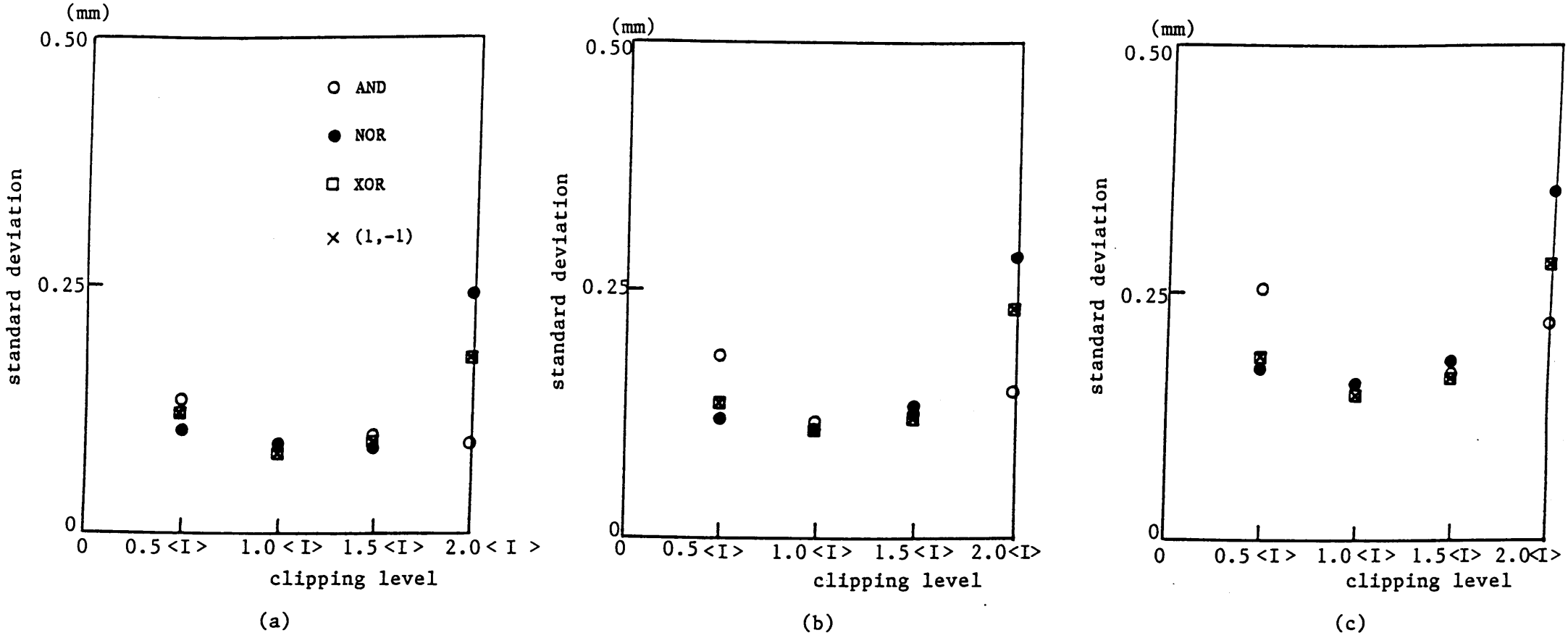

Fig.4-5 Standard deviations of the fluctuations for the peak positions against the various threshold levels. The time offsets are 410, 820, and 1430 ms, from (a) to (c).

may expect that the logical XOR operation for the clipped speckle intensity is superior in accuracy (in a sense of SNR for the peak detection) compared with other logical operations. But this is not always true as is shown in the results in Fig.4-5. Referring the previous theoretical treatment,[6] the accuracy of the peak detections seems to be equal independent of the employment of any logical operation. However, the results obtained here show that the clipping threshold and the method of logical operation are very important when we treat a real experimental data having a finite data length with a possible noise source.

In Ref.8, we have experimentally investigated the probability distribution of the time interval of the clipped speckle intensity. The probability distribution of the time interval may give an important information to choose the clipping threshold. However, the rigorous theory will be needed for the treatment of the time interval distribution of the clipped signal having an arbitrary random process except for the Gaussian process.

4-4. Implementation of one-dimensional speckle clipping correlator

In the conventional analogue correlator, the current signals proportional to two speckle intensities I_1 and I_2 are digitized through an A/D converter which has several gray scales and the digitized signals are processed by using full-bit registers and multiplexers. Therefore, the speed of the calculation is limited by the digitizing bits and the operation speed of the multiplexer. But, for the digital clipping correlation, the full-bit shift register can be reduced to a 1-bit on-off register and the multiplexers can be replaced by simple gates such as AND, XOR, or EX-NOR gates. As a result, high-speed calculation for the correlation function is achieved.

The principle of the one-dimensional digital clipping correlator using EX-NOR gates is shown in Fig.4-6.[48] Two speckle intensity signals I_1 and I_2 are clipped through comparators. The clipped intensity signal I'_1 is fed to a shift register in which the binarized signals "1" and "0" shift by synchronizing a clock. In each shift, a new signal of I'_1 is fed into the first channel of the shift register, while the contents of the remaining channels are shuffled down, the content of the last one being discarded. During the shift operation, the other clipped intensity signal I'_2 is compared with the content of each channel of the shift register through the EX-NOR logic circuits and

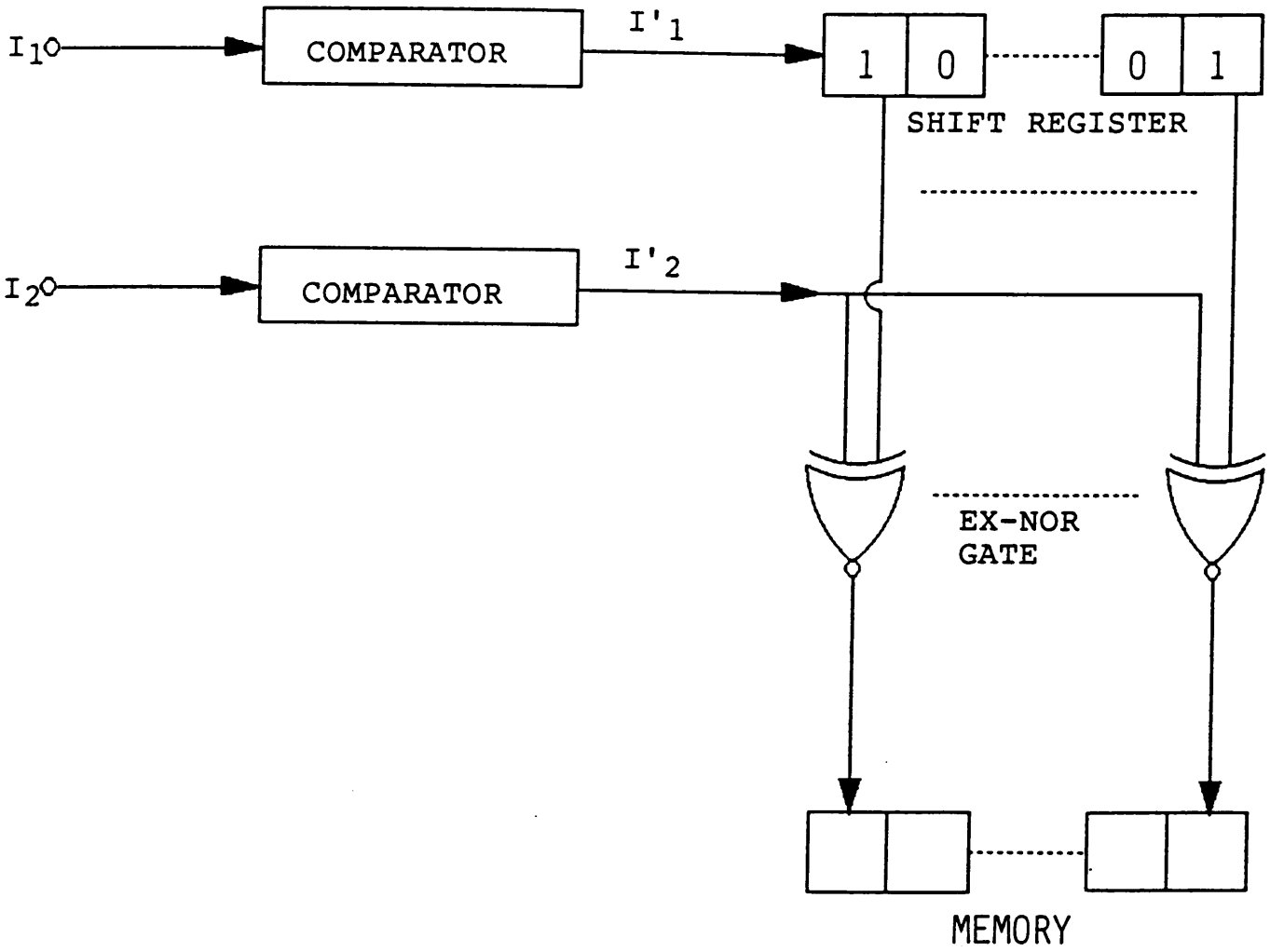

Fig.4-6 Principle of one-dimensional digital clipping correlator

the results are stored in the counter. The continuous operation of the process builds up the cross-correlation function in the store circuits. After the required number of operation, the contents of the memory are read and displayed as the clipped cross-correlation function.

The correlator can be easily realized as a compact instrument by simple electronic circuits when the data length of the signal, i.e., the correlation channel is rather small. However, as the data length becomes large, the counter circuits will become enormous and the speed of the calculation will be slowed down. Furthermore, when we treat a two-dimensional speckle intensity pattern such as the cases for the vector velocity and displacement measurements, the direct expansion of the one-dimensional digital clipping technique to the two-dimensional problem seems to be almost impossible because of the complicated hardware design and the cost for the realization. Thus, a new concept is required to settle the problem. The most useful candidate is the optical parallel processing for the two-dimensional signal. Therefore, in the following chapters, we study about the optical parallel processing for the treatment of a two-dimensional correlation.

Chapter 5. IMPLEMENTATION OF TWO-DIMENSIONAL SPECKLE CLIPPING CORRELATION USING LCTV

5-1. Introduction

The speckle clipping technique discussed in chapter 3 and chapter 4 is a simple and useful approach for a one-dimensional signal, because the required electronics to process the signal is so reduced that the fast calculation of the correlation function can be expected. However, even if we use a digital clipping correlator, it is not sufficient to deal with a large amount of a two-dimensional speckle intensity at high speed. Therefore, an optical correlation method is expected to settle such a difficulty.

In this chapter, we describe the optical correlation method using liquid crystal television (LCTV) based on the Fourier transform property of a lens to implement a two-dimensional speckle clipping correlation. The LCTV has been recently used in the field of optical information processing because of the low cost of the device and the ease of the commercial availability. Though we can expect a high diffraction efficiency of light by using a phase only spatial light modulator, it is difficult to obtain a perfect phase only modulation in a usual twisted nematic LCTV device. Both the intensity and phase modulation ratios through the LCTV panel are affected by the polarization of the input light and become a function of the applied voltage.[43,44] To evaluate a LCTV panel as a phase modulator, the intensity and phase modulation properties of a twisted nematic type LCTV are theoretically and experimentally investigated. The obtained results show that the twisted nematic LCTV can be used as an approximate phase only modulator, especially for a binary signal.

Another interest in this chapter is how to obtain a clear fringe pattern from a binarized speckle signal and clear correlation spots from its Fourier transform. The fringe visibility in the Fourier plane changes depending on the clipping threshold level of an original speckle intensity.[54,55] The relation between the fringe visibility and clipping threshold level is theoretically and experimentally investigated. The effects of the binarization of the fringe pattern at the Fourier plane on the correlation function are also studied.

5-2. Intensity and Phase Modulation Properties of LCTV

5-2-1. Theoretical Treatment

The twisted nematic liquid crystal (LC) is an anisotropic medium that can be treated locally as a uniaxial crystal whose optical axis is parallel to the direction of the molecules. Fig.5-1 shows a theoretical twisted nematic LCTV model which is used in the experiment. The material is inhomogeneous and is locally a uniaxial crystal whose optical axis rotates helically in the direction of twist.

The simplest way of examining the propagation of polarized light along the twist axis of a twisted nematic LC device is by use of Jones calculus.[56] The Jones matrix can be written as a function of the ordinary and extraordinary refraction indices (n_o and n_e) and its direction. For the LC material of thickness d twisted by 90° angle, and when the molecules align with the x-axis at the entrance plane, the Jones matrix for the light having wavelength λ is given by

$$J = \exp(-j\Phi)\begin{bmatrix} \left(\frac{\pi}{2r}\right)\sin(r) & \cos(r) + j\left(\frac{\beta}{r}\right)\sin(r) \\ -\cos(r) + j\left(\frac{\beta}{r}\right)\sin(r) & \left(\frac{\pi}{2r}\right)\sin(r) \end{bmatrix}, \tag{5-1}$$

where

$$\beta = \frac{\pi d}{\lambda}(n_e - n_o), \tag{5-2}$$

$$\Phi = \frac{\pi d}{\lambda}(n_e + n_o), \tag{5-3}$$

$$r = \left\{\left(\frac{\pi}{2}\right)^2 + \beta^2\right\}^{1/2}. \tag{5-4}$$

From above equations, we can recognize that the Jones matrix is a function of only one variable β, except for an unimportant multiplicative phase factor

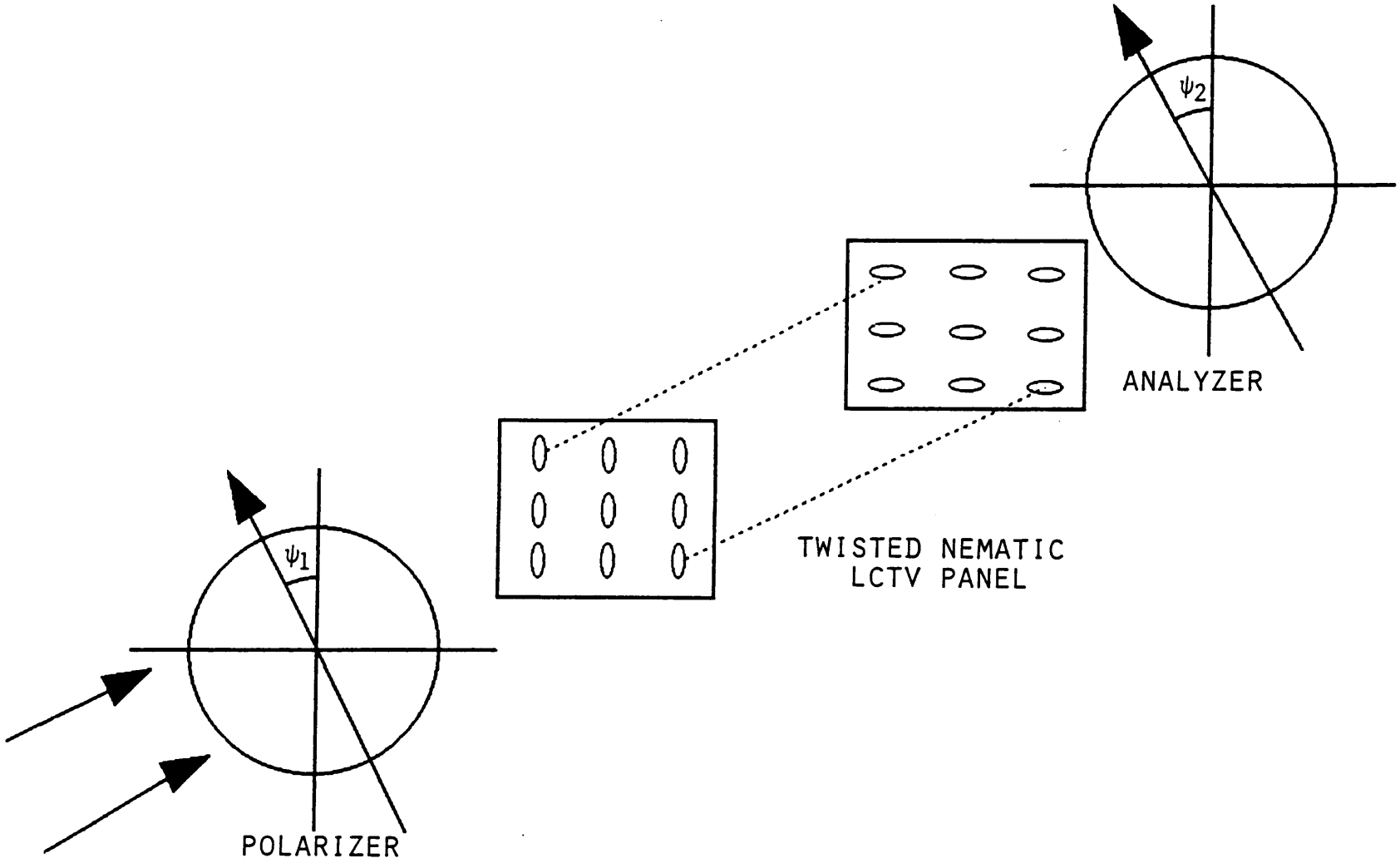

Fig.5-1 Configuration of the LCTV with polarization filters.

exp(-jΦ). When an electric field is applied to the LC device, the parameter β becomes a function of the voltage V between the glass plates through the field dependent refractive index $n_e=n_e(V)$.[44] The normalized parameter β is plotted against the normalized applied voltage V in Fig.5-2. The figure shows that the dependence of β on the applied voltage V is a monotonic decreasing function.

We now proceed to determine the amplitude transmittance and phase shift introduced by the device as a function of β. The LC material is usually sandwiched between a polarizer and an analyzer, in general making angles ψ_1 and ψ_2 with the x-axis, as shown in Fig.5-1. By use of Eq.(5-1) for the Jones matrix, we can easily determine the amplitude and phase transmittance of an incident wave linearly polarized along the direction of the polarizer. Let $\mathbf{E}=(E_x,E_y)=(\cos\psi_1,\sin\psi_1)$ and $\mathbf{E}'=(E'_x,E'_y)$ be the complex amplitudes of the incident and transmitted waves. Straightforward Jones calculus yields

$$\begin{pmatrix} E'_x \\ E'_y \end{pmatrix} = \exp(-j\Phi) \begin{bmatrix} \cos^2\psi_2 & \sin\psi_2\cos\psi_2 \\ \sin\psi_2\cos\psi_2 & \sin^2\psi_2 \end{bmatrix}$$

$$\times \begin{bmatrix} \left(\frac{\pi}{2r}\right)\sin(r) & \cos(r) + j\left(\frac{\beta}{r}\right)\sin(r) \\ -\cos(r) + j\left(\frac{\beta}{r}\right)\sin(r) & \left(\frac{\pi}{2r}\right)\sin(r) \end{bmatrix} \begin{bmatrix} \cos\psi_1 \\ \sin\psi_1 \end{bmatrix} . \qquad (5\text{-}5)$$

In above equation, the vector and the matrix outside the Jones matrix of the LC device represent the contributions of the polarizer and the analyzer, respectively.

Eq.(5-5) yields immediately the intensity transmittance T and phase shift δ:

$$T = \left\{\frac{\pi}{2r}\sin(r)\cos(\psi_1-\psi_2) + \cos(r)\sin(\psi_1-\psi_2)\right\}^2 + \left\{\frac{\beta}{r}\sin(r)\sin(\psi_1+\psi_2)\right\}^2 , \qquad (5\text{-}6)$$

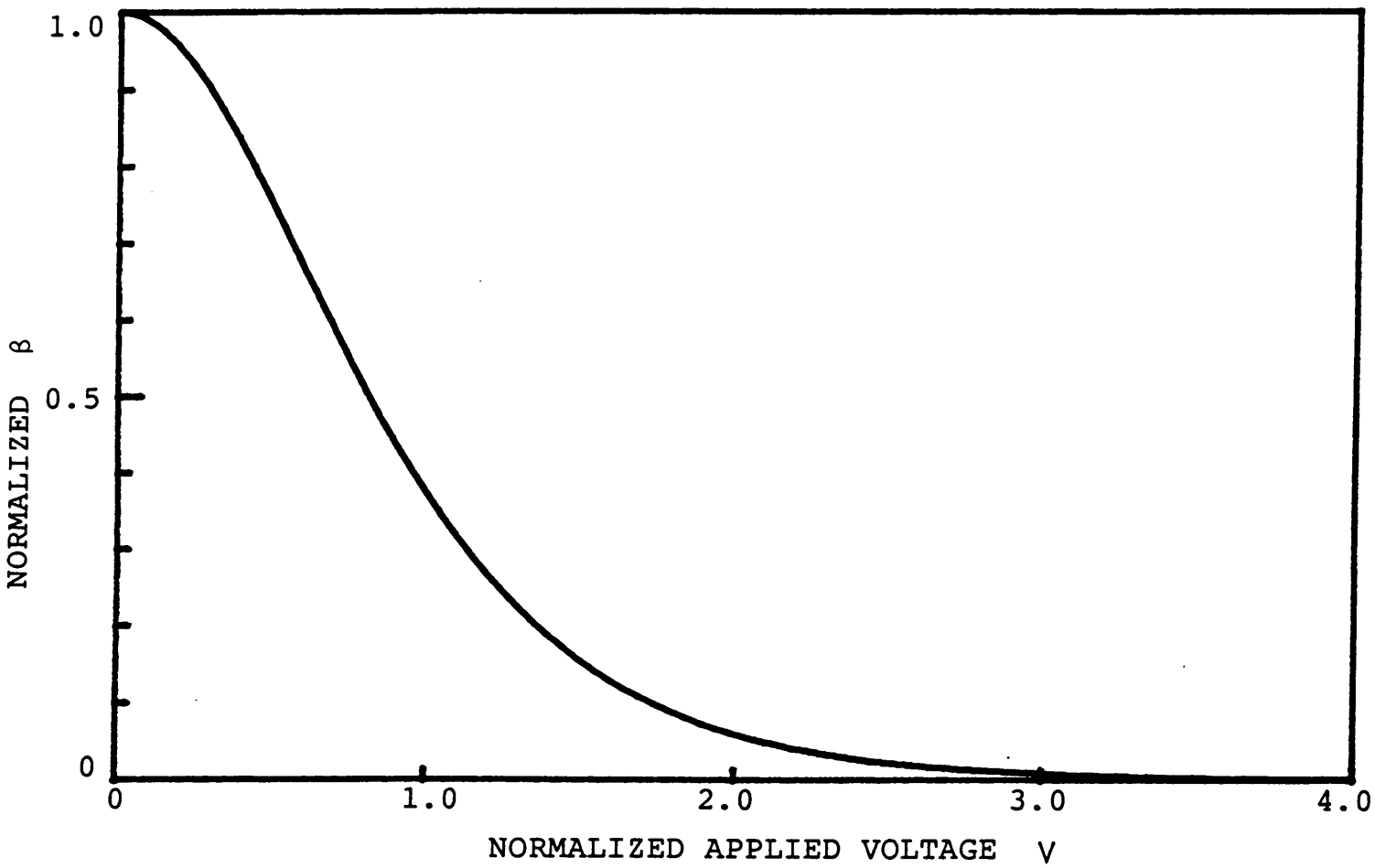

Fig.5-2 Dependence of the normalized parameter β on the normalized applied voltage V.

$$\delta = \beta - \tan^{-1}\frac{\left(\frac{\beta}{r}\right)\sin(r)\sin(\psi_1 + \psi_2)}{\left(\frac{\pi}{2r}\right)\sin(r)\cos(\psi_1 - \psi_2) + \cos(r)\sin(\psi_1 - \psi_2)} \quad . \tag{5-7}$$

For given ψ_1 and ψ_2, both T and δ are functions of one variable, β. These expressions simplify in two special cases which are important in the actual experiments:

Case 1 - when $\psi_1=0^\circ$, $\psi_2=90^\circ$; i.e., the polarizer is orthogonal to the analyzer and parallel to the x-axis:

$$T_{0,90} = 1 - \left(\frac{\pi}{2r}\right)^2 \sin^2(r) \quad , \tag{5-8}$$

$$\delta_{0,90} = \beta + \tan^{-1}\left\{\frac{\beta}{r}\tan(r)\right\} \cong 2\beta \quad , \tag{5-9}$$

where the first and second subscripts denote the angles ψ_1 and ψ_2.

Case 2 - when $\psi_1=90^\circ$, $\psi_2=0^\circ$; i.e., the polarizer is orthogonal to the analyzer and the x-axis:

$$T_{90,0} = 1 - \left(\frac{\pi}{2r}\right)^2 \sin^2(r) \quad , \tag{5-10}$$

$$\delta_{90,0} = \beta - \tan^{-1}\left\{\frac{\beta}{r}\tan(r)\right\} \cong 0 \quad . \tag{5-11}$$

The intensity transmittance T is a monotonic increasing function of β (i.e., a monotonic decreasing function of V) for the both cases. However, the phase shift is an approximately linear function whose slope is 2 in case 1, whereas there is no phase shift in case 2. Thus, not only the intensity modulation but also the phase modulation of the LC device are obtained for the case 1, whereas the device is used only as an intensity modulator for the case 2. This prediction is also verified by the experiments in subsection 5-2-2.

5-2-2. Experiments and Discussions

The LCTV used in the experiment is a projection TV panel of VPJ-700 (Seiko Epson) which is a 90° twisted nematic device with thin film transistors (TFT). The panel consists of 220×320 pixels each having a size of 80×90μm. As is shown in Fig.5-1 for the theoretical model, the liquid crystal molecule director of the LCTV is vertically aligned at the front of the panel while it is twisted by the right angle at the exit face.

After removing the original plastic polarizers from the liquid crystal panels, we evaluate the phase shift by placing the device in one of the arm of a Mach-Zehnder interferometer as illustrated in Fig.5-3, and observe the shift of the interference fringes by the applied voltage.[44] In this figure, the low pass filter is used to eliminate a higher spatial frequency component produced by the electrical matrix of the TFT elements in the LCTV panel.

Fig.5-4(a) is the interference fringe when two different video signals are applied to the upper and lower halves on the LCTV. We can observe the phase shift (the shift of the interference fringe) from the figure. To observe the phase shift more precisely, we conducted the thinning of the interference fringe by an image processing algorithm. Fig.5-4(b) shows the result. The phase difference between the applied video voltages can be clearly seen from this figure.

In Fig.5-5, the intensity transmittance and phase shift are plotted against the input composite video signal levels having a 8-bit gray scale. In Fig.5-5(a), the orientation of the polarizer in Fig.5-1 is aligned to be parallel to the liquid crystal molecule director at the front panel and that of the analyzer is rotated by 90°, i.e., corresponding to the configuration of $(\psi_1,\psi_2)=(0^\circ,90^\circ)$. The phase shift from 0 to 1.2π radians and the normalized intensity transmittance of 0.3~1.0 are obtained in this configuration.

Fig.5-5(b) is the result for the case of $(\psi_1,\psi_2)=(90^\circ,0^\circ)$. The phase modulation is not observed in this configuration, whereas the intensity transmittance is changed by the variation of the video signal.[43,44] Though we can observe no distinct phase change, the intensity modulation has the similar tendency that for the case in Fig.5-5(a). These results are coincident with the theoretical predictions in subsection 5-2-1.

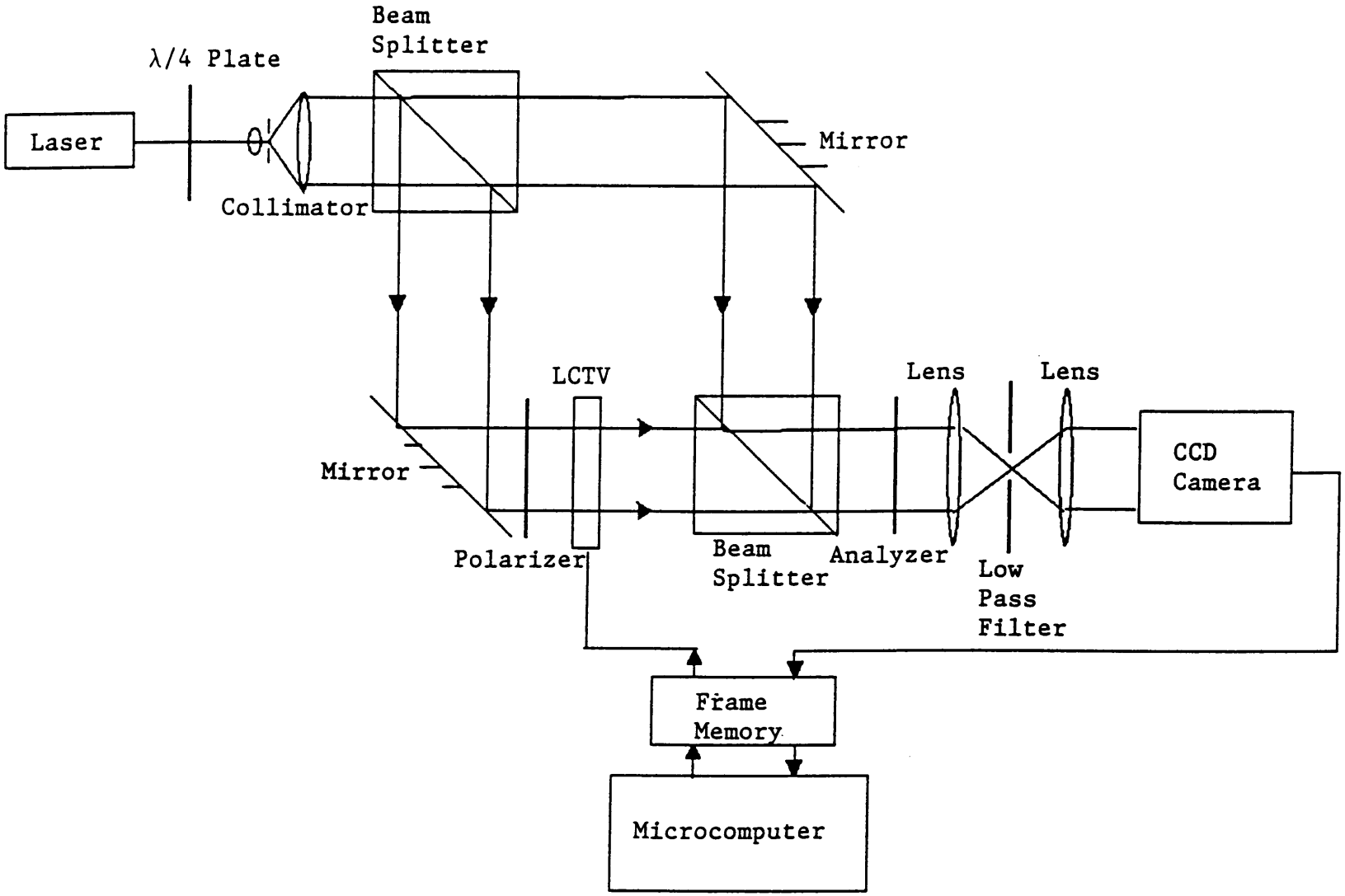

Fig.5-3 Mach-Zehnder interferometer to measure the dependence of phase shift on the applied voltage to the LCTV.

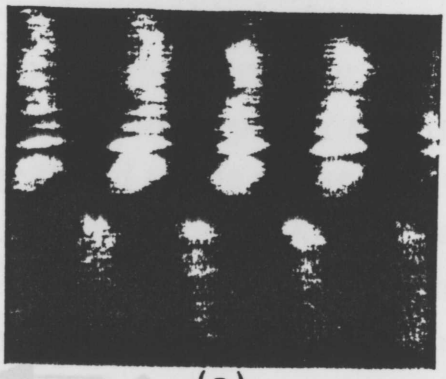

(a)

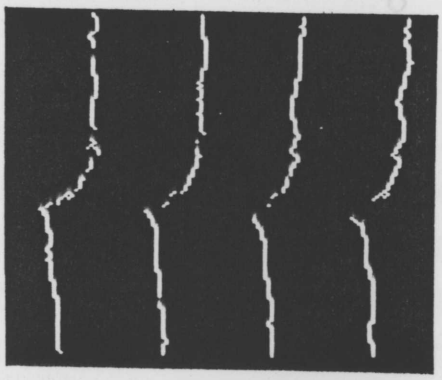

(b)

Fig.5-4 (a) Interference fringe obtained by Mach-Zehnder interferometer when the two different video signals are applied to the upper and lower halves on the LCTV. (b) Thinning of the interference fringe of (a).

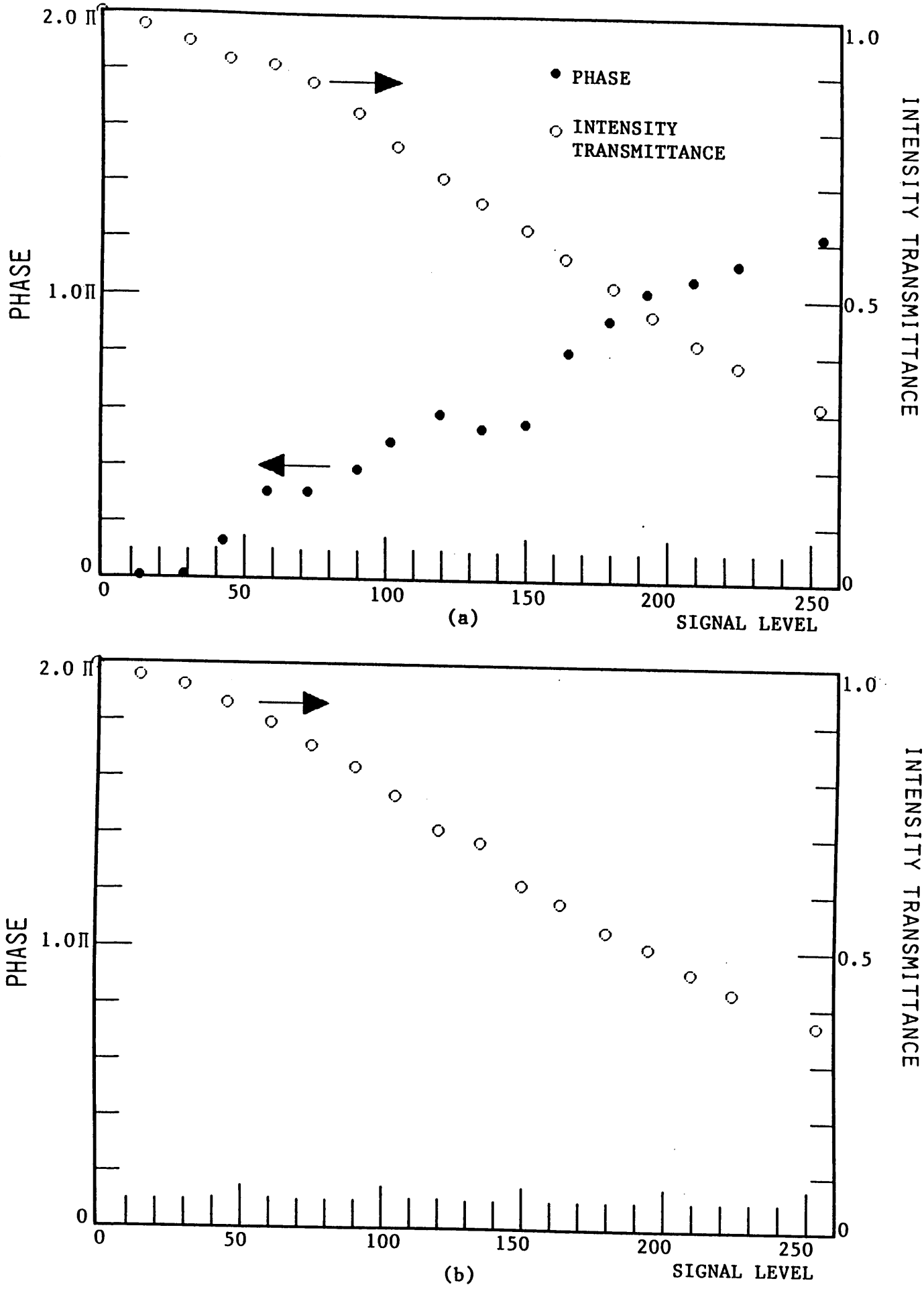

Fig.5-5 Phase and intensity modulation properties of the LCTV at (a) $(\psi_1,\psi_2)=(0^\circ,90^\circ)$ and (b) $(\psi_1,\psi_2)=(90^\circ,0^\circ)$.

Next, we investigated the diffraction efficiency for the LCTV spatial light modulator. In the experimental setup shown in Fig.5-6, the grating pattern having a rectangular wave is used to evaluate the diffraction efficiency. The LCTV panel is illuminated by a collimated light. The transmitted light is Fourier transformed by a lens behind of the panel and detected by a CCD camera at the focal plane of the lens. Fig.5-7(a) shows the result of the intensity distribution of the Fourier power spectrum when the two levels of the grating pattern correspond to the phase values of 0 and π, respectively, under the configuration of $(\psi_1,\psi_2)=(0^\circ,90^\circ)$. The ± 1 order diffraction peaks are clearly seen while the zeroth order term is almost suppressed. The phase modulation effect is dominant in this configuration.

Fig.5-7(b) shows the diffraction pattern under the configuration of $(\psi_1,\psi_2)=(90^\circ,0^\circ)$ when the minimum and maximum intensity transmittance levels in Fig.5-5(b) are used as the binary grating pattern. The strong DC peak has appeared and the ± 1 order diffraction peaks are reduced compared with the pattern in Fig.5-7(a). The LCTV panel behaves as an intensity spatial light modulator in this configuration.

The two dimensional binary cosine hologram of a letter F is also used as the second input pattern to the LCTV. Fig.5-8(a) shows an original image of the letter F and Fig.5-8(b) is its binary cosine hologram having 128×128 pixels calculated by the First Fourier Transform (FFT) algorithm. The black and white pixels are correspond to the phase values of 0 and π in Fig.5-5(a), respectively. Fig.5-8(c) shows the reconstructed image from the binary cosine hologram. The double imaging is observed due to the phase only binary hologram. Though, theoretically, the zeroth order component should be zero, it is not. The several possible reasons for the residual energy at the Fourier plane are as follows: an unwanted intensity modulation through the panel; ununiformity of the phase transmittance of each elements; the aberrations caused by the optical components.

The results show that the phase modulation property of the LCTV rather than the intensity modulation property plays an important role to attain a high diffraction efficiency of light. In particular, the configuration of $(\psi_1,\psi_2)=(0^\circ,90^\circ)$ is suited for the application of LCTV as a spatial light phase modulator, for such as an application to an optical correlator.

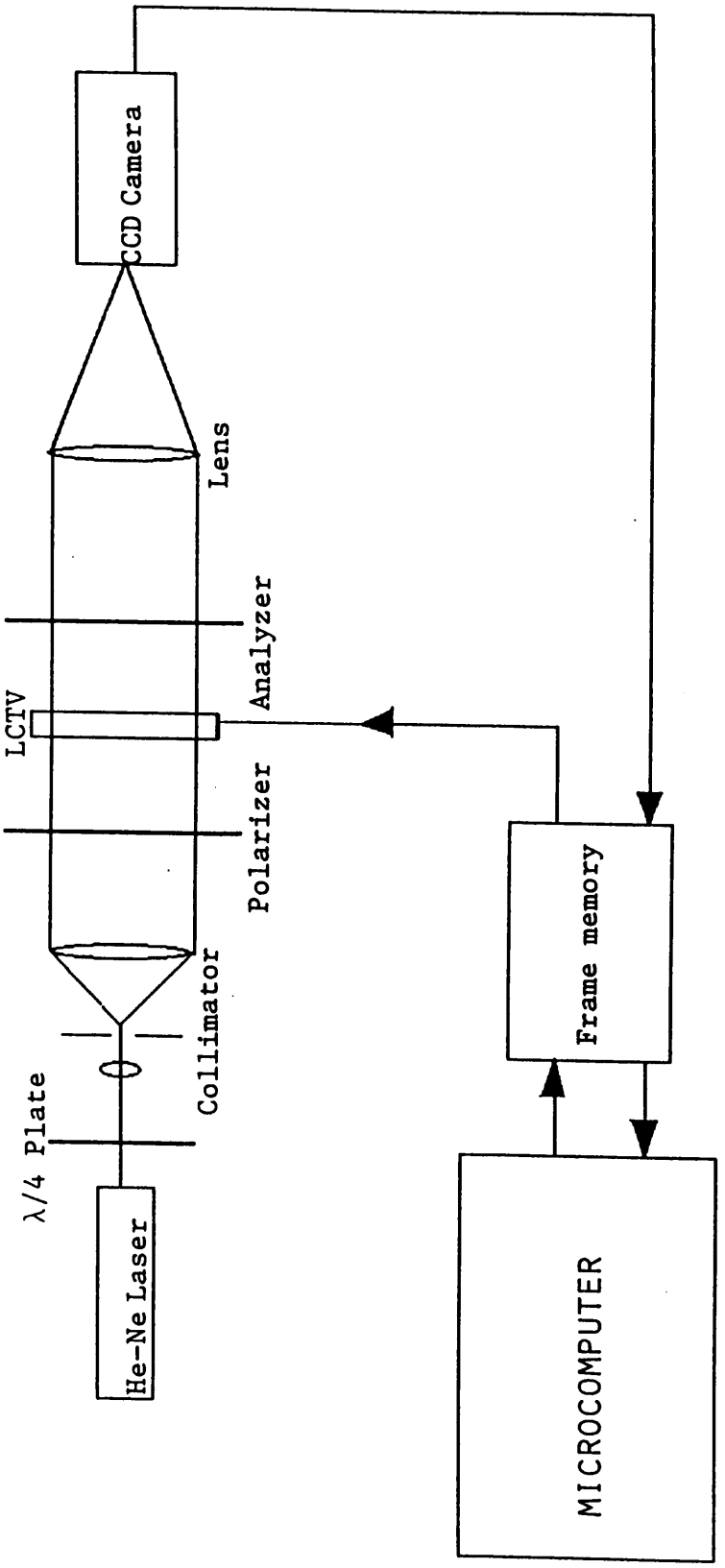

Fig.5-6 Optical system to evaluate the diffraction efficiency of the rectangular wave grating pattern written on the LCTV panel.

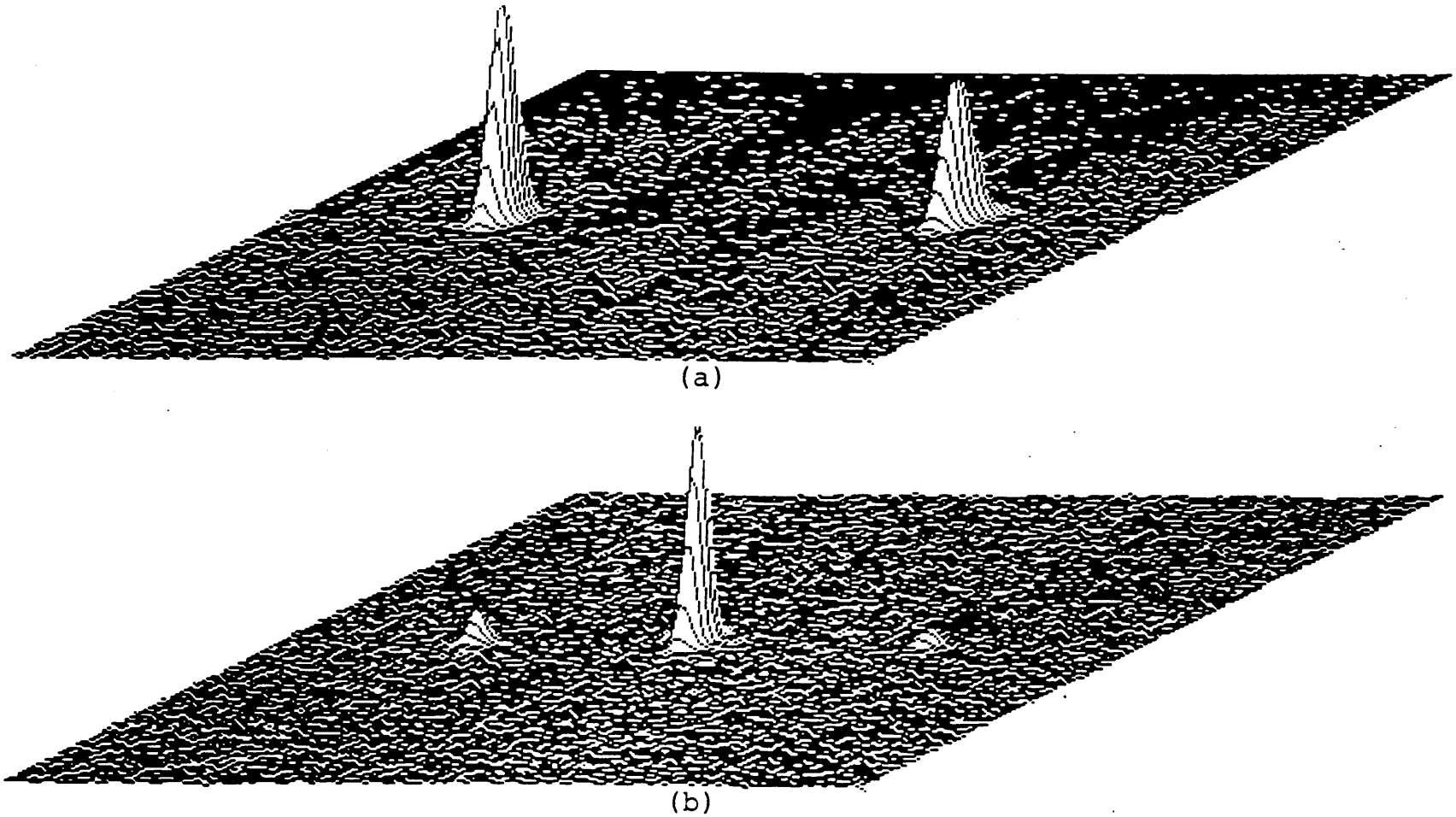

Fig.5-7 Intensity distributions in the Fourier plane produced by the rectangular wave grating: (a) $(\psi_1,\psi_2)=(0^\circ,90^\circ)=$ and (b) $(\psi_1,\psi_2)=(90^\circ,0^\circ)$.

(a)

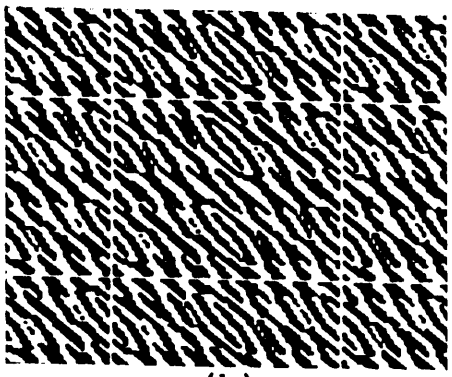

(b)

(c)

Fig.5-8 (a) Input test letter F. (b) Binary phase only filter of letter F. (c) Optical reconstruction of the phase only hologram of the letter F.

5-3. Optical Speckle Clipping Correlation

5-3-1. Theoretical Treatment

The speckle photography method using specklegram is a well known and useful technique for the processing of a two-dimensional speckle pattern.[57] In this section, we discuss the fundamental properties of the optical correlation based on the speckle photography technique. The results in section 5-2 show that the twisted nematic LCTV panel can be used for an approximate phase only modulator, especially for a binary signal. It is also known that the high diffraction efficiency can be obtained by a binary phase only filtering.[17,19] For an optical speckle correlator using LCTV, the binarization of the specklegram plays an important role to obtain a good correlation pattern

In the following discussion, we theoretically study the intensity clipping of the specklegram and the visibility of its Fourier transform. When the specklegram is displayed on a spatial light modulator as a phase modulation signal, the Fourier power spectrum of the input signal should be evaluated by the expansion of the complex exponential function, i.e., $\exp\{if(x)\}$ ($f(x)$ is the specklegram). The theoretical treatment of the binary phase only specklegram and its Fourier transform is straightforward, but the calculation is so complicated that we could not derive the analytical solution. However, the relation between the clipping threshold level of the specklegram and the visibility of its Fourier transform is almost explained by the treatment of intensity clipping in this subsection. In fact, it is found by the later computer simulation and experiment that the relation between the clipping threshold of the specklegram in the intensity clipping and the visibility of its Fourier transformed fringe pattern can be roughly substituted to that for the binary phase only specklegram.

Though here we consider a two-dimensional speckle pattern, we proceed to the theoretical calculations using one-dimensional equations for a simplification of the treatment. The ensemble average of the power spectrum produced by the specklegram at the Fourier plane is written by

$$\langle P(\omega) \rangle = \left\langle \left| \int_{-\infty}^{\infty} \{ I_1(x) + I_2(x) \}\, e^{-i\omega x}\, dx \right|^2 \right\rangle , \tag{5-12}$$

where I_1 and I_2 are the speckle intensities before and after the displacement of a light scattering object, ω is the spatial frequency in the Fourier plane, x denotes the coordinate at the speckle field, and <---> represents an ensemble average. Eq.(5-12) is easily rewritten by

$$<P(\omega)> = \left< \int_{-\infty}^{\infty} \int_{-\infty}^{\infty} \{ I_1(x')I_1(x'') + I_2(x')I_2(x'') + I_1(x')I_2(x'') + I_2(x')I_1(x'') \} \times e^{-i\omega(x' - x'')}\, dx'dx'' \right> . \tag{5-13}$$

Assuming the stationary condition and replacing $x=x'-x''$, Eq.(5-13) becomes

$$<P(\omega)> = \int_{-\infty}^{\infty} \{ R_{11}(x) + R_{22}(x) + R_{12}(x) + R_{21}(x) \} e^{-i\omega x}\, dx . \tag{5-14}$$

In Eq.(5-14), R_{ii} and R_{ij} (i,j = 1,2) represent the auto- and cross-correlation functions made by the two intensities I_1 and I_2, respectively. From the reasonable assumptions for the speckle formation under the illumination of a Gaussian laser beam, we can write each correlation function as follows:

$$R_{11}(x) = R_{22}(x) = \exp\left(-\frac{x^2}{4x_0^2} \right) , \tag{5-15}$$

$$R_{12}(x) = R_{21}(x) = \exp\{-(\alpha\tau)^2\} \exp\left\{ -\frac{(x-v\tau)^2}{4x_0^2} \right\} , \tag{5-16}$$

where x_0 is the spatial size of the averaged speckle, τ is the time offset between the two exposures, v is the velocity of the object (here, we assume that the object is moving as a constant velocity), and α represents a parameter corresponding to the speckle decorrelation during the object

motion. Substituting Eqs.(5-15) and (5-16) into Eq.(5-14), the intensity distribution of the power spectrum is calculated by

$$<P(\omega)> = \exp\{ - (x_o\omega)^2 \}[1 + \exp\{ - (\alpha\tau)^2 \} \cos(v\tau\omega)] , \tag{5-17}$$

where we neglect the unnecessary constant coefficient. Fig.5-9(a) shows an example of the power spectra calculated from Eq.(5-17) for x_o=0.07(mm), τ=1.70(s), v=1.00(mm/s), and α=0.50(1/s). In the following calculations, the same parameter values are used.

Next, we consider the power spectrum produced by the clipped specklegram at the Fourier plane. The clipped correlation functions corresponding to Eqs.(5-15) and (5-16) are expanded by infinite series as the same manner in chapter 2. Thus the clipped correlation function are written by

$$R'_{ii}(x) = \sum_{n=0}^{\infty} \exp(-2b)\{ L_n^{(-1)}(b) \}^2 R_{ii}^n(x) , \tag{5-18}$$

$$R'_{ij}(x) = \sum_{n=0}^{\infty} \exp(-2b)\{ L_n^{(-1)}(b) \}^2 R_{ij}^n(x) . \tag{5-19}$$

Substituting Eqs.(5-18) and (5-19) into Eq.(5-14), the power spectrum for the clipped specklegram is calculated as

$$<P(\omega)> = \exp(-2b) \sum_{n=1}^{\infty} \frac{1}{n} \left\{ L_n^{(-1)}(b) \right\}^2 \exp\left\{ - \frac{1}{n} (x_o\omega)^2 \right\}$$

$$\times [1 + \exp\{ - n(\alpha\tau)^2 \} \cos(v\tau\omega)] . \tag{5-20}$$

Fig.5-9(b) and (c) show the plots of the power spectrum calculated from Eq.(5-20) for the clipping levels of 0.2<I> and 1.0<I>. We can see from

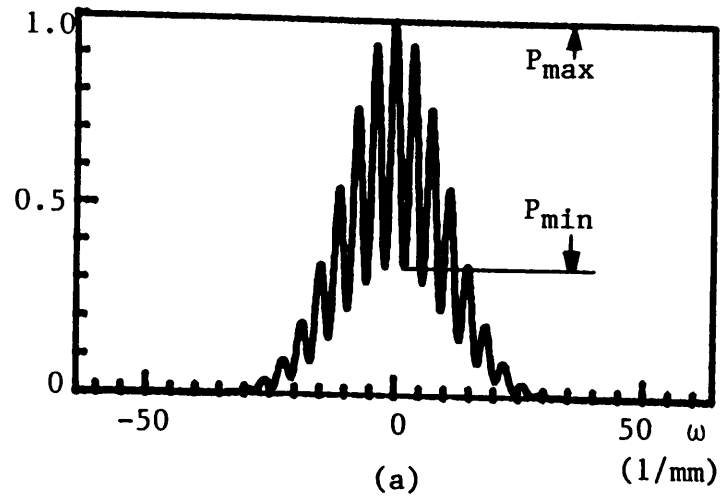

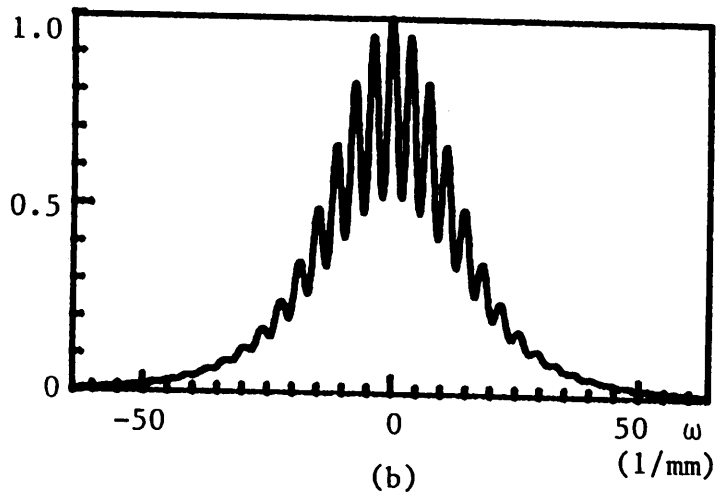

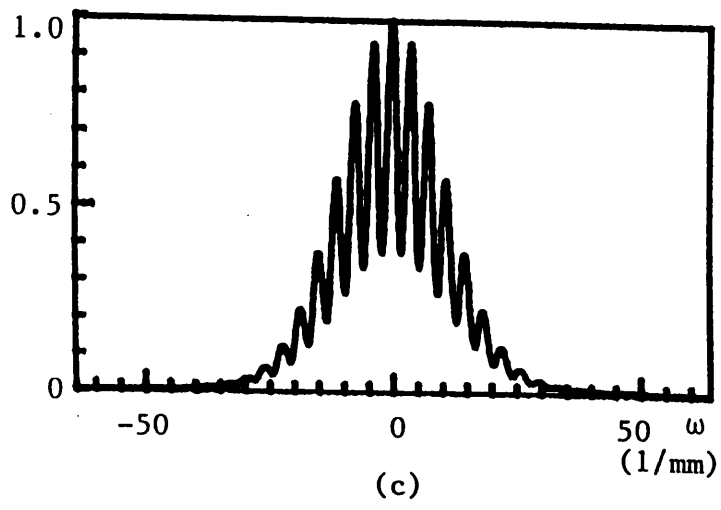

Fig.5-9 (a) Theoretical intensity curve for the nonclipped case calculated from Eq.(5-17). Theoretical intensity curves for the clipped case calculated from Eq.(5-20) at the clipping thresholds of (b) 0.2<I> and (c) 1.0<I>.

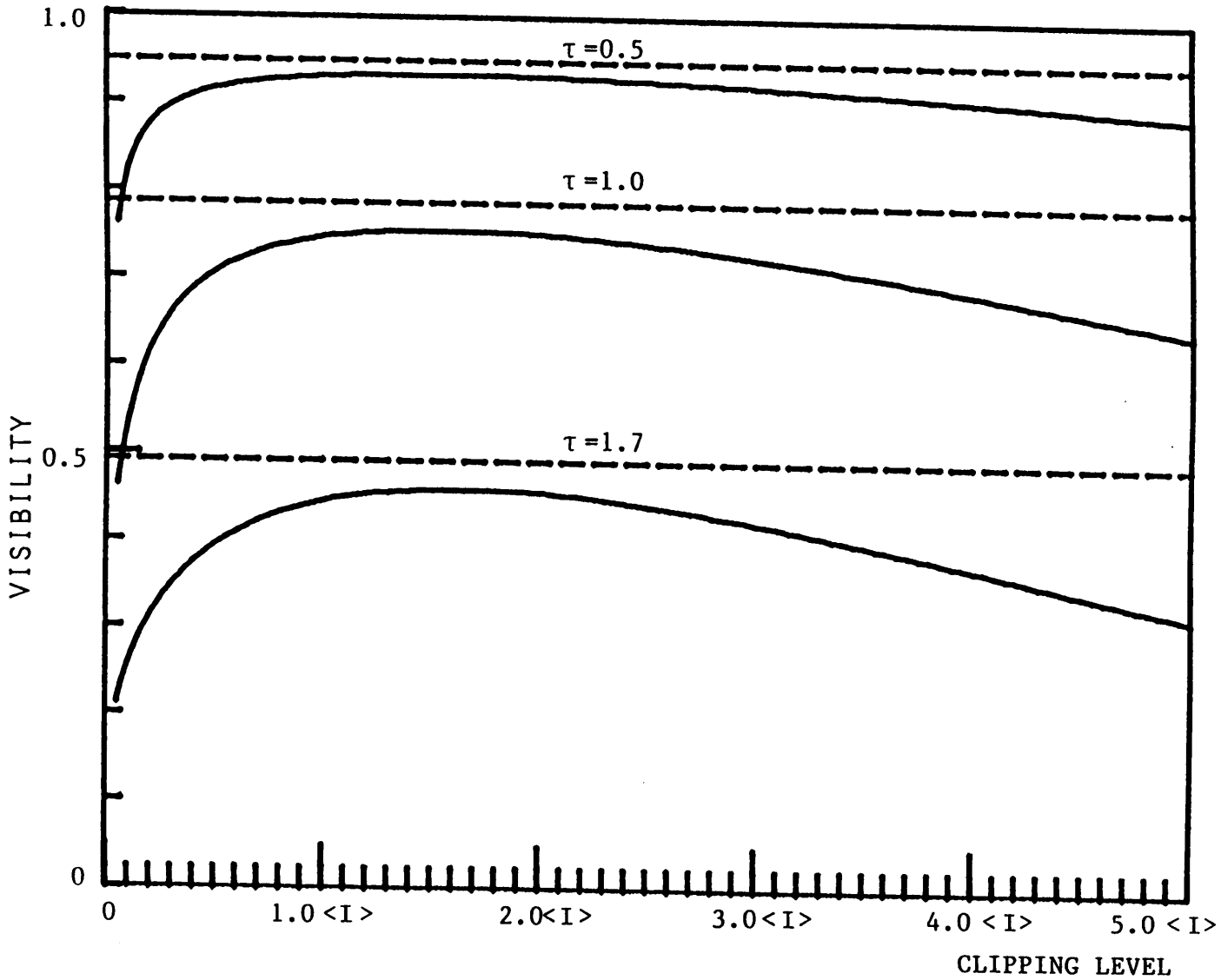

Fig.5-10 The variation of the fringe visibility versus the clipping level for several values of the time offset.

this figure that the visibility of the fringe depends on the clipping level and the higher frequency components are enhanced compared with that for the nonclipped case. To observe more precisely the dependence of the clipping level on the visibility, we define the visibility of the fringe as is in the usual manner

$$V = \frac{P_{max} - P_{min}}{P_{max} + P_{min}} . \qquad (5\text{-}21)$$

P_{max} and P_{min} in Eq.(5-21) are the maximum and minimum intensity values at the Fourier plane as is shown in Fig.5-9.

Fig.5-10 shows the visibilities of the fringes versus the clipping level for the several time offsets. For comparison, the broken lines show the visibilities for the nonclipped cases. We can see from this figure that the visibility for the clipped specklegram is always less than that for the nonclipped one and that the difference grows as the time offset increases. However, the visibility for the clipped case has roughly the same value as that for the nonclipped one around the average clipping level. Therefore, we can expect a clear Fourier fringe pattern by choosing the clipping level and the time offset appropriately.

5-3-2. Computer Simulation

In this subsection, we investigate the effects of the binarizations of the specklegram on the fringe visibility at the Fourier plane. Fig.5-11(a) shows a specklegram consisting of 256×256 pixels to be treated by the computer simulation. Each speckle pattern is separated by 15 pixels along the horizontal direction. The process to make the specklegram is as follows. At first, a speckle pattern of a 8-bit gray scale having 512×512 pixels is experimentally detected by a CCD camera and stored in a microcomputer. Then, the bias level of the video signal is subtracted from the original pattern. From this 512×512 points speckle pattern, two speckle patterns each having the area of 256×256 pixels separated by the offset are chosen and added by the microcomputer, thus forming the specklegram. In Fig.5-11(a), the normalized intensities of the specklegram are distributed over the phase values from 0 to π. Although there might be the optimum phase value for

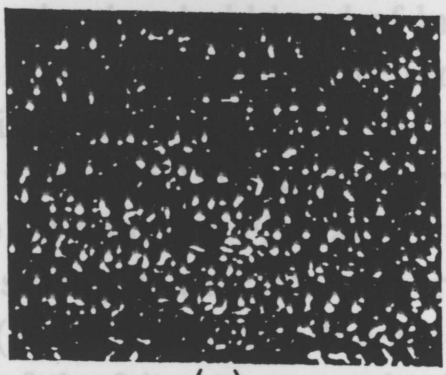

(a)

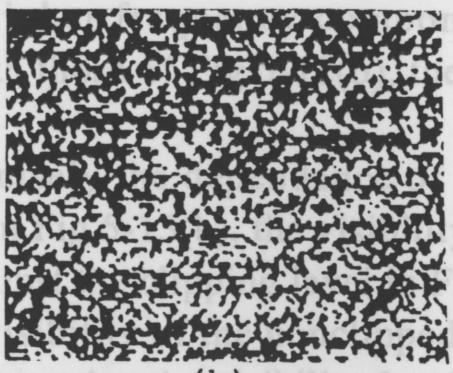

(b)

Fig.5-11 (a) Nonclipped specklegram and (b) clipped specklegram.

the normalization, the phase modulation depth is limited in our LCTV spatial light modulator (our LCTV panel shown in subsection 5-2-2 has roughly the phase modulation range from 0 to π).

On the other hand, Fig.5-11(b) shows the clipped specklegram obtained by binarizing the pattern at the threshold level of ln2<I>. As is discussed in chapter 2, the number of the data points above threshold is the same as that below threshold at this threshold level. The two levels in this figure correspond to the phase values of 0 and π, respectively.

By the two-dimensional complex FFT algorithm, the Fourier power spectra, i.e., the Young's fringes, are calculated from these specklegrams in a computer. Fig.5-12(a) shows an one-dimensional intensity distribution across the center spot of the fringe pattern obtained from the nonclipped specklegram. We can only see a spike-like DC term in this figure. Another intensity distribution perpendicular to the fringe pattern shifted by five pixels from the DC center peak is shown in Fig.5-12(b). Fig.5-13 is the results calculated for the clipped specklegram. The suppression of the zero order diffraction term such as a typical effect of a binary phase hologram is observed in Fig.5-13(a). The DC component in Fig.5-13(a) calculated by the Fourier transform of Fig. 5-11(b) is just canceled because the binary only phase filter is generated by assigning the phase values 0 for the signal +1 and π for -1, and the number of the pixels for the two phase values in Fig.5-11(b) becomes equal to each other at the threshold level of ln2<I>. Because of the DC suppression, we can observe the higher diffraction orders of the fringe. Though the higher frequency components in Fig.5-13(b) are enhanced compared with those of Fig.5-12(b), the fringe visibility slightly decreases.

To observe more precisely the dependence of the clipping level on the fringe visibility shown in Fig.5-13(b), the visibility of the fringe defined by Eq.(5-21) is plotted against the clipping level in Fig.5-14. For comparison, the broken line is the visibility of the nonclipped case shown in Fig.5-12. We can see from this figure that the visibility for the clipped specklegram is always less than that for the nonclipped one, however, it approximately approaches to that of the nonclipped one around the average threshold level. These results coincide with those of the numerical calculation for the intensity clipping in subsection 5-3-1.

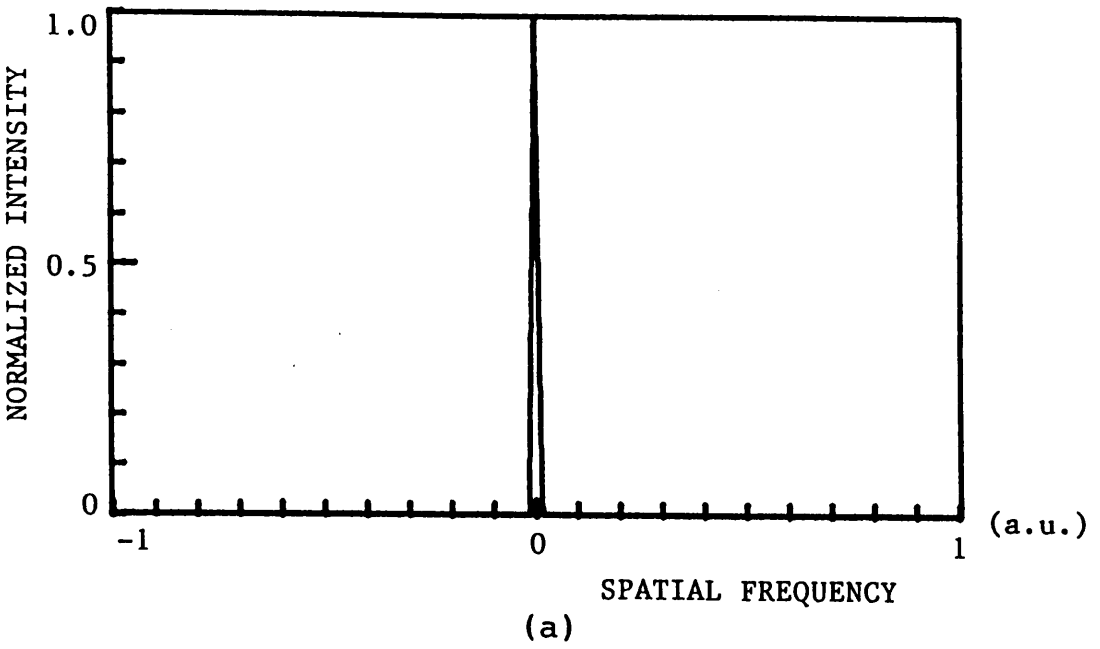

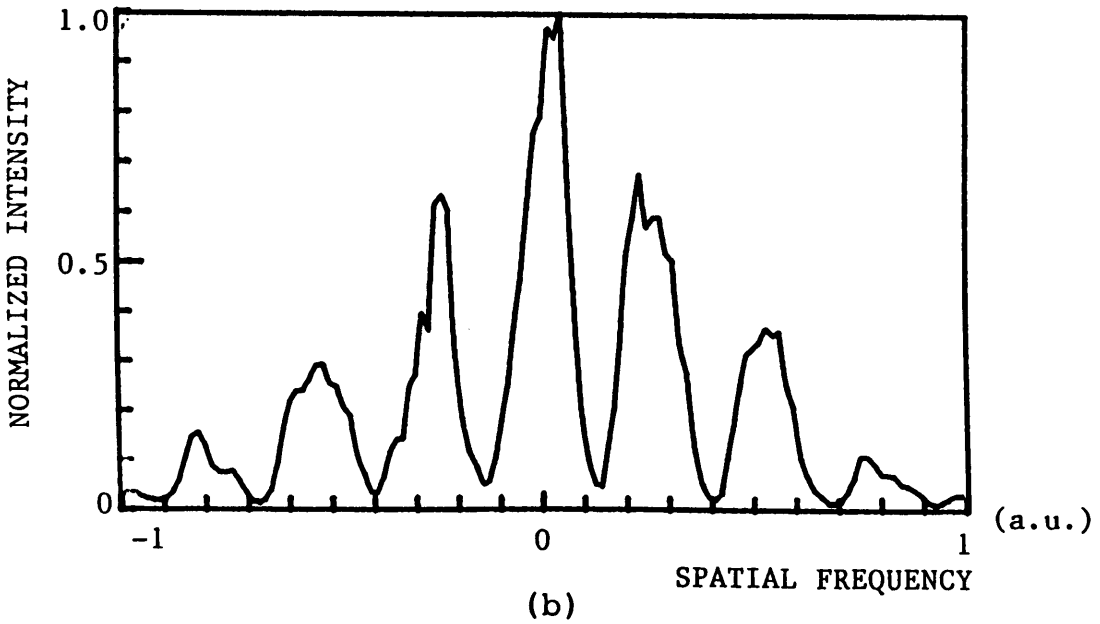

Fig.5-12 Fringe intensities calculated by the Fourier transform of Fig.5-11: (a) intensity distribution across the DC spot and (b) intensity distribution shifted from the DC spot.

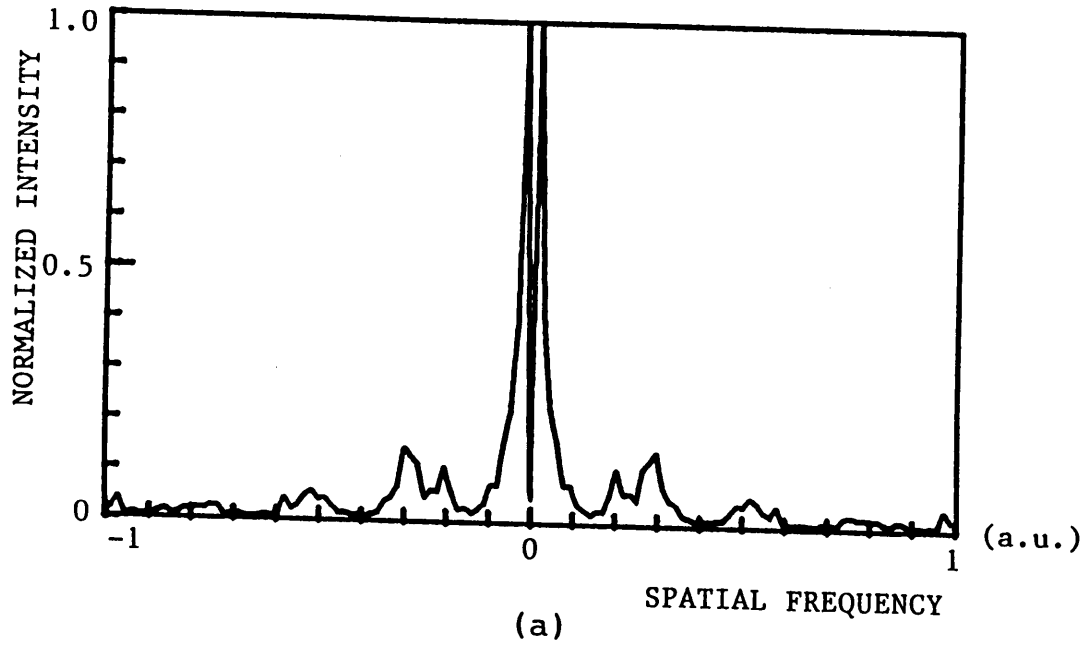

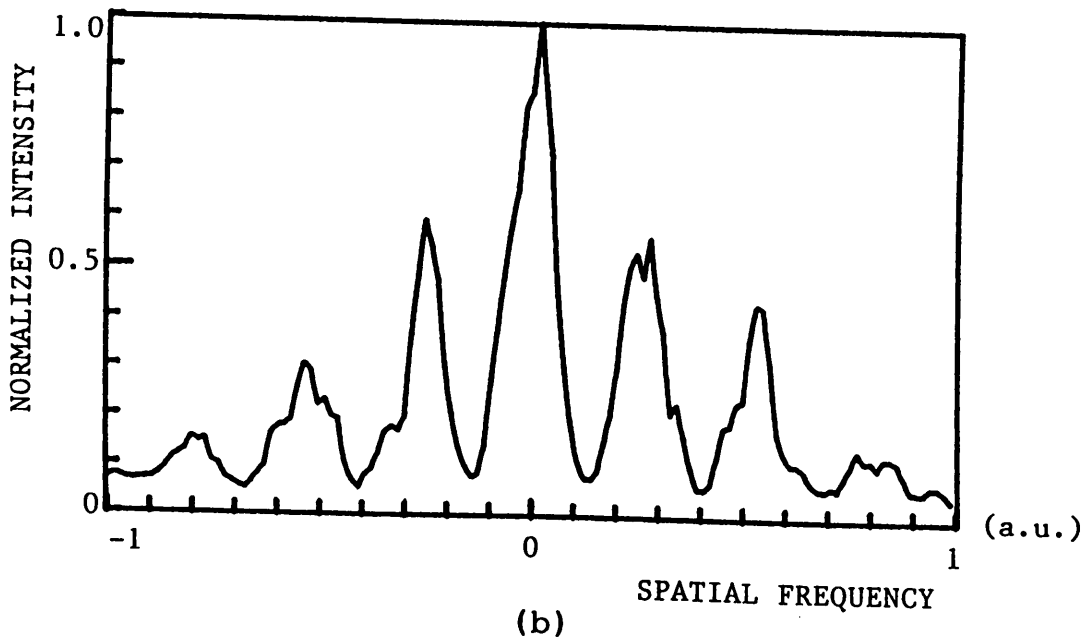

Fig.5-13 Fringe intensities calculated by Fourier transform of Fig.5-11(b): (a) intensity distribution across the DC spot and (b) intensity distribution shifted from DC spot.

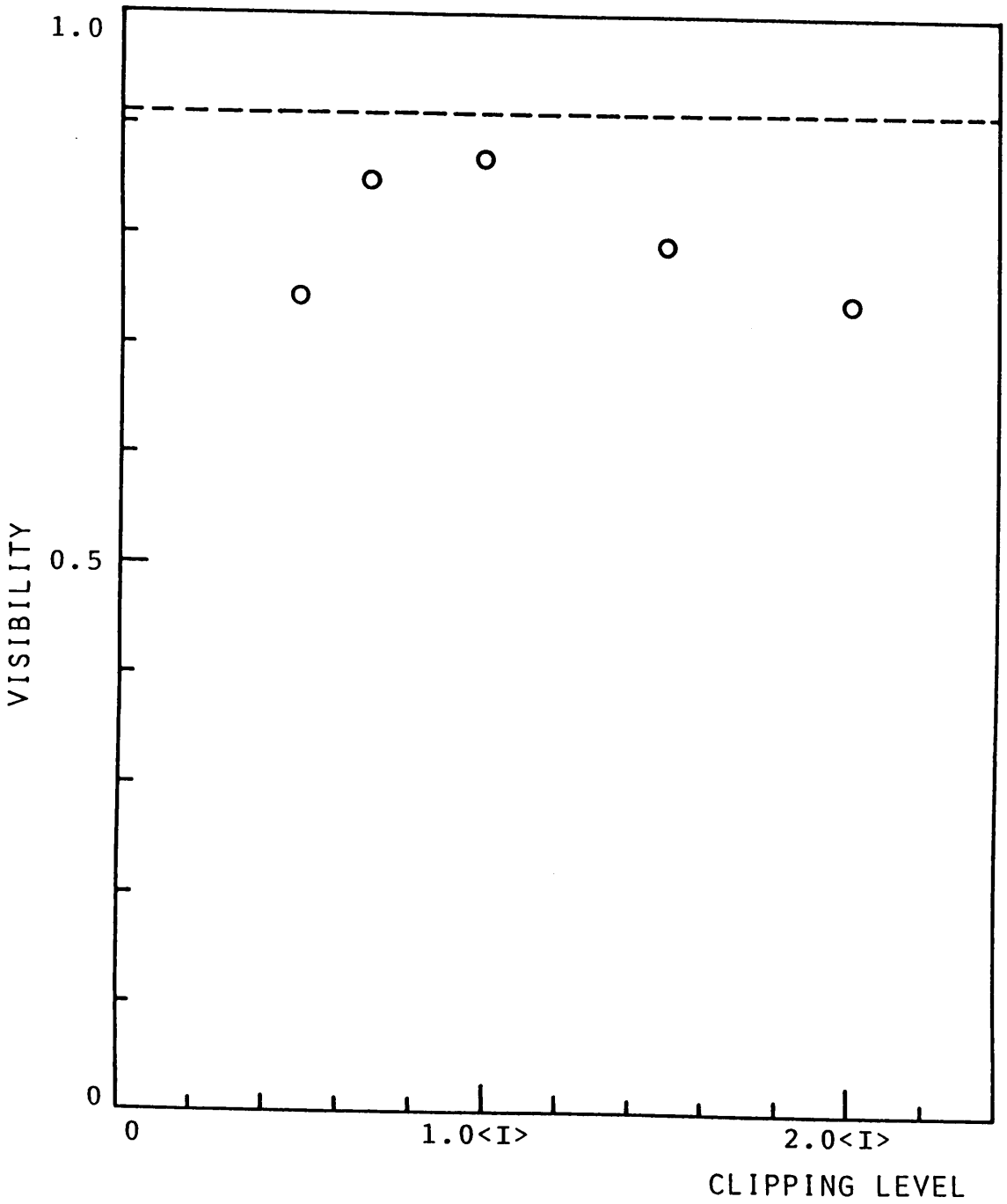

Fig.5-14 Plots of the fringe visibilities against the clipping threshold obtained by the computer simulation. A broken line shows the fringe visibility in the nonclipped case.

5-3-3. Experiments and Discussions

The power spectrum and correlation patterns are optically calculated from the specklegram shown in Fig.5-11 in the experimental setup in Fig.5-6. Fig.5-15 shows the power spectra under the intensity modulation condition in Fig.5-5(b). Fig.5-15(a) is the fringe pattern calculated from the specklegram having the intensity distribution from the minimum to maximum transmittance levels in Fig.5-5(b). Fig.5-15(b) shows the fringe pattern for the clipped specklegram having only two values of the minimum and maximum intensity transmittances. Under the intensity modulation for the LCTV, the diffracted fringes are buried in the large DC term, so that we can hardly observe them.

On the other hand, Fig.5-16 is the example of the fringe patterns which are calculated by using the phase modulation regime under the configuration in Fig.5-5(a). Fig.5-16(a) is the fringe pattern obtained from the specklegram distributed over the phase values from 0 to π while Fig.5-16(b) is one from the clipped specklegram having two phase values of 0 and π. The DC components in Fig.5-16 are suppressed more than those in Fig.15. In particular, we can clearly see the fringes to the higher diffraction orders in Fig.5-16(b). It is recognized that the phase modulation, especially the binary phase modulation, has the advantage of obtaining the high diffraction efficiency of light.

Next, the effect of the clipping threshold on the fringe visibility is investigated. To observe the intensity distribution more precisely, the CCD camera at the focal plane of the lens in Fig.5-6 is replaced by a PIN photodiode which has a wide dynamic range of the light detection. The PIN photodiode is mounted on a linearly moving X-table driven by a stepping motor and scanned to detect the intensity distribution under the control of a microcomputer. Figs.5-17 and 5-18 show the obtained fringe intensity distributions when the phase modulation effect is dominant. These figures correspond to the simulations of Figs.5-12 and 5-13. Comparing between Figs.5-17 and 5-18, it is seen that the signal clipping has the advantages of the suppression of the DC component and the enhancement of the higher diffraction orders. However, the fringe visibility of Fig.5-18(b) is slightly less than that of Fig.5-17(b). Fig.5-19 shows the dependence of the fringe visibility on the clipping threshold. The broken line is the fringe visibility

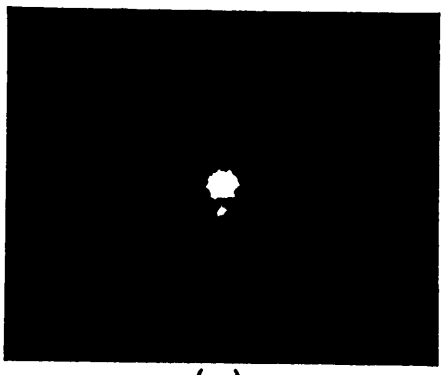

(a)

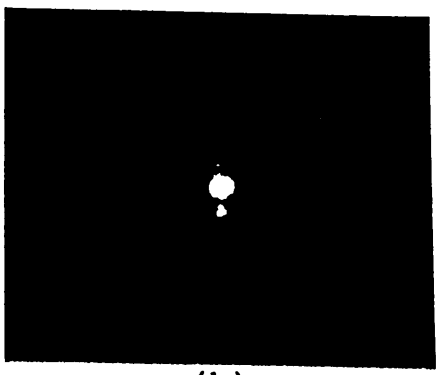

(b)

Fig.5-15 Fringe patterns produced by the Fourier transform of Fig.5-11 under the intensity modulation of the LCTV: (a) nonclipped case and (b) clipped case.

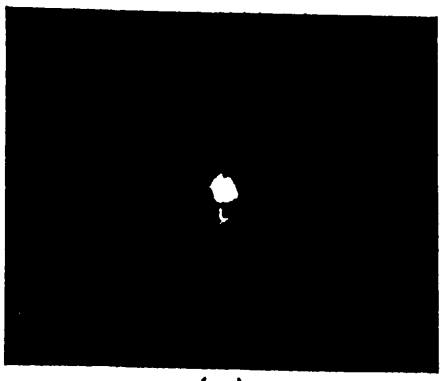

(a)

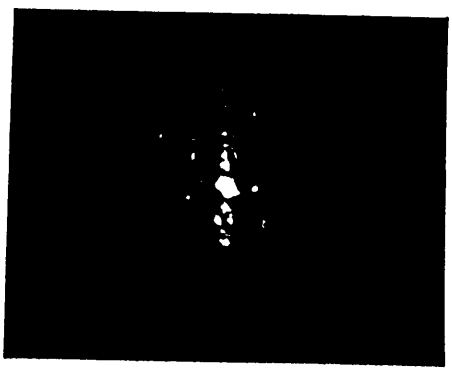

(b)

Fig.5-16 Fringe patterns under the phase modulation of the LCTV: (a) nonclipped case and (b) clipped case.

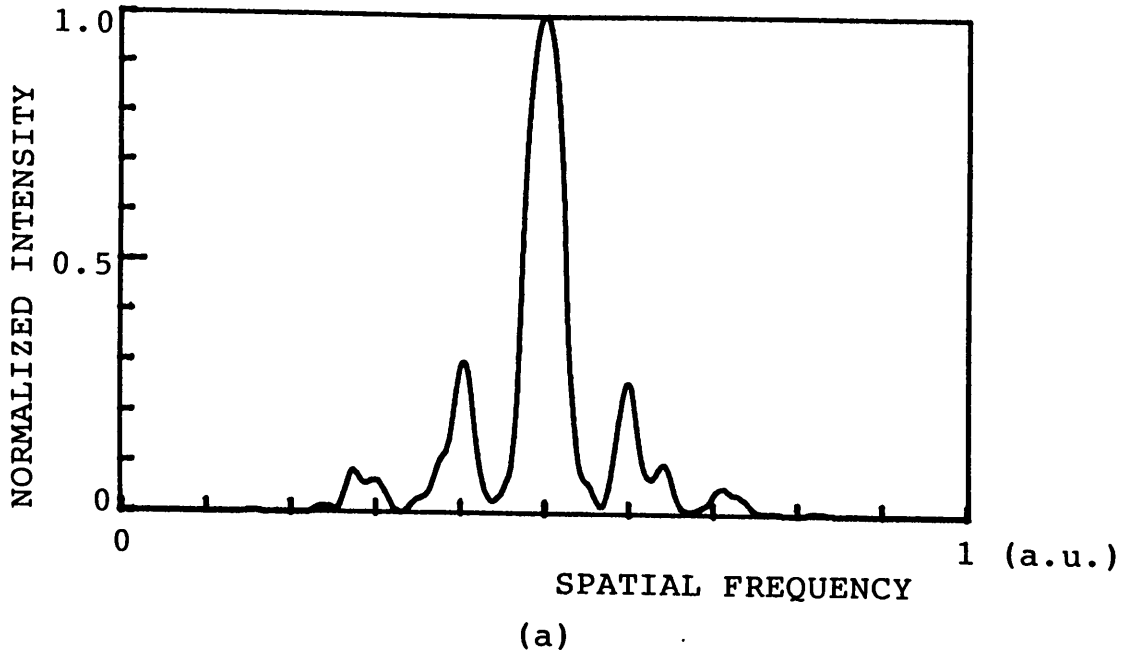

(a)

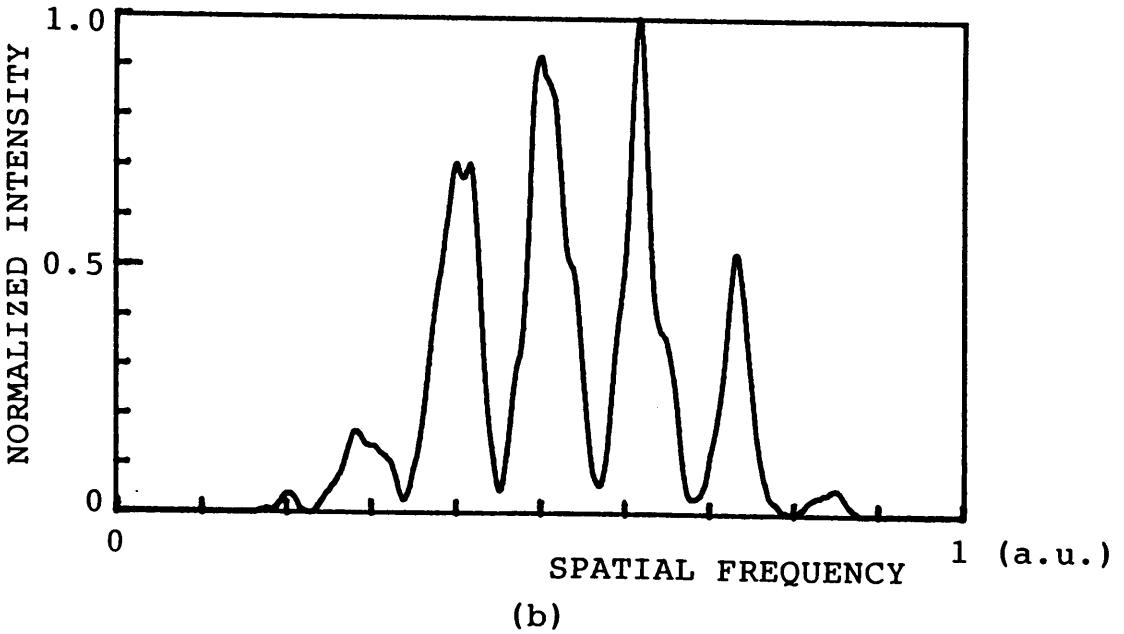

(b)

Fig.5-17 One-dimensional intensity distributions of the fringe patterns in Fig.5-16 (a): (a) intensity distribution across the DC spot and (b) intensity distribution shifted from the DC spot.

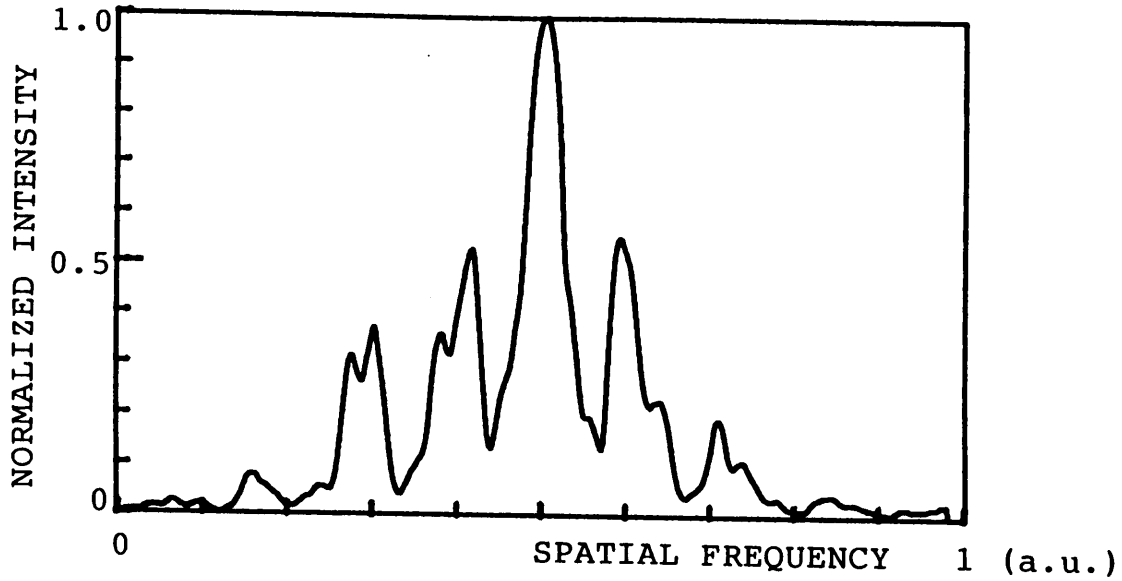

(a)

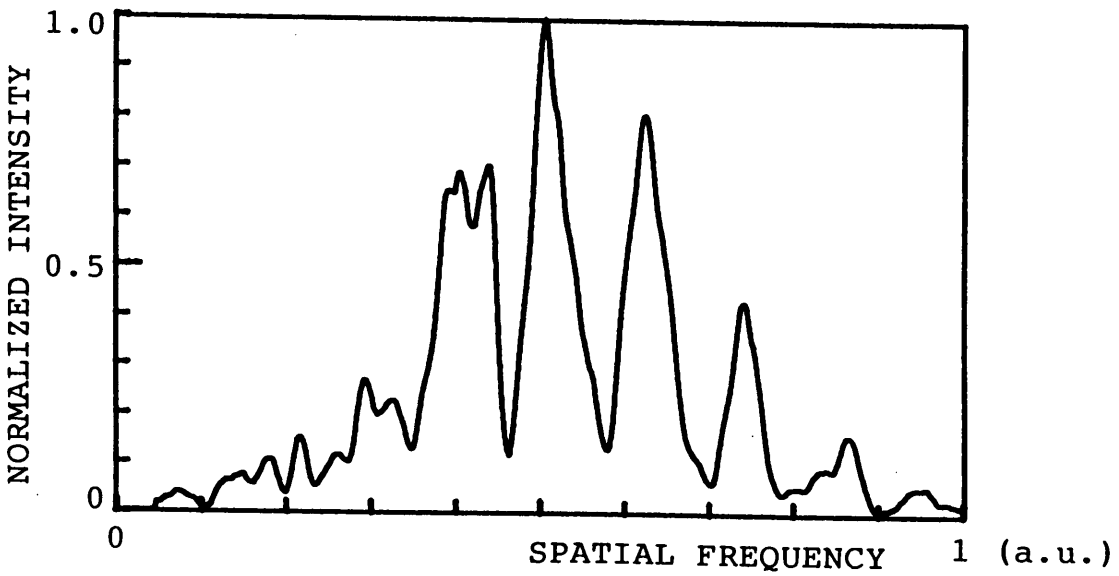

(b)

Fig.5-18 One-dimensional intensity distributions in Fig.5-16(b): (a) intensity distribution across the DC spot and (b) intensity distribution shifted from the DC spot.

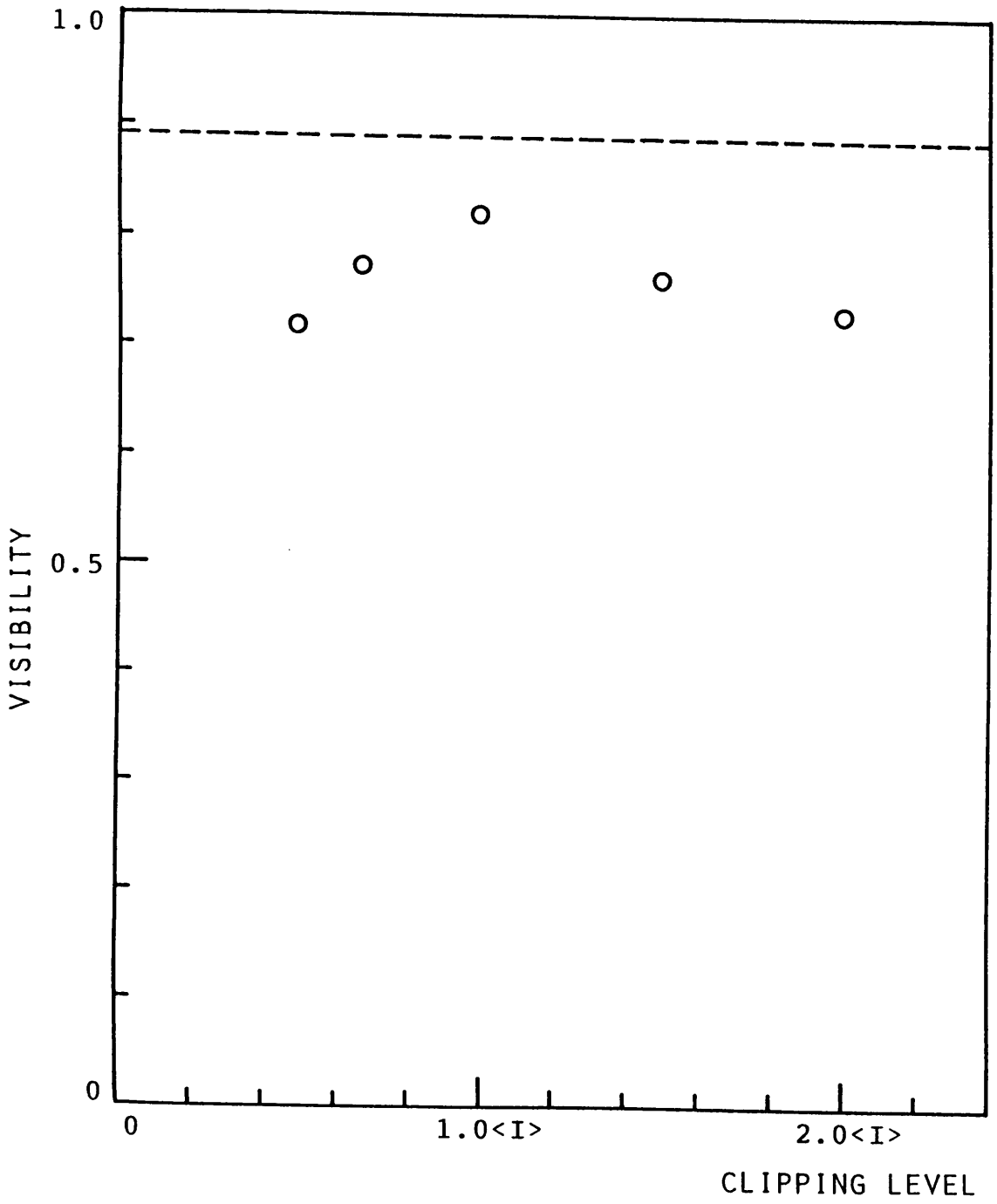

Fig.5-19 Experimental plots of the fringe visibilities against the clipping threshold.

of the nonclipped case. The experimental results in Fig.5-19 are almost coincident with those of the computer simulation in Fig.5-14. From the figure, the high visibility of the fringe can be obtained at the clipping threshold around the average intensity level.

In the previous treatment, by the binarization of the speckle intensity at a certain threshold level, the DC diffraction term was so reduced that we could clearly observe the high diffraction orders of the fringes. Binarizing the fringe pattern, the further improvement of the correlation signal is expected due to the nonlinear effect; i.e., the higher peak value and narrower width of the correlation spots.[21,27] The method is advantageous to compensate the weak points of the LCTV panel for the application to a spatial light modulator such as an insufficient phase modulation property and a low space band width product.

The fringe pattern shown in Fig.5-16(b) is again displayed on the LCTV in the experimental setup in Fig.5-6. By the optical Fourier transform of the fringe pattern, i.e., the Fourier transform of the power spectrum, we obtain the correlation pattern. Fig.5-20(a) shows the correlation function calculated from the fringe pattern shown in Fig.5-16(b); the signal levels of the fringe pattern to be fed to the LCTV are normalized and distributed over the phase values from 0 to π. The two correlation spots are observed along the horizontal direction, but they are not distinct because of the strong DC term.

Next, the fringe pattern is binarized at the average intensity level and displayed on the LCTV as the binary phase values of 0 and π radians. Fig.5-20(b) shows the Fourier transform of the binary fringe pattern. By the Fourier transform of the binary fringe pattern, the correlation spots are clearly seen better than that in Fig.5-20(a). To observe the intensity distribution more precisely, Fig.5-21 shows one-dimensional intensity distributions across the direction of the diffraction spots detected by a PIN photodiode. The correlation peak obtained from the binary fringe pattern is five times higher than that for the nonclipped case. The relation between the correlation peak to the DC peak ratio and the clipping threshold for the fringe pattern is calculated and shown in Fig.5-22. The figure shows that the best SNR occurs at the average threshold.

In this section, we investigate the effects of the binarizations both of the input specklegram and its Fourier fringe on the diffraction efficiency at the

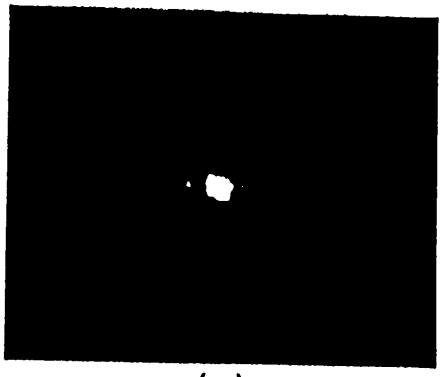

(a)

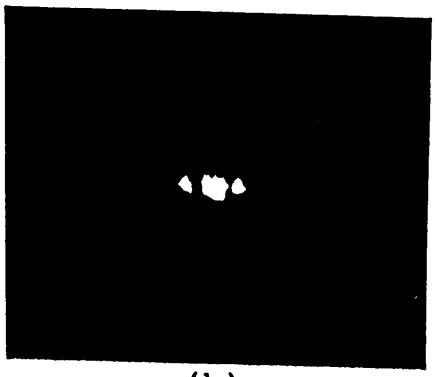

(b)

Fig.5-20 Correlation patterns produced by the Fourier transform of the phase modulation patterns of Fig.5-16(b): (a) the nonclipped fringe pattern and (b) the clipped fringe pattern.

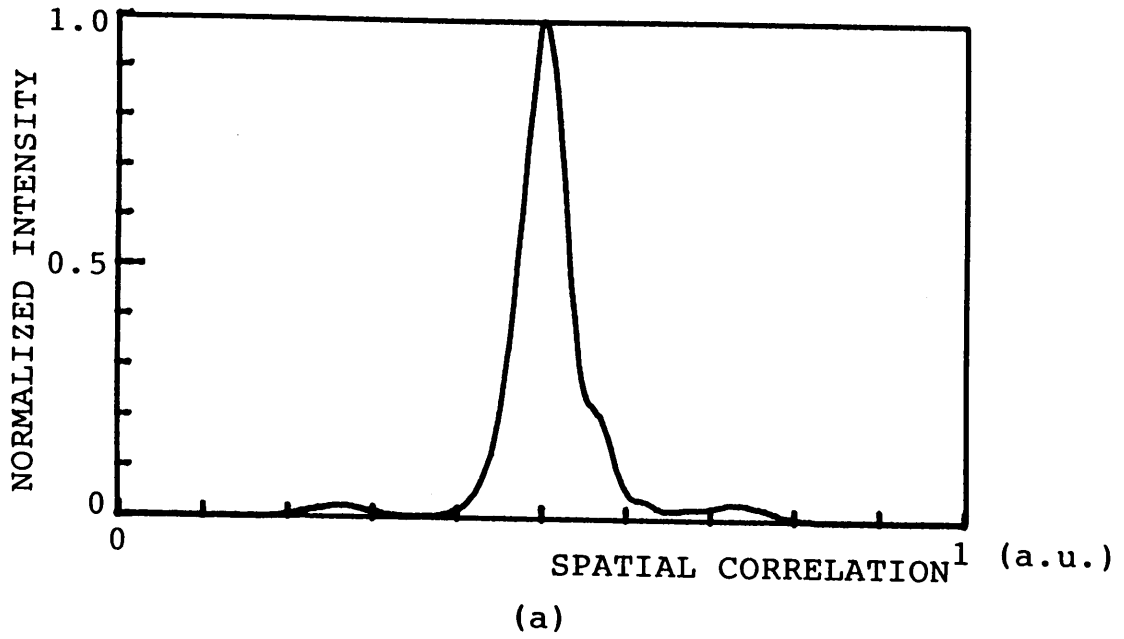

(a)

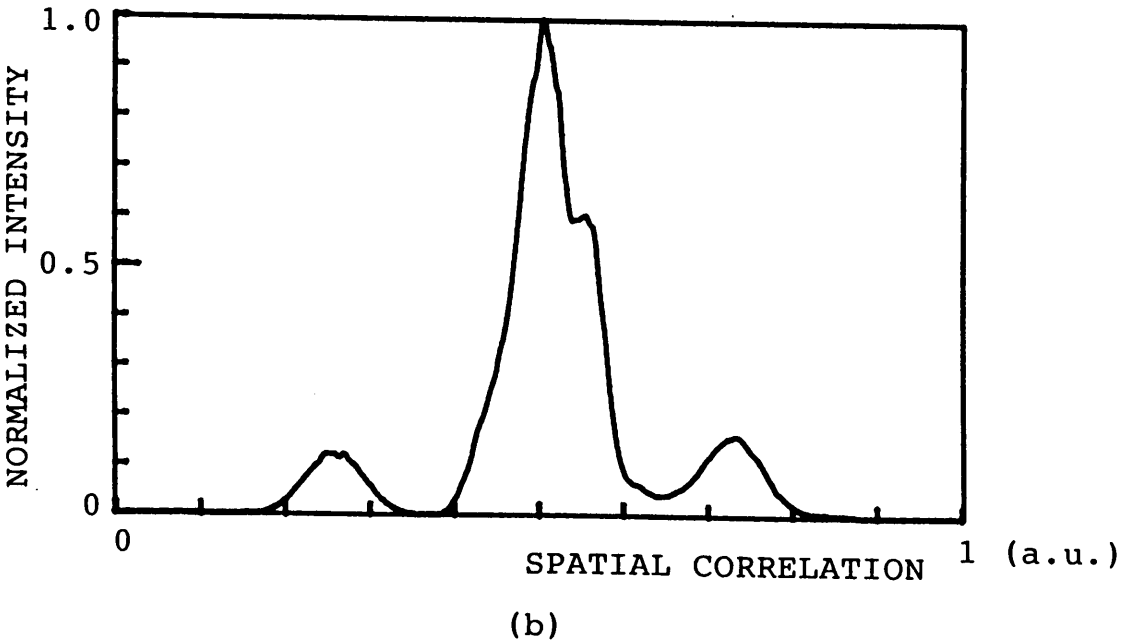

(b)

Fig.5-21 One-dimensional intensity distributions of the correlation functions of Fig.5-20 (a) and (b) along the line to the ±1 order diffraction spots.

	correlation peak	DC peak	correlation peak / DC peak
nonclipping	144	5809	0.025
0.4 <I>	148	2802	0.053
0.6 <I>	290	2794	0.104
0.8 <I>	353	3001	0.118
1.0 <I>	363	2884	0.126
1.2 <I>	299	3656	0.082
1.4 <I>	229	4105	0.056
1.6 <I>	174	5086	0.034

Fig.5-22 Diffraction efficiency of the binary phase only fringe at the correlation plane for the various clipping threshold.

correlation plane when we use the LCTV as a spatial light modulator. It is found that the correlation signal is enhanced by the binarization and, thus, we can expect the simple architecture and high performance of the optical correlator by the binary phase only filtering.

Chapter 6. OPTICAL CORRELATOR FOR SPECKLE INTERFEROMETRY

6-1. Introduction

The fundamentals of the optical correlation using a LCTV for the processing of a two-dimensional speckle pattern are studied in chapter 5. It is shown that the binarization of the signals both for the input specklegram and the fringe pattern improves the diffraction efficiency of light at the correlation plane. In this chapter, we propose a new optical correlation system using nonlinear Optic RAM detectors and LCTVs.[58-64]

Using the Optic RAM detector, we can immediately obtain the two-dimensional binarized signals within the detector at an arbitrary threshold level of the input light intensity. Thus, we need no electronic circuit like a comparator for a clipped light intensity, so that we can realize the simple and first detection of the signal. A basic description of this application is as follows: (1) the dynamic speckle patterns are detected as the binary signals by the nonlinear Optic RAM detector; (2) from the detected speckle signals, the two-dimensional correlation function is optically calculated by using the phase modulation property of the LCTV; and (3) the information of the object such as a displacement or a velocity is analyzed from the obtained correlation function. To demonstrate the usefulness of the system, the vector velocity measurement of a light scattering object is conducted.

6-2. Nonlinear Optic RAM Detector

The IS32 Optic RAM detector array (Micron Technology) we used in the experiment is basically the same device as a dynamic random access memory (DRAM) chip except for removal of the opaque cover from its top surface. Marron and Morris investigated the statistical properties of clipped speckle intensity using the Optic RAM detector.[6] The Optic RAM detector which consists of 256×256 elements each measuring 6.4×6.4μm has attractive features: the binarization of a two-dimensional speckle pattern is performed for an arbitrary threshold level of the light intensity; and each cell can be used as a point detector because of its random access property.

A DRAM is usually controlled by a refresh cycle which charges up regularly to keep the content of the memory cell correct. If light falls on the

DRAM cell while the refresh cycle is disabled the incident light causes the charge stored in the memory cell to decay at a rate proportional to the incident light intensity. Usually, this is called as a soft error effect and harmful for the memory function. However, the effect can be applied to the detection of input light level. The Optic RAM is originally designed as a light detector based on the soft error effect of DRAM.

Basic operation is as follows (See Fig.6-1).

STEP1 After the refresh cycle to keep the content of the memory cell (the process is regularly set by a timed interruption command from a microcomputer), the memory cell is initialized by writing a logical 1 into all memory cells. This process is a preparation for light detection.

STEP2 By disabling the refresh cycle for a certain time offset by the software program, the charge stored in the memory cell starts to decay proportionally to the level of the incident light. Comparing the remaining charge with a reference voltage, the content of each memory cell is replaced by "1" or "0" corresponding to above or below the threshold intensity level. This operation may be considered as a kind of exposure in photography.

STEP3 Finally, the binarized intensity pattern stored in the Optic RAM is accessed by the I/O command and sent to the microcomputer.

From above operations, we can consider that the Optic RAM detector includes a 1-bit AD converter in itself. This property is applied to the optical threshold logic operation for the successive two intensity patterns.[65] Setting a certain threshold level to the Optic RAM, the only superposed intensity level of the different two intensity patterns above the threshold, i.e., logical AND pattern, can be detected by the cell, whereas at a lower threshold level, the logical OR pattern is obtained. We can arbitrarily adjust the threshold level by changing the exposure time and the reference voltage to the Optic RAM detector.

6-3. Optical Correlator for Doubly Exposed Clipped Speckle

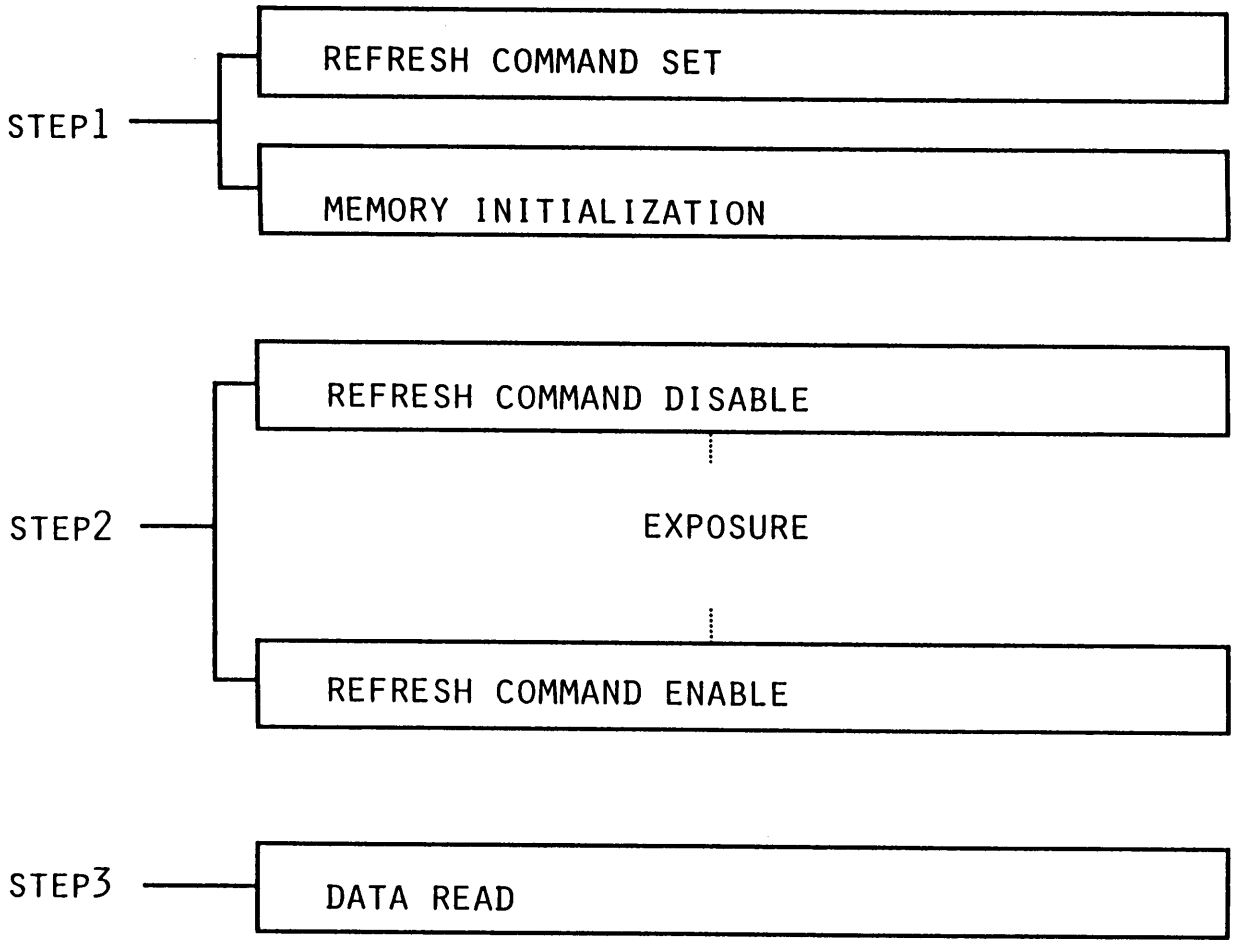

Fig.6-1 Flow chart for the intensity detection by the Optic RAM.

In chapter 5, it is shown that the performance of the optical correlator using the LCTV is improved by the binarization of the signals not only for the input specklegram but also for the fringe pattern obtained by its Fourier transform. Based on the results, we propose the system for calculating the correlation function using the phase modulation property of LCTV and the Optic RAM detector which enable the nonlinear detection of signals.[59,64]

The system for the detection of speckle patterns and the realization of the nonlinear optical correlator are shown in Fig.6-2. A rotating ground glass plate of #400 mounted on a two-dimensional x-z stage is illuminated by a plane wave of a 5mW laser diode (λ=780nm). The Optic RAM detector has the maximum sensitivity around the laser light wavelength. The object is imaged by a two-lens imaging system (f=100mm) together with a pinhole (r=1.5mm). A time dependent clipped specklegram (the logical OR pattern between before and after the displacements of the clipped speckle patterns) is detected by the Optic RAM. During the exposure time, the speckle pattern to be detected is considered as a frozen pattern. Strictly speaking, there is a distribution of the separations between the speckle pairs on the Optic RAM because of the finite sizes of the laser light illumination to the rotating ground glass plate and the detection area of the Optic RAM. However, this effect is not so serious in this optical setup and can be ignored because the detector area is considerably small compared with the imaging area on the detection plane.

After the allocation of the binary pattern to the two signal values corresponding to the phase shifts 0 and π by the microcomputer, they are sent to the LCTV through a frame memory. Illuminating the LCTV panel by a collimated light from a 5mW He-Ne laser, the phase modulated signal is Fourier transformed by a lens behind of the panel. Another Optic RAM located at the focal plane of the lens detects the Fourier transformed pattern as a binary signal. By changing the exposure time or the threshold voltage to the Optic RAM detector by the microcomputer, we can appropriately adjust the threshold level of the detection for the fringe intensity . After storing the binary fringe pattern in the microcomputer, it is again displayed on the LCTV panel as a phase pattern having two levels of 0 and π. Fourier transforming it by the same optical system, the correlation pattern is detected by a CCD camera in Fig.6-2.

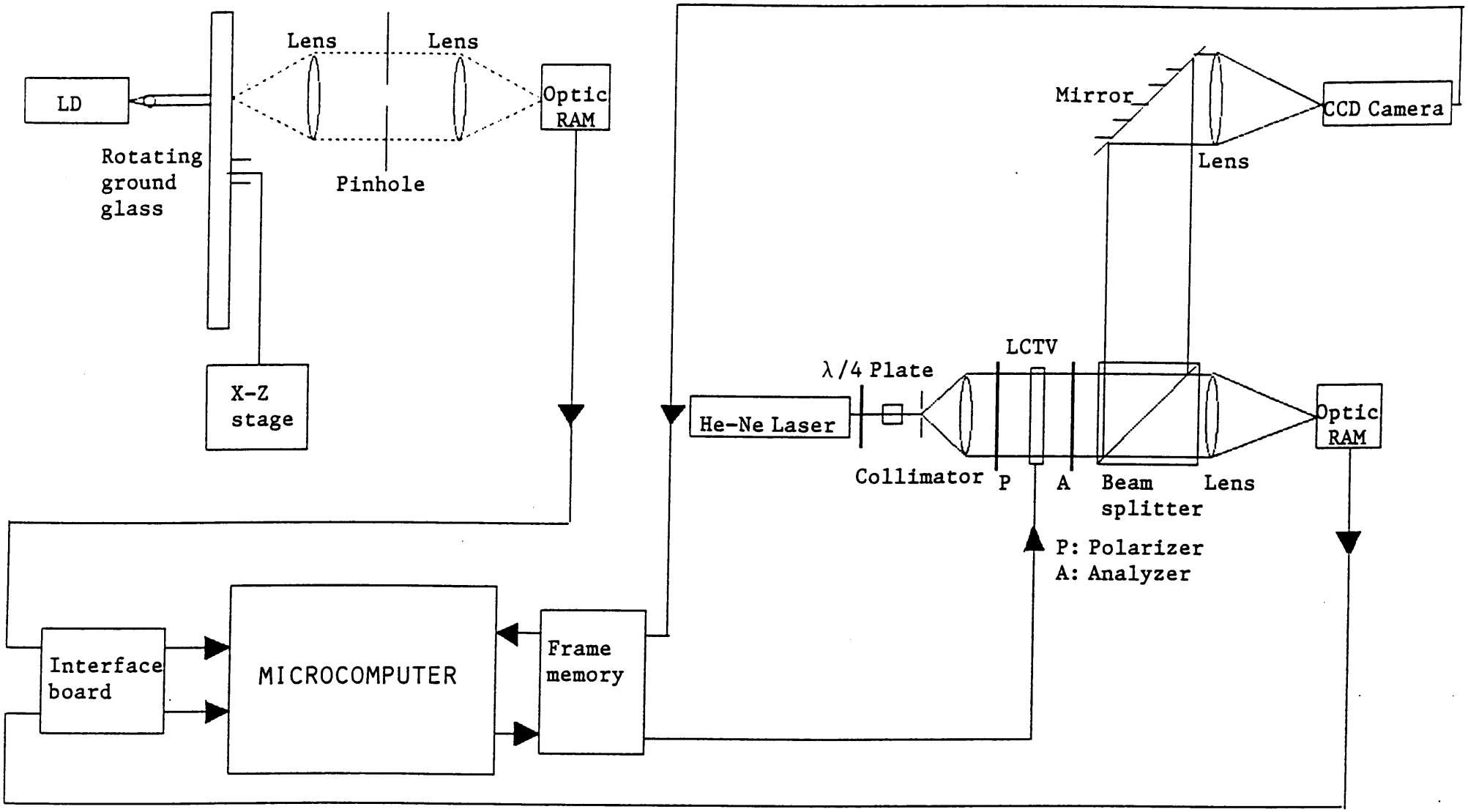

Fig.6-2 Speckle detection system and implementation of the nonlinear optical correlator.

Fig.6-3(a) shows the binary specklegram taken by the system. We can recognize the clipped speckle pairs in Fig.6-3(a). Fig.6-3(b) is the power spectrum calculated by the Fourier transform of Fig.6-3(a) and detected by the Optic RAM detector as a binary signal. The five fringes can be seen in this figure. Fig.6-3(c) is the output pattern of the optical correlator obtained by the Fourier transform of Fig.6-3(b). We can see the clear correlation spots in the diagonal direction. The whole time to obtain the correlation signal was about 2.0 second. However, the processing time may be easily shortened to the video rate by the hardware installation.

By using this system, we conducted an in-plane velocity measurement at seven points on the glass plate by shifting the x-z stage to the line perpendicular to the optical axis. The result is shown in Fig.6-4. The horizontal axis is the radius from the rotating center of the plate while the vertical axis is the distance between the ±1 order diffraction peaks of the correlation output which is proportional to the object velocity. The DC term shown in Fig.6-3(c) always appears in the correlation pattern and affects the precise detection of the correlation signals. However, we can easily eliminate the DC term from the correlation pattern by masking the pattern optically or electronically since the term is stationary during the measurement. From the good linear relation between the correlation distance and radius of the rotating center in the figure, it is shown that the system can be used for the practical velocity measurement of a light scattering object.

6-4. Optical Joint Transform Correlator Using Clipped Speckle Intensity

In section 6-3, the nonlinear optical correlator for doubly clipped speckle intensity is proposed and applied to the velocity measurement of a rotating ground glass plate. Although the method is useful to obtain the magnitude of an object velocity, its direction can not be determined. In this section, we provide an improved method to obtain both the magnitude and direction of the object velocity at the same time by the joint transform correlation.[11,40,60] The basic operation of the optical correlation using LCTV has been already described in previous section, so that we only discuss the merit of the joint transform correlation method.

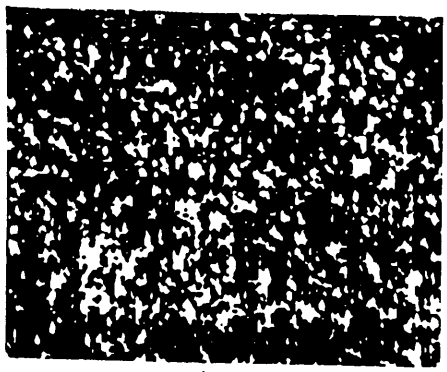

(a)

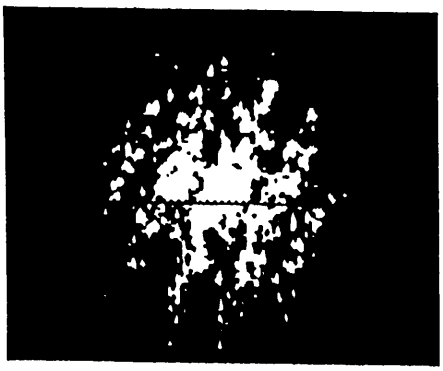

(b)

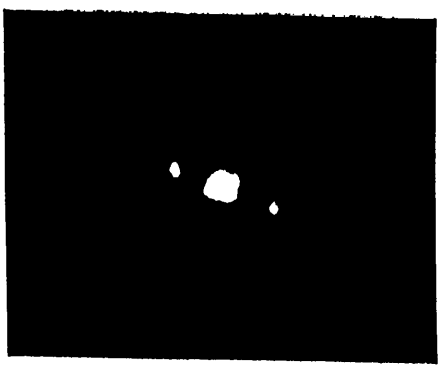

(c)

Fig.6-3 (a) Clipped specklegram detected by the Optic RAM detector. (b) Binary fringe pattern produced by the Fourier transform of the specklegram. (c) Correlation output by the Fourier transform of (b).

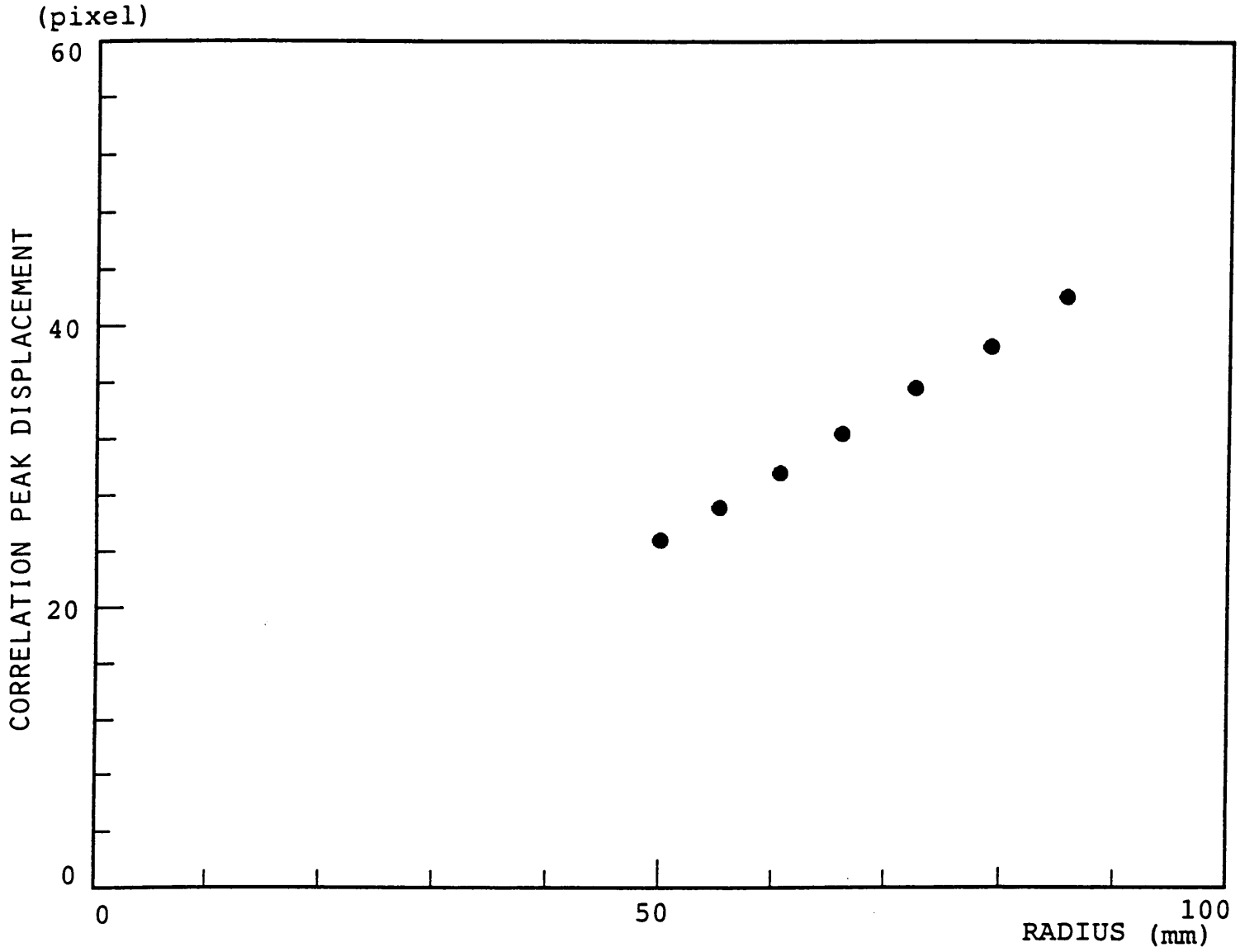

Fig.6-4 Result of the velocity measurement by the proposed system.

The system configuration is shown in Fig.6-5. The same optical imaging system shown in Fig.6-2 is used for the detection of speckle pattern, whereas the two LCTV panels and CCD cameras are used for the realization of the optical correlator. The display panel (Citizen UB250) which has 160 horizontal and 146 vertical pixels in an area 50mm by 38mm is used in the experiment. In the joint transform correlation, the two speckle patterns separated by a certain time offset are displayed on the upper and lower sides of the LCTV as is shown in Fig.6-6(a). We can obtain not only the magnitude but also the direction of the object velocity because the resulting correlation spots locate at the distance from the origin centered at the offset distance and their derivation from the offset represents the sign of the velocity. The fringe separation or the correlation distance is determined by the spatial offset of the two speckle patterns. The fringe pattern involves a large DC component because of the low contrast ratio and the imperfect phase modulation of the LCTV. The DC components at the Fourier and correlation planes are optically blocked by the DC cut masks in front of the detectors.

The operation of joint transform optical correlator is as follows. A time dependent speckle pattern is detected twice by the Optic RAM detector and displayed at the upper and lower sides on the LCTV LCTV1 with a certain spatial separation. Illuminating LCTV1 by a collimated light from a 5mW He-Ne laser, a phase modulated speckle signal is Fourier transformed by a lens behind the panel. Filtered out all but near the zeroth order diffraction beam by a filter and enlarged the pattern by an objective lens, the transmitted signal is imaged onto the screen and detected by a CCD camera CCD1 as a power spectrum. The screen has a DC cut mask by which the zeroth order component of the diffraction is eliminated. This image is immediately displayed on the LCTV LCTV2 through CCD1. The power spectrum displayed on LCTV2 is optically Fourier transformed in the same manner as the above treatment. Finally, the correlation signal is detected by a CCD camera CCD2 and sent to the microcomputer through a frame memory.

The experimental results are shown in Fig.6-6. Fig.6-6(a) is an example of two speckle patterns displayed on the LCTV. In this case, the illuminating spot on the ground glass plate is located on the vertical line which crosses the rotating center, namely , the Y component of the velocity is zero. Fig.6-6(b)

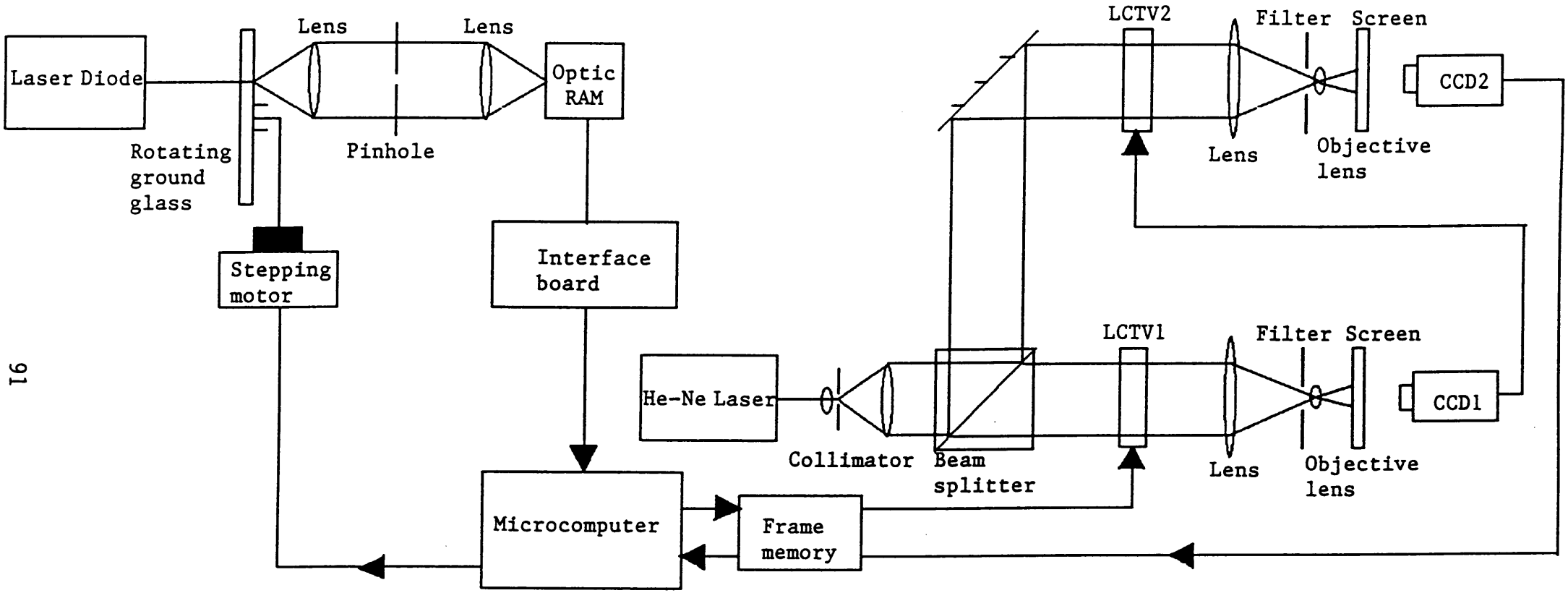

Fig.6-5 Schematic diagram of the speckle detection and the optical correlation.

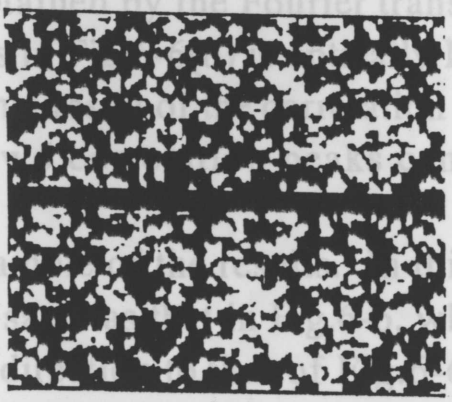

(a)

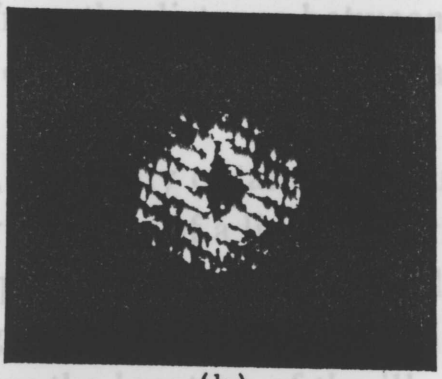

(b)

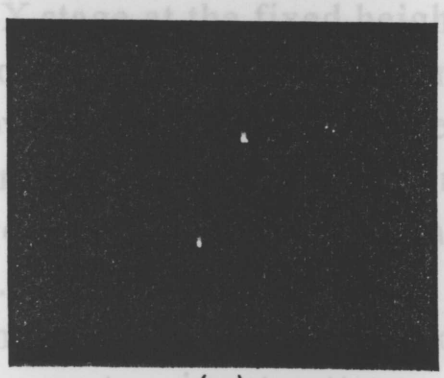

(c)

Fig.6-6 Results (a) Example of speckle patterns of the successive two exposures displayed on the first LCTV panel. (b) Fringe pattern obtained by the optical Fourier transform of (a). (c) Correlation output of (b).

is the fringe pattern obtained by the Fourier transform of Fig.6-6(a). The power spectrum such as in Fig.6-6(b) is optically Fourier transformed again. Fig.6-6(c) shows the final result of the correlation pattern taken by the CCD camera CCD2. The two correlation peaks can be seen in the diagonal direction.

Fig.6-7 is another example of the results. In this case, the location of the illuminating spot is the same as that in Fig.6-6, while the ground glass plate rotates in the opposite direction to that of Fig.6-6. The fringe patterns or the correlation spots in Fig.6-6 and Fig.6-7 are symmetrically situated against the vertical line which intersects the correlation origin. These results show that the proposed method here can be used to determine not only the magnitude of the object velocity but also its direction. The magnitude of the velocity is calculated from the distance between the origin and one of the correlation peaks. The direction of it is also obtained from the direction of the correlation peaks.

By using this system, we easily obtain the locus of the correlation spots produced by an arbitrary motion of a light scattering object. In Fig.6-5, the rotating ground glass plate is mounted on the linearly movable X stage driven by the stepping motor under the control of the microcomputer, so that we can easily change the location of the illuminating spot on the glass plate which has an arbitrary vector velocity $\mathbf{v}=(v_x,v_y)$.

We conducted velocity measurement at five points on the glass plate by shifting the X stage by a step of 10mm. Because the rotating glass plate is linearly shifted by the X stage at the fixed height from its rotating center, i.e., the X components of the velocities at the illuminating spots always have the same value as is shown in Fig.6-8. In each measurement, the location of the peak spot of the correlation function is obtained from the output of the optical correlator proposed here and displayed successively on the microcomputer display.

In the joint transform correlator, the correlation peaks corresponding to the offset distance between two input patterns always appear at a certain distance from the correlation origin, even if the speckle patterns do not change between the successive exposures, i.e., the ground glass plate is halt. In the following discussion, we only concern the correlation plane above the horizontal line which crosses the correlation origin and we choose the correlation spot produced by the same two speckle patterns as a new origin

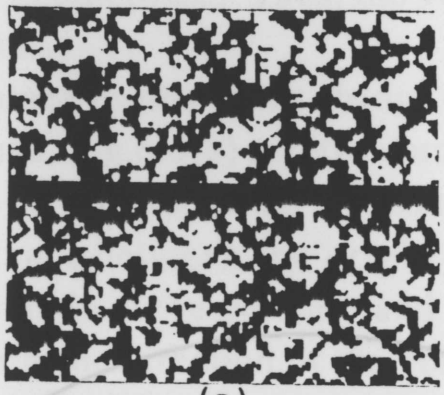

(a)

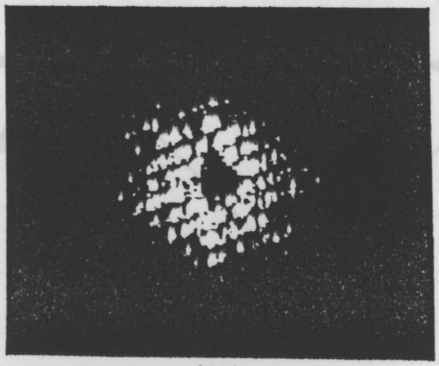

(b)

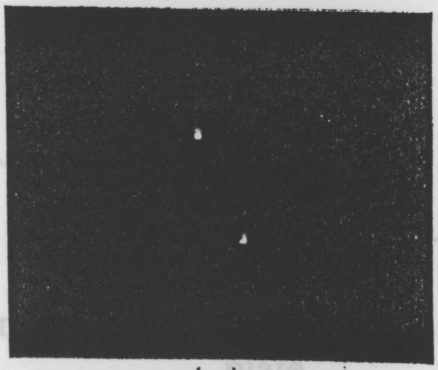

(c)

Fig.6-7 Results obtained for the case when the rotating direction of the glass plate is reversed to that of Fig.6-6: (a) speckle patterns, (b) fringe pattern, and (c) correlation output.

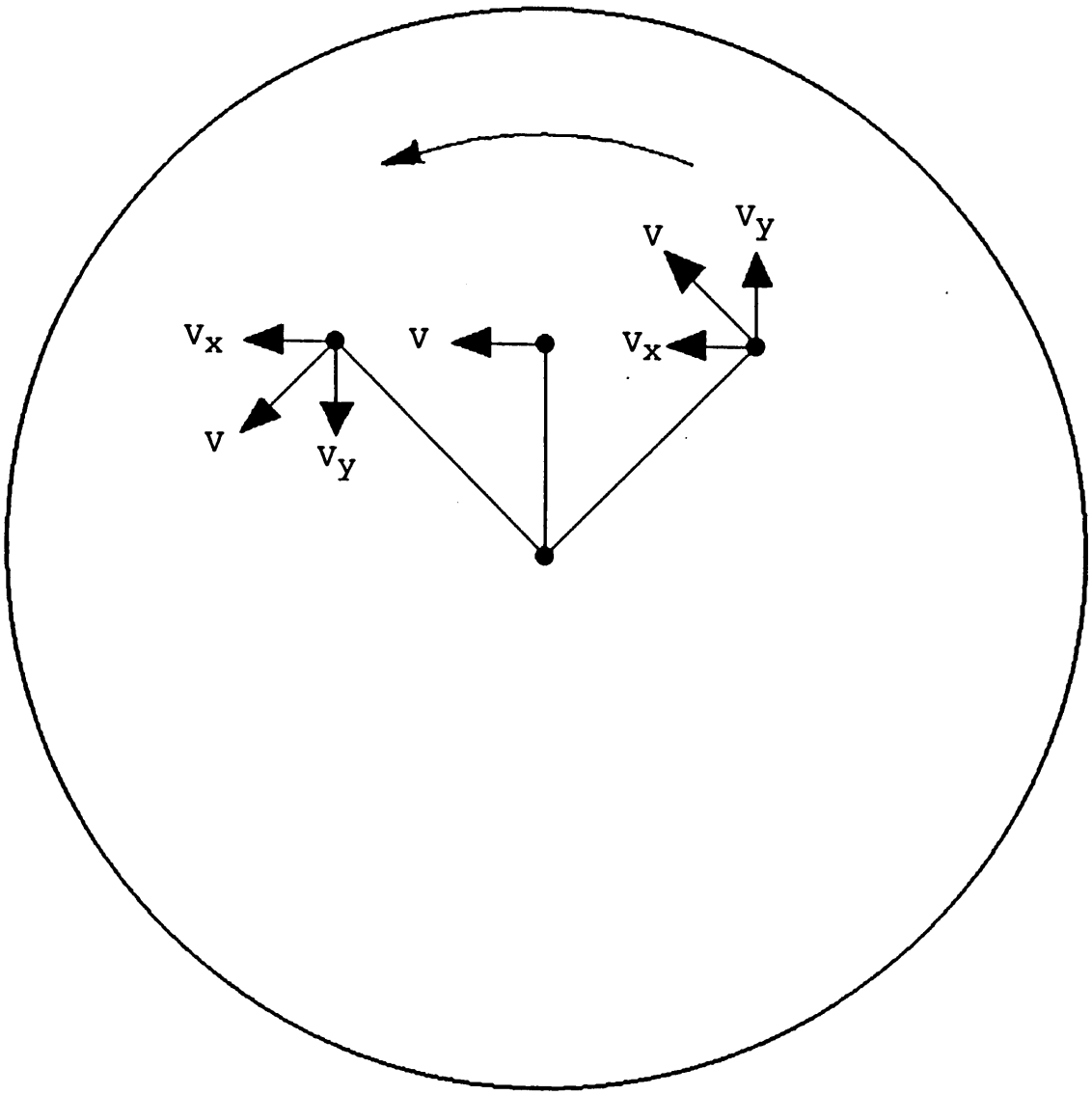

Fig.6-8 Vector coordinates at the various positions on the ground glass plate.

of the coordinate (X,Y) in that plane. Then, the vector velocity can be easily displayed in the new plane.

Fig.6-9 shows the obtained results of the change of the vector velocities due to the shifts of the X stage. Fig.6-9(a) and (b) correspond to the results when the glass plate rotates in the clockwise and counter-clockwise directions, respectively. The distance between the origin (X,Y)=(0,0) and a circle correspond to the magnitude of the velocity and the direction of the circle from the origin represents the direction of the velocity. In both Figs.6-9(a) and (b), the X components of the velocities have the same speed. This means the fact that each measurement is made at a fixed illumination height from the rotating glass center. As the ground glass plate rotates in opposite directions in Figs.6-9(a) and (b), the obtained correlation spots are located at the right hand side or the left hand side in the correlation plane corresponding to the clockwise or counter-clockwise rotation of the plate. In Fig.6-9(b), though the X components of the velocity should have the same value for each data, there is a fluctuation of the data points. The fluctuation is one pixel in the X direction, so that the error can be considered as the deviation of the data within the resolution of the image detection system. There is also a fluctuation of the data points for the Y components of the velocity due to the low resolution of the imaging system. The deviation of the data is also within its resolution. This problem may be settled by choosing appropriately the optical constants in the imaging system, such as an appropriate choice of the magnifications of the objective lenses.

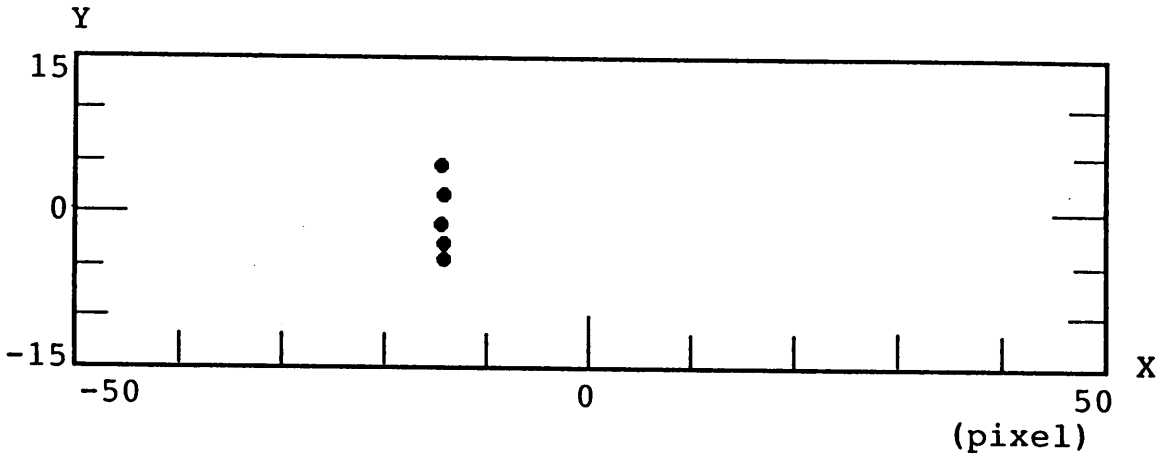

(a)

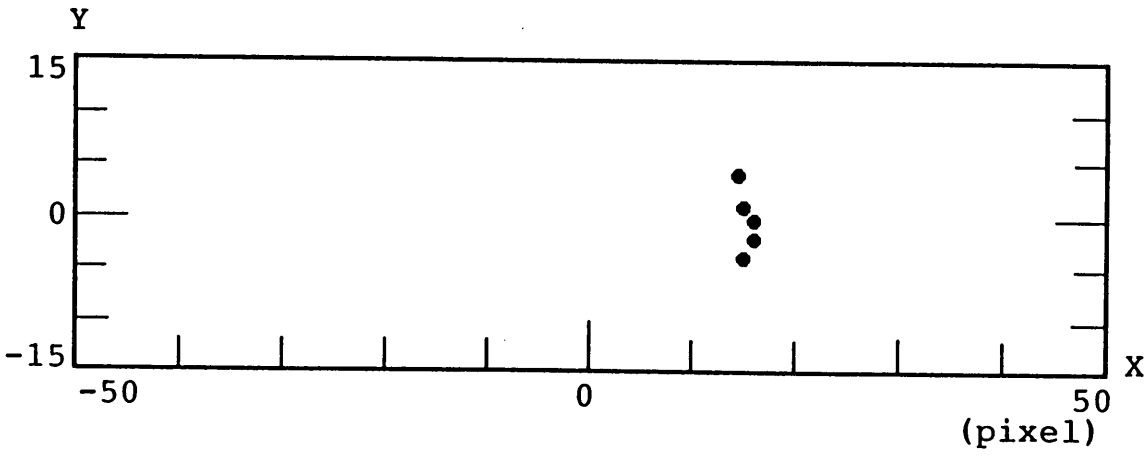

(b)

Fig.6-9 Output correlation spots correspond to vector velocities in various positions at the rotating glass plate. The rotating directions of the glass plate are opposite to each other between (a) and (b).

Chapter 7. CONCLUSIONS

The present thesis has described the statistical properties of clipped speckle pattern and its applications to optical correlator.

In chapter 3, the accuracy of the peak detection of the clipped cross-correlation function has been studied by using a computer simulation. The clipped correlation function for both the pure and modified translation states of speckle patterns have been investigated. In the pure speckle translation such as in a two-lens imaging system, the peak fluctuation of the clipped cross-correlation function is smaller than that of nonclipped one when there is no additive noise to the speckle signal. However, it is found that the accuracy of the peak detection is affected by a noise but the effect is not serious when the noise level is small. It is proved that the clipping technique has an advantage of the accurate detection of the peak position.

As an another example, the accuracy of the peak detection for the clipped correlation in a single lens imaging system, i.e., the modified translation state of a speckle pattern, has been investigated. The accurate measurement of the peak detection is expected for a small value of the correlation offset, while the peak fluctuation becomes large as the offset increases corresponding to the decrease of the height of the correlation peak.

The clipping technique of the speckle signal is suitable for the accurate detection of the peak position in the cross-correlation function, especially for the speckle having a pure translation state, and it is also useful for the speckle of the modified translation state when the correlation offset is not so large. It was also noted that it is possible to detect a small peak deviation from the correlation origin and, as a result, a fine displacement measurement compared to the speckle size is achieved by using the clipping technique.

In chapter 4, the accuracy of the peak detection of the correlation function has been examined for several logical operations of a clipped speckle intensity. The experimental results are compared with the theoretical predictions. It has been proved that the (1,-1) logic for the clipping signal has the same meanings as the logical XOR operation because the clipped intensity has only two levels which are above or below threshold. Referring to the previous theoretical treatment,[6] it is pointed out that the accuracies of the peak detections are equal independent of the employment of any logical operations. However, the obtained results show that except for the

equivalence between the logical XOR and (1,-1) operations, the accuracy of the peak detection varies depending on the clipping threshold level and the employment of the logical operations. The results are very important in the real measurement having a finite data length with a possible noise source.

In chapter 5, the phase and intensity modulation properties of LCTV as a spatial light modulator have been investigated for the implementation of an optical correlator. The phase shift from 0 to 1.2π radians and intensity transmittance variations of 0.3~1.0 in the LCTV panel have been obtained. As the LCTV panel used in the experiment is a twisted nematic type, we can not realize a perfect phase only modulation. A liquid crystal device such as a homogeneous alignment type is suited for an ideal phase only spatial light modulator.[66] However, it is found that we can attain approximate phase only modulation for the twisted nematic LCTV for the certain configuration of the polarization filters and the ranges of the applied video signals.

The effects of the clipping threshold level of a specklegram on the visibility of the fringe pattern in the Fourier plane have been theoretically and experimentally studied. The results of numerical calculation and computer simulation show that the binarization of the specklegram enhances the higher diffracted orders of the Fourier transformed fringe, but the visibility of the fringe pattern decreases compared with the nonclipped one. However, it is also found that the fringe visibility for clipped case roughly approaches to that for the nonclipped one by setting the threshold level around the average value of the speckle intensity. The results have been verified by the experiments using the twisted nematic LCTV as a spatial light modulator. The correlation signal is improved by the further binarization of fringe pattern.

In chapter 6, based on the results in previous chapters, the nonlinear optical correlator for the processing of a two-dimensional speckle signal has been proposed by using the phase modulation property of LCTV together with the combination of nonlinear Optic RAM light detectors. To demonstrate the usefulness of the system, the velocity measurement of a light scattering object has been conducted. Although it is useful to obtain the magnitude of an object velocity, its direction can not be determined. Thus, an improved method to obtain both the magnitude and direction of the object velocity at the same time has been presented by using a joint transform correlation.

The obtained results show that the combination of Optic RAM detector and commercially available LCTV is efficient for the implementation of the optical correlator. The Optic RAM detector basically has the same properties as a DRAM which has a large memory capacity, a fast access to the data, and a low cost of the device. Considering the good availability of these devices, the proposed method is promising for the real-time optical correlator.

In conclusion, the present thesis has presented the statistical properties of clipped speckle intensity. The various significant results have been found not only from the fundamental point of view but also for the applications. The new optical correlator has been proposed for the velocity measurement of a light scattering object. As the proposed system consists of a low power laser diode and simple optical elements, it is suitable for the industrial purpose demanding for low cost and compactness.

It is finally pointed out that new optical devices are now under development as a spatial light modulator. The spatial light modulator using a ferroelectric liquid crystal device which can operate much faster than usual ones has been developed.[67,68] Since it can operate by only two states of the molecule director, the signal binarizations investigated here are directly applied to the nonlinear optical correlator. Using this device, all optical real-time correlator consisting of optical write-in and optical read-out devices will be realized in future.

Acknowledgements

I am grateful to Dr. J. Ohtsubo for his continuous guidance and constant encouragement throughout the present work, without which this thesis would not have been possible. I would also like to thank Professor N. Okamoto, Professor T. Kubo, Professor A. Sasaki, and Associate Professor T. Iwai for valuable discussions and experimental advice. My deep appreciation should also be extended to Dr. T. H. Barnes, Mr. T. Sonehara, Mr. H. Sakai, and Mr. K. Ohkubo for many useful discussions and experimental support. Acknowledgement is also made to the other members at this laboratory, for their various supports with which the present thesis has been successfully accomplished.

References

1. H. M. Pedersen, " Theory of speckle-correlation measurements using nonlinear detectors, " J. Opt. Soc. Am. A **1**, 850 (1984).
2. J. Ohtsubo, " Intensity clipping correlation of speckle patterns, " Appl. Opt. **24**, 746 (1985).
3. J. H. Churnside, " Speckle correlation measurements using clipped intensity signals, " Appl. Opt. **24**, 2488 (1985).
4. J. Marron and M. Morris, " Correlation properties of clipped laser speckle, " J. Opt. Soc. Am. A **2**, 1403 (1985).
5. J. Marron, A. J. Martino, and G. M. Morris, " Generation of random arrays using clipped laser speckle, " Appl. Opt. **25**, 26 (1986).
6. J. Marron and G. M. Morris, " Correlation measurements using clipped laser speckle, " Appl. Opt. **25**, 789 (1986).
7. R. Barakat, " Clipped correlation functions of aperture integrated laser speckle, " Appl. Opt. **25**, 3885 (1986).
8. J. Ohtsubo and A. Ogiwara, " Effects of clipping threshold of clipped speckle intensity, " Opt. Commun. **65**, 73 (1988).
9. A. Ogiwara and J. Ohtsubo, " Maximum dynamic range of clipped correlation of integrated laser speckle intensity, " J. Opt. Soc. Am. A **5**, 403 (1988).
10. A. Vander Lugt, " Signal detection by complex spatial filtering, " IEEE Trans. Inf. Theory **IT-10** 748 (1964).
11. C. S. Weaver and J. W. Goodman, " A technique for optically convolving two functions, " Appl. Opt. **5**, 1248 (1966).
12. J. Grinberg, A. Jacobson, W. P. Bleha, L. Miller, L. Fracs, D. Boswell, and G. Myer, " New real time noncoherent to coherent light image converter: hybrid field effect liquid crystal light valve, " Opt. Eng. **14**, 217 (1975).
13. W. P. Bleha, L. T. Lipton, E. Wiener-Avnear, J. Grinberg, P. G. Reif, D. P. Casasent, H. B. Brown, and B. V. Markevitch, " Application of liquid crystal light valve to real time optical data processing, " Opt. Eng. **17**, 371 (1978).
14. J. L. Horner, " Light utilization in optical correlators, " Appl. Opt. **21**, 4511 (1982).
15. J. L. Horner and P. D. Gianino, " Phase-only matched filtering, " Appl.

Opt. **23**, 812 (1984).
16. P. D. Gianino and J. L. Horner, " Additional properties of the phase-only correlation filter, " Opt. Eng. **23**, 695 (1984).
17. J. L. Horner and J. R. Leger, " Pattern recognition with binary phase-only filters, " Appl. Opt. **24**, 609 (1985).
18. J. L. Horner and P. D. Gianino, " Applying the phase-only filter concept to the synthetic discriminant function correlation filter, " Appl. Opt. **24**, 851 (1985).
19. J. L. Horner and H. O. Bartelt, " Two-bit correlation, " Appl. Opt. **24**, 2889 (1985).
20. M. A. Flavin and J. L. Horner, " Amplitude encoded phase-only filters, " Appl. Opt. **28**, 1692 (1989).
21. B. Javidi and C. J. Kuo, " Joint transform image correlation using a binary spatial light modulator at the Fourier plane, " Appl. Opt. **27**, 663 (1988).
22. B. Javidi and S. F. Odeh, " Multiple object identification by bipolar joint transform correlation, " Opt. Eng. **27**, 295 (1988).
23. B. Javidi, D. A. Gregory, and J. L. Horner, " Single modulator joint transform correlator architectures, " Appl. Opt. **28**, 411 (1989).
24. B. Javidi and J. L. Horner, " Single spatial light modulator joint transform correlator, " Appl. Opt. **28**, 1027 (1989).
25. B. Javidi, " Comparison of binary joint transform correlators and phase-only matched filter correlators, " Opt. Eng. **28**, 267 (1989).
26. B. Javidi, J. L. Horner, and H. J. Caulfield, " Deconvolution using nonlinear joint transform correlator, " Opt. Commun. **70**, 369 (1989).
27. B. Javidi, " Nonlinear joint power spectrum based optical correlation, " Appl. Opt. **28**, 2358 (1989).
28. B. Javidi, " Synthetic discriminant function-based binary nonlinear optical correlator, " Appl. Opt. **28**, 2490 (1989).
29. B. Javidi and J. L. Horner, " Multifunction nonlinear signal processor: deconvolution and correlation, " Opt. Eng. **28**, 837 (1989).
30. B. Javidi, H. J. Caulfield, and J. L. Horner, " Image deconvolution by nonlinear signal processing, " Appl. Opt. **28**, 3106 (1989).
31. B. Javidi, " Nonlinear matched filter based optical correlation, " Appl. Opt. **28**, 4518 (1989).
32. B. Javidi, " Comparison of nonlinear joint transform correlator and

nonlinear matched filter based correlator, " Opt. Commun. **75**, 8 (1990).
33. B. Javidi, C. Ruiz, and J. Ruiz, " Image deconvolution by a logarithmic exponential nonlinear joint transform process, " Appl. Opt. **29**, 685 (1990).
34. B. Javidi, " Generalization of the linear matched filter concept to nonlinear matched filters, " Appl. Opt. **29**, 1215 (1990).
35. B. Javidi, " Image enhancement by nonlinear joint transform processing, " Opt. Commun. **76**, 325 (1990).
36. F. T. S. Yu and X. J. Lu, " A real-time programmable joint transform correlator, " Opt. Commun. **52**, 10 (1984).
37. F.T. S. Yu and J. E. Ludman, " Microcomputer-based programmable optical correlator for automatic pattern recognition and identification, " Opt. Lett. **11**, 395 (1986).
38. F. T. S. Yu, S. Jutamulia, and D. A. Gregory, " Real-time liquid crystal TV XOR- and XNOR-gate binary image subtraction technique, " Appl. Opt. **26**, 2738 (1987).
39. F. T. S. Yu, S. Jutamulia, and D. A. Gregory, " Optical parallel logic gates using inexpensive liquid-crystal televisions, " Opt. Lett. **12**, 1050 (1987).
40. F. T. S. Yu, S. Jutamulia, T. W. Lin, and D. A. Gregory, " Adaptive real-time pattern recognition using a liquid crystal TV based joint transform correlator, " Appl. Opt. **26**, 1370 (1987).
41. B. Bates and P. C. Miller, " Liquid crystal television in speckle metrology, " Appl. Opt. **27**, 2816 (1988).
42. B. Bates, P. C. Miller and W. Luchuan, " Liquid-crystal television optical gates applied to real-time speckle metrology, " J. Mod. Opt. **36**, 317 (1989).
43. T. H. Barnes, T. Eiju, K. Matsuda, and N. Ooyama, " Phase-only modulation using a twisted nematic liquid crystal television, " Appl. Opt. **28**, 4845 (1989).
44. K. Lu and B. E. A. Saleh, " Theory and design of the liquid crystal TV as an optical spatial phase modulator, " Opt. Eng. **29**, 240 (1990).
45. E. C. Tam, F. T. S. Yu, D. A. Gregory, and R. D. Juday, " Data association multiple target tracking using a phase mostly liquid crystal television, " Opt. Eng. **29**, 1114 (1990).
46. D. A. Gregory, J. A. Loudin, J. C. Kirsh, E. C. Tam, and F. T. S. Yu,

" Using the hybrid modulating properties of liquid crystal television, " Appl. Opt. **30**, 1374 (1991).
47. J. C. Dainty, Ed., *Laser Speckle and Related Phenomena* 2nd Ed. (Springer-Verlag, Berlin, 1984).
48. J. Ohtsubo and A. Ogiwara, " Clipping of laser speckle signal and its applications, " Oyobutsuri (in Japanese) **58**, 1463 (1989).
49. A. Ogiwara and J. Ohtsubo, " Accuracy of peak detection in speckle clipping correlation, " Appl. Opt. **29**, 2632 (1990).
50. J. Ohtsubo, " Non-Gaussian speckle: a computer simulation, " Appl. Opt. **21**, 4167 (1982).
51. J. Ohtsubo, " The second-order statistics of speckle patterns, " J. Opt. (Paris) **12**, 129 (1981).
52. J. Marron, " Accuracy of Fourier-magnitude estimation from speckle intensity correlation, " J. Opt. Soc. Am. A **5**, 864 (1988).
53. A. Ogiwara, T. Suzuki, J. Ohtsubo, " Speckle clipping correlation using various logical operations, " Opt. Eng. **30**, 1547 (1991).
54. K. Shigeta, Master Thesis (in Japanese), Facul. Eng. Shizuoka Univ., Chap. 5 (1989).
55. A. Ogiwara and J. Ohtsubo, " Real-time nonlinear optical correlator in speckle metrology, " SPIE Proc. **1564**, (1991).
56. A. Yariv and P. Yeh, *Optical Waves in Crystals*, Chap. 5, (Wiley, New York, 1984).
57. R. K. Erf, *Speckle Metrology*, Chap. 5, (Academic Press, New York, 1978).
58. A. Ogiwara, H. Sakai, T. Utakouji, and J. Ohtsubo, " Real-time joint transform correlator using speckle clipping technique, " SPIE Proc. **1319**, 428 (1990).
59. A. Ogiwara, H. Sakai, and J. Ohtsubo, " Real-time optical correlator for doubly exposed clipped speckle, " Opt. Commun. **78**, 213 (1990).
60. A. Ogiwara, H. Sakai, and J. Ohtsubo, " Real-time optical joint transform correlator for velocity measurement using clipped speckle intensity, " Opt. Commun. **78**, 322 (1990).
61. A. Ogiwara, H. Sakai, K. Ohkubo, and J. Ohtsubo, " Application of liquid crystal TV in speckle pattern measurement, " Proceedings of 7th meeting on lightwave sensing technology (in Japanese) 67 (1991).
62. A. Ogiwara and J. Ohtsubo, " Real-time optical joint transform

correlator using nonlinear detector in speckle metrology, " Kogaku (in Japanese) **20**, 277 (1991).
63. A. Ogiwara and J. Ohtsubo, " Optical correlator for speckle interferometry, " Reports of the graduate school of electronic science and technology, Shizuoka Univ. (in Japanese) **12**, 95 (1991).
64. A. Ogiwara, H. Sakai, and J. Ohtsubo, "Application of LCTV to nonlinear speckle correlator, " Opt. Commun. **86**, 513 (1991).
65. D. G. Feitelson, *Optical Computing*, p. 169, (The MIT Press, Cambridge, 1988).
66. D. A. Yocky, T. H. Barnes, K. Matsumoto, N. Ooyama, and K. Matsuda, " Simple measurement of the phase modulation capability of liquid crystal phase-only light modulators, " Optik **84**, 140 (1990).
67. S. Yamamoto, T. Ebihara, N. Kato, H. Hoshi, " Ferroelectric liquid crystal spatial light modulator using a hydrogenated amorphous silicon as a photoconductor, " FLC' 89, 59 (1989).
68. S. Yamamoto, R. Sekura, J. Yamanaka, T. Ebihara, N. Kato, and H. Hoshi, " Optical pattern recognition with LAPS-SLM / Light addressed photoconductor and smectic C* liquid crystal spatial light modulator, " SPIE Proc. **1211**, 273 (1990).

List of papers by the author

1. J. Ohtsubo and A. Ogiwara, " Effects of clipping threshold of clipped speckle intensity, " Opt. Commun. **65**, 73 (1988).
2. A. Ogiwara and J. Ohtsubo, " Maximum dynamic range of clipped correlation of integrated laser speckle intensity, " J. Opt. Soc. Am. A **5**, 403 (1988).
3. J. Ohtsubo and A. Ogiwara, " Clipping of laser speckle signal and its applications, " Oyobutsuri (in Japanese) **58**, 1463 (1989).
4. A. Ogiwara and J. Ohtsubo, " Accuracy of peak detection in speckle clipping correlation, " Appl. Opt. **29**, 2632 (1990).
5. A. Ogiwara, H. Sakai, T. Utakouji, and J. Ohtsubo, " Real-time joint transform correlator using speckle clipping technique, " SPIE Proc. **1319**, 428 (1990).
6. A. Ogiwara, H. Sakai, and J. Ohtsubo, " Real-time optical correlator for doubly exposed clipped speckle, " Opt. Commun. **78**, 213 (1990).
7. A. Ogiwara, H. Sakai, and J. Ohtsubo, " Real-time optical joint transform correlator for velocity measurement using clipped speckle intensity, " Opt. Commun. **78**, 322 (1990).
8. A. Ogiwara, H. Sakai, K. Ohkubo, and J. Ohtsubo, " Application of liquid crystal TV in speckle pattern measurement, " Proceedings of 7th meeting on lightwave sensing technology (in Japanese) 67 (1991).
9. A. Ogiwara and J. Ohtsubo, " Real-time optical joint transform correlator using nonlinear detector in speckle metrology, " Kogaku (in Japanese) **20**, 277 (1991).
10. A. Ogiwara and J. Ohtsubo, " Optical correlator for speckle interferometry, " Reports of the Graduate School of Electronic Science and Technology, Shizuoka Univ. (in Japanese) **12**, 95 (1991).
11. A. Ogiwara and J. Ohtsubo, " Real-time nonlinear optical correlator in speckle metrology, " SPIE Proc. **1564**, (1991).
12. A. Ogiwara, T. Suzuki, and J. Ohtsubo, " Speckle clipping correlation using various logical operations, " Opt. Eng. **30**, 1547 (1991).
13. A. Ogiwara, H. Sakai, and J. Ohtsubo, " Application of LCTV to nonlinear speckle correlator, " Opt. Commun. **86**, 513 (1991).
14. A. Ogiwara and J. Ohtsubo, " Effect of clipping threshold to optical binary speckle correlator using LCTV, " submitted for publication.

15. A. Ogiwara, H. Sakai, and J. Ohtsubo, " Applications of optic RAM detector in speckle metrology, " submitted for publication.

口頭発表

1. 荻原昭文、大坪順次：「スペックルクリッピング強度の統計」　第３４回応用物理学関係連合講演会　(1987.4).
2. 荻原昭文、大坪順次：「積分されたスペックルクリッピング強度の統計的特性」第４８回応用物理学会学術講演会　(1987.10).
3. 荻原昭文、大坪順次：「スペックル強度相互相関におけるピーク位置検出の高精度化」　第３５回応用物理学関係連合講演会　(1988.3).
4. 荻原昭文、大坪順次：「スペックル強度相関における信号レベルとダイナミックレンジの関係」　第３６回応用物理学関係連合講演会　(1989.3).
5. 荻原昭文、大坪順次：「スペックル強度相関における異なった論理演算を用いた精度評価」　第５０回応用物理学会学術講演会　(1989.9).
6. 荻原昭文、酒井宏明、大坪順次：「光ＲＡＭ検出器を用いたスペックルクリッピング相関」　第３７回応用物理学関係連合講演会　(1990.3).
7. A. Ogiwara, H. Sakai, T. Utakouji, and J. Ohtsubo, " Real-time joint transform correlator using speckle clipping technique, " ICO-15 (Garmisch Partenkirchen, Germany, 1990.8).
8. 荻原昭文、酒井宏明、大坪順次：「クリップされたスペックルグラムを用いた光学的相関法」　第５１回応用物理学会学術講演会　(1990.10).
9. 荻原昭文、大坪順次：「スペックルパターンを用いた光学的相関法における二値化信号特性」　第５１回応用物理学会学術講演会　(1990.10).
10. 荻原昭文、酒井宏明、大坪順次：「非線形検出器を用いたスペックル光相関計」第３８回応用物理学関係連合講演会　(1991.3).
11. 荻原昭文、大久保和展、酒井宏明、大坪順次：「スペックルパターン計測への液晶ＴＶの応用」　第７回光波センシング技術研究会　(1991.5).
12. J. Ohtsubo and A. Ogiwara, " Real-time nonlinear optical correlator in speckle metrology, " SPIE 36th International technical symposium (San Diego, USA., 1991.7).
13. 荻原昭文、大坪順次：「液晶ＴＶを用いたスペックルパターン計測法における回折効率の改善」　第５２回応用物理学会学術講演会　(1991.10).
14. 酒井宏明、荻原昭文、大坪順次：「液晶ＴＶの偏光変調を用いた画像の減算」第５２回応用物理学会学術講演会　(1991.10).
15. 大久保和展、荻原昭文、大坪順次：「空間光変調素子としての液晶テレビの特性評価」第５２回応用物理学会学術講演会　(1991.10).
16. A. Ogiwara and J. Ohtsubo, " Optical speckle correlator using the phase modulation property of liquid crystal television, " OSA Annual meeting (San Jose, USA., 1991.11).

17. 荻原昭文、大坪順次：「液晶ＴＶを用いたスペックルパターン計測法におけるしきい値の影響」第３９回応用物理学関係連合講演会　(1992.3).
18. 大久保和展、荻原昭文、大坪順次：「空間光変調素子としての液晶テレビの特性評価」第３９回応用物理学関係連合講演会　(1992.3).
19. 渡邊実、荻原昭文、大坪順次：「微小レンズアレイとＬＣＴＶを用いた光アソシアトロン」第３９回応用物理学関係連合講演会　(1992.3).